

CAPITAL UNIVERSITY OF SCIENCE & TECHNOLOGY,
ISLAMABAD



Peristaltic Flow of Newtonian and Non-Newtonian Fluids

by

Aqila Shaheen

A thesis submitted in partial fulfillment for the
degree of Doctor of Philosophy

in the
Faculty of Computing
Department of Mathematics

July 2017

Peristaltic Flow of Newtonian and Non-Newtonian Fluids

By
Aqila Shaheen

A research thesis submitted to the Department of Mathematics, Capital University of
Science and Technology, Islamabad in partial fulfillment of the requirements for the
degree of

DOCTOR OF PHILOSOPHY IN MATHEMATICS



DEPARTMENT OF MATHEMATICS
CAPITAL UNIVERSITY OF SCIENCE AND TECHNOLOGY
ISLAMABAD
2017

Copyright © 2017 by Miss Aqila Shaheen

All rights reserved. No part of this thesis may be reproduced, distributed, or transmitted in any form or by any means, including photocopying, recording, or other electronic or mechanical methods, by any information storage and retrieval system without the prior written permission of the author.

Peristaltic Flow of Newtonian and Non-Newtonian Fluids

**By
Aqila Shaheen
(PA133005)**

**Prof. Dr. Changhoon Lee
Yonsei University, Seoul, South Korea
(Foreign Evaluator No. 1)**

**Dr. Gazanfer Unal
Yeditepe University, Istanbul, Turkey
(Foreign Evaluator No. 2)**

**Dr. Shafqat Hussain
(Thesis Supervisor)**

**Dr. Muhammad Sagheer
(Head, Department of Mathematics)**

**Dr. Muhammad Abdul Qadir
(Dean, Faculty of Computing)**

**DEPARTMENT OF MATHEMATICS
CAPITAL UNIVERSITY OF SCIENCE & TECHNOLOGY
ISLAMABAD**



**CAPITAL UNIVERSITY OF SCIENCE & TECHNOLOGY
ISLAMABAD**

Expressway, Kahuta Road, Zone-V, Islamabad
Phone: +92-51-111-555-666 Fax: +92-51-4486705
Email: info@cust.edu.pk Website: <https://www.cust.edu.pk>

CERTIFICATE OF APPROVAL

This is to certify that the research work presented in the thesis, entitled “**Peristaltic Flow of Newtonian and Non-Newtonian Fluids**” was conducted under the supervision of **Dr. Shafqat Hussain**. No part of this thesis has been submitted anywhere else for any other degree. This thesis is submitted to the **Department of Mathematics** in partial fulfillment of the requirements for the degree of Doctor in Philosophy in the field of **Mathematics, Department of Mathematics, Capital University of Science and Technology**.

Student Name : Ms. Aqila Shaheen (PA133005)

Examination Committee :

- (a) External Examiner 1: Dr. Tanvir Akbar Kiani
Assistant Professor
CIIT, Islamabad
- (b) External Examiner 2: Dr. Asim Aziz
Assistant Professor
CEME, NUST, Islamabad
- (c) Internal Examiner : Dr. Muhammad Sagheer
Associate Professor
Capital University of Science &
Technology, Islamabad

Supervisor Name : Dr. Shafqat Hussain
Associate Professor
Capital University of Science &
Technology, Islamabad

Name of HoD : Dr. Muhammad Sagheer
Associate Professor
Capital University of Science &
Technology, Islamabad

Name of Dean : Dr. Muhammad Abdul Qadir
Professor
Capital University of Science &
Technology, Islamabad



**CAPITAL UNIVERSITY OF SCIENCE & TECHNOLOGY
ISLAMABAD**

Expressway, Kahuta Road, Zone-V, Islamabad
Phone: +92-51-111-555-666 Fax: +92-51-4486705
Email: info@cust.edu.pk Website: <https://www.cust.edu.pk>

AUTHOR'S DECLARATION

I, Ms. Aqila Shaheen (Registration No. PA133005), hereby state that my PhD thesis titled, 'Peristaltic Flow of Newtonian and Non-Newtonian Fluids' is my own work and has not been submitted previously by me for taking any degree from Capital University of Science and Technology, Islamabad or anywhere else in the country/ world.

At any time, if my statement is found to be incorrect even after my graduation, the University has the right to withdraw my PhD Degree.

(Ms. Aqila Shaheen)

Dated: 21 June, 2017

Registration No : PA133005



**CAPITAL UNIVERSITY OF SCIENCE & TECHNOLOGY
ISLAMABAD**

Expressway, Kahuta Road, Zone-V, Islamabad
Phone: +92-51-111-555-666 Fax: +92-51-4486705
Email: info@cust.edu.pk Website: <https://www.cust.edu.pk>

PLAGIARISM UNDERTAKING

I solemnly declare that research work presented in the thesis titled “**Peristaltic Flow of Newtonian and Non-Newtonian Fluids**” is solely my research work with no significant contribution from any other person. Small contribution/ help wherever taken has been duly acknowledged and that complete thesis has been written by me.

I understand the zero tolerance policy of the HEC and Capital University of Science and Technology towards plagiarism. Therefore, I as an author of the above titled thesis declare that no portion of my thesis has been plagiarized and any material used as reference is properly referred/ cited.

I undertake that if I am found guilty of any formal plagiarism in the above titled thesis even after award of PhD Degree, the University reserves the right to withdraw/ revoke my PhD degree and that HEC and the University have the right to publish my name on the HEC/ University Website on which names of students are placed who submitted plagiarized thesis.

Dated: 21 June, 2017

(Ms. Aqila Shaheen)
Registration No. PA133005

Publications List

It is certified that following publications have been made out of the research work that has been carried out for this thesis.

Journal Papers

1. S. Nadeem, A. Shaheen, S. Hussain, Physiological breakdown of Jeffrey six-constant nanofluid in an endoscope with non-uniform wall, *Journal of Applied Physics Letters*, 5, 127143, (2015).
2. S. Nadeem, A. Munim, A. Shaheen, and S. Hussain, Physiological breakdown of Carreau due to ciliary motion, *Journal of Applied Physics Letter*, 6, 035125, (2016).
3. A. Shaheen, S. Hussain, and S. Nadeem, Physiological flow of Jeffrey six-constant fluid model due to ciliary motion, *Communication in Theoretical Physics*, 66: 701-708, (2016).

Dedicated to

My loving father and mother

Whose prayers have always been a source of great inspiration for me

My caring and supporting husband

Who've always given me perpetual love and care

Contents

List of Figures	vii
Symbols	viii
Acknowledgement	x
1 Introduction	1
1.1 Thesis contribution	4
1.2 Scheme of the thesis	5
2 Physiological breakdown of Jeffrey six-constant nanofluid flow in an endoscope with nonuniform wall	8
2.1 Problem Formulation	9
2.2 Solution of the problem	12
2.2.1 Exact Solution	12
2.2.2 Homotopy Perturbation Method	13
2.3 Results and discussions	16
2.4 Conclusion	24
3 Simulation of mixed convection flow for physiological breakdown of Jeffrey six-constant fluid model with convective boundary condition	25
3.1 Problem Formulation	25
3.2 Solution of the problem	29
3.2.1 Exact Solution	29
3.2.2 Homotopy Perturbation Method	29
3.3 Results and discussions	31
3.4 Conclusion	39
4 Physiological breakdown of Sisko fluid with convective boundary condition in a uniform tube	40
4.1 Mathematical Formulation	40
4.2 Solution Methodology	44
4.3 Results and discussions	46
4.4 Conclusion	59

5	Physiological flow of Carreau fluid due to ciliary motion	60
5.1	Model of the Problem	60
5.2	Solution Methodology	63
5.3	Results and discussions	66
5.4	Conclusion	76
6	Metachronal wave analysis for Non-Newtonian fluid under thermo- phersis and brownian motion effects	77
6.1	Introduction	77
6.2	Model of the Problem	77
6.3	Solution Methodology	82
6.4	Results and discussions	84
6.5	Conclusion	91
7	Physiological flow of Jeffrey six-constant fluid due to ciliary motion	92
7.1	Formulation of the Problem	93
7.2	Solution Methodology	96
	7.2.1 Perturbation solution	96
7.3	Results and discussions	98
7.4	Conclusion	106
8	Conclusion	107
8.1	Future work	108
	Bibliography	110
	Appendix A	116
	Appendix B	117
	Appendix C	118

List of Figures

2.1	Geometry of the problem.	9
2.2	Variation of temperature for N_b when $N_t = 8, Z = 0.2, r_1 = 0.1, a_0 = 0.01$ and $\lambda = 0.1, \phi = 0.02$	18
2.3	Variation of temperature for N_t when $N_b = 8, Z = 0.2, r_1 = 0.1, a_0 = 0.01$ and $\lambda = 0.1, \phi = 0.02$	18
2.4	Variation of concentration for N_b when $N_t = 8, Z = 0.2, r_1 = 0.1,$ $a_0 = 0.01$ and $\lambda = 0.1, \phi = 0.02$	18
2.5	Variation of concentration for N_t when $N_b = 8, Z = 0.2, r_1 = 0.1,$ $a_0 = 0.01$ and $\lambda = 0.1, \phi = 0.02$	19
2.6	Variation of velocity for α when $N_t = 8, Z = 0.2, r_1 = 0.1, a_0 = 0.01$ and $\lambda = 0.1, \phi = 0.02, N_b = 8, \alpha_1 = 8$	19
2.7	Variation of velocity for M when $N_t = 8, Z = 0.2, r_1 = 0.1, a_0 = 0.01$ and $\lambda = 0.1, \phi = 0.02, N_b = 8, \alpha_1 = 8, \alpha = 0.03$	19
2.8	Variation of pressure rise for α when $N_t = 8, Z = 0.2, r_1 = 0.1, a_0 = 0.01$ and $\lambda = 0.1, \phi = 0.02, \alpha_1 = 8, M = 0.9$	20
2.9	Variation of frictional force (inner tube) for α when $N_t = 8, Z = 0.2,$ $r_1 = 0.1, a_0 = 0.01$ and $\lambda = 0.1, \phi = 0.02, \alpha_1 = 8, N_b = 0.03, M = 0.9$	20
2.10	Variation of frictional force (outer tube) for α when $N_t = 8, Z = 0.2,$ $r_1 = 0.1, a_0 = 0.01$ and $\lambda = 0.1, \phi = 0.02, \alpha_1 = 8, M = 0.9$	20
2.11	Variation of pressure rise for M when $N_t = 8, Z = 0.2, r_1 = 0.1, a_0 = 0.01$ and $\lambda = 0.1, \phi = 0.02, \alpha_1 = 8, \alpha = 0.03, N_b = 7$	21
2.12	Variation of frictional force (inner tube) for M when $N_t = 8, Z = 0.2,$ $r_1 = 0.1, a_0 = 0.01$ and $\lambda = 0.1, \phi = 0.02, \alpha_1 = 8, \alpha = 0.03, N_b = 7$	21
2.13	Variation of frictional force (outer tube) for M when $N_t = 8, Z = 0.2,$ $r_1 = 0.1, a_0 = 0.01$ and $\lambda = 0.1, \phi = 0.02, \alpha_1 = 8, \alpha = 0.03, N_b = 7$	21
2.14	Pressure gradient $\frac{dp}{dz}$ for sinusoidal wave when $N_t = 8, Z = 0.2, r_1 = 0.1,$ $a_0 = 0.01$ and $\lambda = 0.1, N_b = 7, \alpha_1 = 8, \alpha = 0.03, M = 0.9$	22
2.15	Pressure gradient $\frac{dp}{dz}$ for multisinusoidal wave when $N_t = 8, Z = 0.2,$ $r_1 = 0.1, a_0 = 0.01$ and $\lambda = 0.1, N_b = 7, \alpha_1 = 8, \alpha = 0.03, M = 0.9$	22
2.16	Pressure gradient $\frac{dp}{dz}$ for Trapizodioal wave when $N_t = 8, Z = 0.2, r_1 =$ $0.1, a_0 = 0.01$ and $\lambda = 0.1, N_b = 7, \alpha_1 = 8, \alpha = 0.03, M = 0.9$	22
2.17	Streamlines pattern for sinusoidal wave when $N_t = 8, Z = 0.2, r_1 = 0.1,$ $a_0 = 0.01$ and $\lambda = 0.1, \phi = 0.02, \alpha_1 = 8, \alpha = 0.03, M = 0.9$	23
2.18	Streamlines pattern for multisinusoidal wave when $N_t = 8, Z = 0.2,$ $r_1 = 0.1, a_0 = 0.01$ and $\lambda = 0.1, \phi = 0.02, \alpha_1 = 8, \alpha = 0.03, M = 0.9$	23
2.19	Streamlines pattern for Trapizodioal wave when $N_t = 8, Z = 0.2, r_1 =$ $0.1, a_0 = 0.01$ and $\lambda = 0.1, \phi = 0.02, \alpha_1 = 8, \alpha = 0.03, M = 0.9$	23
3.1	Geometry of the problem.	26

3.2	Variation of temperature for B when $Z = 0.23$, $\epsilon = 0.22$, $\kappa = 2.55$	33
3.3	Variation of temperature for κ when $Z = 0.23$, $\epsilon = 0.22$, $B = 2.55$	33
3.4	Variation of velocity for α when $Z = 0.23$, $\epsilon = 0.22$, $\kappa = 2.55$, $\eta = \frac{\pi}{4}$, $B = 0.22$, $G_r = 1.5$, $\alpha_1 = 0.4$, $\alpha_2 = 0.6$	33
3.5	Variation of velocity for κ when $Z = 0.23$, $\epsilon = 0.22$, $\alpha = 0.22$, $\eta = \frac{\pi}{4}$, $B = 0.22$, $\alpha_1 = 0.22$, $\alpha_2 = 0.4$, $G_r = 1.5$	34
3.6	Variation of velocity for B when $Z = 0.23$, $\epsilon = 0.22$, $\kappa = 2.55$, $\eta = \frac{\pi}{4}$, $\alpha = 0.22$, $\alpha_1 = 0.22$, $\alpha_2 = 0.4$, $G_r = 1.5$	34
3.7	Variation of velocity for G_r when $Z = 0.23$, $\epsilon = 0.22$, $\eta = \frac{\pi}{4}$, $\alpha = 0.22$, $\alpha_1 = 0.22$, $\alpha_2 = 0.4$, $B = 0.22$	34
3.8	Variation of pressure rise for λ_1 when $Z = 0.23$, $\epsilon = 0.01$, $\eta = \frac{\pi}{4}$, $\alpha_1 =$ 0.22 , $\alpha_2 = 0.4$, $G_r = 1.5$, $B = 1.5$	35
3.9	Variation of frictional forces for λ_1 when $Z = 0.23$, $\epsilon = 0.01$, $\eta = \frac{\pi}{4}$, $\alpha_1 = 0.22$, $\alpha_2 = 0.4$, $G_r = 1.5$, $B = 1.5$	35
3.10	Variation of pressure rise for α when $Z = 0.23$, $\epsilon = 0.01$, $\eta = \frac{\pi}{4}$, $\alpha_1 = 0.22$, $\alpha_2 = 0.4$, $G_r = 1.5$, $B = 1.5$	35
3.11	Variation of frictional forces for α when $Z = 0.23$, $\epsilon = 0.01$, $\eta = \frac{\pi}{4}$, $\alpha_1 = 0.22$, $\alpha_2 = 0.4$, $G_r = 1.5$, $B = 1.5$	36
3.12	Variation of pressure rise for λ_2 when $Z = 0.23$, $\epsilon = 0.01$, $\eta = \frac{\pi}{4}$, $\alpha_1 =$ 0.22 , $\alpha_2 = 0.4$, $G_r = 1.5$, $B = 1.5$	36
3.13	Variation of frictional forces for λ_2 when $Z = 0.23$, $\epsilon = 0.01$, $\eta = \frac{\pi}{4}$, $\alpha_1 = 0.22$, $\alpha_2 = 0.4$, $G_r = 1.5$, $B = 1.5$	36
3.14	Pressure gradient $\frac{dp}{dz}$ for sinusoidal wave when $Z = 0.23$, $\eta = \frac{\pi}{4}$, $\alpha_1 = 0.22$, $\alpha_2 = 0.4$, $G_r = 1.5$, $B = 1.5$	37
3.15	Pressure gradient $\frac{dp}{dz}$ for multisinusoidal wave when $Z = 0.23$, $\eta = \frac{\pi}{4}$, $\alpha_1 = 0.22$, $\alpha_2 = 0.4$, $G_r = 1.5$, $B = 1.5$	37
3.16	Pressure gradient $\frac{dp}{dz}$ for trapizodioal wave when $Z = 0.23$, $\eta = \frac{\pi}{4}$, $\alpha_1 =$ 0.22 , $\alpha_2 = 0.4$, $G_r = 1.5$, $B = 1.5$	37
3.17	Streamlines pattern for sinusoidal wave $Z = 0.23$, $\epsilon = 0.01$, $\eta = \frac{\pi}{4}$, $\alpha_1 = 0.22$, $\alpha_2 = 0.4$, $G_r = 1.5$, $B = 1.5$	38
3.18	Streamlines pattern for multisinusoidal wave $Z = 0.23$, $\epsilon = 0.01$, $\eta = \frac{\pi}{4}$, $\alpha_1 = 0.22$, $\alpha_2 = 0.4$, $G_r = 1.5$, $B = 1.5$	38
3.19	Streamlines pattern for trapizodioal $Z = 0.23$, $\epsilon = 0.01$, $\eta = \frac{\pi}{4}$, $\alpha_1 = 0.22$, $\alpha_2 = 0.4$, $G_r = 1.5$, $B = 1.5$	38
4.1	A physical sketch of the problem.	41
4.2	Variation of temperature for b when $Z = 0.23$, $\epsilon = 0.22$, $\kappa = 2.55$, $M = 0.09$, $B_k = 0.23$	48
4.3	Variation of temperature for B_k when $Z = 0.23$, $\epsilon = 0.22$, $\kappa = 2.55$, $M = 0.09$, $b = 0.23$	48
4.4	Variation of temperature for M when $Z = 0.23$, $\epsilon = 0.22$, $\kappa = 2.55$, $b = 0.01$, $B_k = 0.23$	48
4.5	Variation of temperature graph for κ when $Z = 0.23$, $\epsilon = 0.22$, $b = 0.01$, $M = 0.09$, $B_k = 0.23$	49
4.6	Variation of nanoparticle concentration graph for B_k when $M = 0.09$, $Z = 0.2$, $S_T = 0.8$, $\lambda = 0.1$, $\epsilon = 0.22$, $S_H = 0.8$	49
4.7	Variation of nanoparticle concentration graph for M when $B_k = 0.09$, $Z = 0.2$, $S_T = 0.8$, $\lambda = 0.1$, $\epsilon = 0.22$, $S_H = 0.8$	49

4.8	Variation of nanoparticle concentration graph for b when $M = 0.09$, $Z = 0.2$, $S_T = 0.8$, $\lambda = 0.1$, $\epsilon = 0.22$, $S_H = 0.8$.	50
4.9	Variation of nanoparticle concentration graph for S_H when $M = 0.09$, $Z = 0.2$, $S_T = 0.8$, $\lambda = 0.1$, $\epsilon = 0.22$, $b = 0.01$.	50
4.10	Variation of nanoparticle concentration graph for S_T when $M = 0.09$, $Z = 0.2$, $b = 0.01$, $\lambda = 0.1$, $\epsilon = 0.22$, $S_H = 0.8$.	50
4.11	Variation of velocity graph for M when $b = 0.01$, $Z = 0.2$, $S_T = 0.8$, $\lambda = 0.1$, $\epsilon = 0.22$, $S_H = 0.8$.	51
4.12	Variation of shear stress graph for b when $M = 0.09$, $Z = 0.2$, $S_T = 0.8$, $\lambda = 0.1$, $\epsilon = 0.22$, $S_H = 0.8$.	51
4.13	Variation of shear stress graph for M when $b = 0.01$, $Z = 0.2$, $S_T = 0.8$, $\lambda = 0.1$, $\epsilon = 0.22$, $S_H = 0.8$.	51
4.14	Variation of pressure rise graph for b when $M = 0.09$, $Z = 0.2$, $S_T = 0.8$, $\lambda = 0.1$, $\epsilon = 0.22$, $S_H = 0.8$.	52
4.15	Variation of frictional forces graph for b when $M = 0.09$, $Z = 0.2$, $S_T = 0.8$, $\lambda = 0.1$, $\epsilon = 0.22$, $S_H = 0.8$.	52
4.16	Variation of pressure rise graph for ϵ when $M = 0.09$, $Z = 0.2$, $S_T = 0.8$, $\lambda = 0.1$, $b = 0.01$, $S_H = 0.8$.	52
4.17	Variation of frictional forces graph for ϵ when $M = 0.09$, $Z = 0.2$, $S_T = 0.8$, $\lambda = 0.1$, $b = 0.01$, $S_H = 0.8$.	53
4.18	Variation of pressure rise for M when $b = 0.01$, $Z = 0.2$, $S_T = 0.8$, $\lambda = 0.1$, $\epsilon = 0.22$, $S_H = 0.8$.	53
4.19	Variation of frictional forces for M when $b = 0.01$, $Z = 0.2$, $S_T = 0.8$, $\lambda = 0.1$, $\epsilon = 0.22$, $S_H = 0.8$.	53
4.20	Pressure gradient $\frac{dp}{dz}$ for sinusoidal wave when $M = 0.09$, $Z = 0.2$, $S_T = 0.8$, $\lambda = 0.1$, $b = 0.01$, $S_H = 0.8$.	54
4.21	Pressure gradient $\frac{dp}{dz}$ for multisinusoidal wave when $M = 0.09$, $Z = 0.2$, $S_T = 0.8$, $\lambda = 0.1$, $b = 0.01$, $S_H = 0.8$.	54
4.22	Pressure gradient $\frac{dp}{dz}$ for Trapizoidal wave when $M = 0.09$, $Z = 0.2$, $S_T = 0.8$, $\lambda = 0.1$, $b = 0.01$, $S_H = 0.8$.	54
4.23	Pressure gradient $\frac{dp}{dz}$ for b when $M = 0.09$, $Z = 0.2$, $S_T = 0.8$, $\lambda = 0.1$, $\epsilon = 0.01$, $S_H = 0.8$.	55
4.24	Pressure gradient $\frac{dp}{dz}$ for M when $\epsilon = 0.22$, $Z = 0.2$, $S_T = 0.8$, $\lambda = 0.1$, $b = 0.01$, $S_H = 0.8$.	55
4.25	Streamlines pattern for sinusoidal wave $M = 0.09$, $Z = 0.2$, $S_T = 0.8$, $\lambda = 0.1$, $b = 0.01$, $S_H = 0.8$.	55
4.26	Streamlines pattern for multisinusoidal wave $M = 0.09$, $Z = 0.2$, $S_T = 0.8$, $\lambda = 0.1$, $b = 0.01$, $S_H = 0.8$.	56
4.27	Streamlines pattern for Trapizoidal wave $M = 0.09$, $Z = 0.2$, $S_T = 0.8$, $\lambda = 0.1$, $b = 0.01$, $S_H = 0.8$.	56
4.28	Streamlines pattern for $b = 0.01$ when $M = 0.09$, $Z = 0.2$, $S_T = 0.8$, $\lambda = 0.1$, $\epsilon = 0.01$, $S_H = 0.8$.	56
4.29	Streamlines pattern for $b = 0.02$ when $M = 0.09$, $Z = 0.2$, $S_T = 0.8$, $\lambda = 0.1$, $\epsilon = 0.01$, $S_H = 0.8$.	57
4.30	Streamlines pattern for $b = 0.03$ when $M = 0.09$, $Z = 0.2$, $S_T = 0.8$, $\lambda = 0.1$, $\epsilon = 0.01$, $S_H = 0.8$.	57
4.31	Streamlines pattern for $b = 0.04$ when $M = 0.09$, $Z = 0.2$, $S_T = 0.8$, $\lambda = 0.1$, $\epsilon = 0.01$, $S_H = 0.8$.	57

4.32	Streamlines pattern for $M = 1$ when $\epsilon = 0.09, Z = 0.2, S_T = 0.8, \lambda = 0.1, b = 0.01, S_H = 0.8$.	58
4.33	Streamlines pattern for $M = 2$ when $\epsilon = 0.09, Z = 0.2, S_T = 0.8, \lambda = 0.1, b = 0.01, S_H = 0.8$.	58
4.34	Streamlines pattern for $M = 3$ when $\epsilon = 0.09, Z = 0.2, S_T = 0.8, \lambda = 0.1, b = 0.01, S_H = 0.8$.	58
5.1	A physical sketch of the problem	61
5.2	Variation of velocity for n when $Q = 0.3, \xi = 0.7, \delta = 0.8, \gamma = 0.7, W_e = 0.9$.	67
5.3	Variation of velocity for W_e when $\delta = 0.3, \xi = 0.7, \gamma = 0.8, Q = 0.7, W_e = 0.9$.	67
5.4	Variation of velocity for ξ when $\delta = 0.3, n = 0.7, \gamma = 0.8, Q = 0.7, W_e = 0.9$.	67
5.5	Variation of velocity for Q when $\delta = 0.3, \xi = 0.6, \gamma = 0.8, n = 0.2, W_e = 0.9$.	68
5.6	Variation of pressure gradient for n when $\delta = 0.3, \xi = 0.6, \gamma = 0.8, Q = 0.7, W_e = 0.9$.	68
5.7	Variation of pressure gradient for Q when $\delta = 0.3, \xi = 0.6, \gamma = 0.8, n = 0.6, W_e = 0.9$.	68
5.8	Variation of pressure gradient for W_e when $\gamma = 0.3, Q = 0.6, n = 0.8, \delta = 0.5, \xi = 0.6$.	69
5.9	Variation of pressure gradient for ξ when $\gamma = 0.3, Q = 0.6, n = 0.8, W_e = 0.5, \delta = 0.9$.	69
5.10	Variation of pressure gradient for δ when $\gamma = 0.6, Q = 0.5, \xi = 0.8, n = 0.5, W_e = 0.9$.	69
5.11	Variation of pressure gradient for γ when $\xi = 0.1, \delta = 0.1, Q = 0.1, W_e = 0.5, n = 0.3$.	70
5.12	Variation of pressure gradient for n when $Q = 0.1, W_e = 0.1, \gamma = 0.1, \xi = 0.5, \delta = 0.3$.	70
5.13	Variation of pressure rise for W_e when $Q = 0.1, n = 0.1, \xi = 0.1, \delta = 0.5, b = 0.3$.	70
5.14	Variation of pressure rise for δ when $Q = 0.1, n = 0.1, \xi = 0.1, \gamma = 0.5, b = 0.3$.	71
5.15	Variation of pressure rise for γ when $Q = 0.1, \xi = 0.1, b = 0.1, n = 0.5, W_e = 0.3$.	71
5.16	Variation of pressure rise for ξ when $Q = 0.1, b = 0.1, W_e = 0.1, n = 0.5, \gamma = 0.3$.	71
5.17	Streamlines for different value of $Q = 0.1, \xi = 0.1, n = 0.1, W_e = 0.1, Q = 0.5, \gamma = 0.3$.	72
5.18	Streamlines for different value of $Q = 0.1, W_e = 0.1, n = 0.1, \gamma = 0.1, \delta = 0.5, \xi = 0.3$.	72
5.19	Streamlines for different value of $Q = 0.1, W_e = 0.1, n = 0.1, \gamma = 0.1, \delta = 0.5, \xi = 0.3$.	72
5.20	Streamlines for different value of $Q = 0.1, W_e = 0.1, n = 0.1, \gamma = 0.1, \delta = 0.5, \xi = 0.3$.	73
5.21	Streamlines for different value of $Q = 0.1, W_e = 0.1, n = 0.1, \gamma = 0.1, \delta = 0.5, \xi = 0.3$.	73
5.22	Streamlines for different value of $Q = 0.1, W_e = 0.1, n = 0.1, \gamma = 0.1, \delta = 0.5, \xi = 0.3$.	73

5.23 Streamlines for different value of $Q = 0.1, W_e = 0.1n = 0.1, \gamma = 0.1, \delta = 0.5, \xi = 0.3$	74
5.24 Streamlines for different value of $Q = 0.1, W_e = 0.1n = 0.1, \gamma = 0.1, \delta = 0.5, \xi = 0.3$	74
5.25 Streamlines for different value of $Q = 0.1, W_e = 0.1n = 0.1, \gamma = 0.1, \delta = 0.5, \xi = 0.3$	74
5.26 Streamlines for different value of $Q = 0.1, W_e = 0.1n = 0.1, \gamma = 0.1, \delta = 0.5, \xi = 0.3$	75
5.27 Streamlines for different value of $Q = 0.1, W_e = 0.1n = 0.1, \gamma = 0.1, \delta = 0.5, \xi = 0.3$	75
5.28 Streamlines for different value of $Q = 0.1, W_e = 0.1n = 0.1, \gamma = 0.1, \delta = 0.5, \xi = 0.3$	75
6.1 A physical sketch of the problem	78
6.2 Velocity for different values of α_1 when $\alpha = 0.28, \delta = 0.43, B = 0.87, \epsilon = 0.12, N_t = 0.8, N_b = 0.7, G_r = 5.57$	85
6.3 Velocity for different values of ϵ when $\alpha = 0.28, \delta = 0.43, B = 0.87, N_t = 0.8, N_b = 0.7, G_r = 5.57$	85
6.4 Velocity for different values of M when $\alpha = 0.28, \delta = 0.43, B = 0.87, \epsilon = 0.12, N_t = 0.8, N_b = 0.7, G_r = 5.57$	85
6.5 Temperature for different values of N_t when $\alpha = 0.28, \delta = 0.43, B = 0.87, \epsilon = 0.12, N_b = 0.7, G_r = 5.57$	86
6.6 Concentration for different values of N_b when $\alpha = 0.28, \delta = 0.43, B = 0.87, \epsilon = 0.12, N_t = 0.8, G_r = 5.57$	86
6.7 Concentration for different values of N_t when $\alpha = 0.28, \delta = 0.43, B = 0.87, \epsilon = 0.12, N_b = 0.7, G_r = 5.57$	86
6.8 Pressure rise for different values of α_1 when $\alpha = 0.28, \delta = 0.43, B = 0.87, \epsilon = 0.12, N_t = 0.8, N_b = 0.7, G_r = 5.57, M = 0.9$	87
6.9 Frictional forces for different values of α_1 when $\alpha = 0.28, \delta = 0.43, B = 0.87, \epsilon = 0.12, N_t = 0.8, N_b = 0.7, G_r = 5.57, M = 0.9$	87
6.10 Pressure rise for different values of ϵ when $\alpha = 0.28, \delta = 0.43, B = 0.87, N_t = 0.8, N_b = 0.7, G_r = 5.57, M = 0.9$	87
6.11 Frictional forces for different values of ϵ when $\alpha = 0.28, \delta = 0.43, B = 0.87, N_t = 0.8, N_b = 0.7, G_r = 5.57, M = 0.9$	88
6.12 Pressure rise for different values of α_3 when $\alpha = 0.28, \delta = 0.43, B = 0.87, \epsilon = 0.12, N_t = 0.8, N_b = 0.7, G_r = 5.57, M = 0.9$	88
6.13 Frictional forces for different values of α_3 when $\alpha = 0.28, \delta = 0.43, B = 0.87, \epsilon = 0.12, N_t = 0.8, N_b = 0.7, G_r = 5.57, M = 0.9$	88
6.14 Pressure gradient for different values of ϵ when $\alpha = 0.28, \delta = 0.43, B = 0.87, \alpha_3 = 0.12, N_t = 0.8, N_b = 0.7, G_r = 5.57, M = 0.9$	89
6.15 Pressure gradient for different values of G_r when $\alpha = 0.28, \delta = 0.43, B = 0.87, \epsilon = 0.12, N_t = 0.8, N_b = 0.7, \alpha_3 = 5.57, M = 0.9$	89
6.16 Pressure gradient for different values of N_t when $\alpha = 0.28, \delta = 0.43, B = 0.87, \epsilon = 0.12, \alpha_3 = 0.8, N_b = 0.7, G_r = 5.57, M = 0.9$	89
6.17 Streamlines for different values of $\alpha_1 = 0.1$ when $\alpha = 0.28, \delta = 0.43, B = 0.87, \epsilon = 0.12, N_t = 0.8, N_b = 0.7, G_r = 5.57, M = 0.9$	90
6.18 Streamlines for different values of $\alpha_1 = 0.3$ when $\alpha = 0.28, \delta = 0.43, B = 0.87, \epsilon = 0.12, N_t = 0.8, N_b = 0.7, G_r = 5.57, M = 0.9$	90

6.19	Streamlines for different values of $\alpha_1 = 0.5$ when $\alpha = 0.28, \delta = 0.43, B = 0.87, \epsilon = 0.12, N_t = 0.8, N_b = 0.7, G_r = 5.57, M = 0.9$	90
7.1	Variation of temperature graph for α_1 when $Z = 0.75, \epsilon = 0.22, M = 0.2, B_r = 0.22, \alpha = 0.22, \beta = 1.5, \alpha_2 = 0.6$	99
7.2	Variation of temperature for α_1 when $Z = 0.75, \epsilon = 0.22, M = 0.2, B_r = 0.22, \alpha = 0.22, \beta = 1.5, \alpha_1 = 0.6$	99
7.3	Variation of temperature for B_r when $Z = 0.75, \epsilon = 0.22, M = 0.2, \alpha_1 = 0.22, \alpha = 0.22, \beta = 1.5, \alpha_2 = 0.6$	99
7.4	Variation of temperature for ϵ when $Z = 0.75, B_r = 0.22, M = 0.2, \alpha_1 = 0.22, \alpha = 0.25, \beta = 1.5, \alpha_2 = 0.6$	100
7.5	Variation of nanoparticle concentration for α_1 when $Z = 0.75, B_r = 0.22, M = 0.2, \epsilon = 0.22, \alpha = 0.25, \beta = 1.5, \alpha_2 = 0.6, S_T = 0.7, S_H = 0.5$	100
7.6	Variation of nanoparticle concentration for α_2 when $Z = 0.75, B_r = 0.22, M = 0.2, \epsilon = 0.22, \alpha = 0.25, \beta = 1.5, \alpha_1 = 0.6, S_T = 0.7, S_H = 0.5$	100
7.7	Variation of nanoparticle concentration for S_T when $Z = 0.75, B_r = 0.22, M = 0.2, \epsilon = 0.22, \alpha = 0.25, \beta = 1.5, \alpha_1 = 0.6, \alpha_2 = 0.7, S_H = 0.5$	101
7.8	Variation of nanoparticle concentration for S_H when $Z = 0.75, B_r = 0.22, M = 0.2, \epsilon = 0.22, \alpha = 0.25, \beta = 1.5, \alpha_1 = 0.6, \alpha_2 = 0.7, S_T = 0.5$	101
7.9	Variation of velocity for α_2 when $Z = 0.75, B_r = 0.22, M = 0.2, \epsilon = 0.22, \alpha = 0.25, \beta = 1.5, \alpha_1 = 0.7$	101
7.10	Variation of velocity for ϵ when $Z = 0.75, B_r = 0.22, M = 0.2, \alpha_1 = 0.22, \alpha = 0.25, \beta = 1.5, \alpha_2 = 0.27$	102
7.11	Variation of Pressure rise for α_1 when $Z = 0.23, \epsilon = 0.01, \alpha_1 = 0.22, \alpha_2 = 0.4, \beta = 1.5, B_r = 1.5, S_T = 0.7, S_H = 0.5$	102
7.12	Variation of frictional force for α_1 when $Z = 0.23, \epsilon = 0.01, \alpha = 0.22, \alpha_2 = 0.4, \beta = 1.5, B_r = 1.5, S_T = 0.7, S_H = 0.5$	102
7.13	Variation of Pressure rise for α_2 when $Z = 0.23, \epsilon = 0.01, \alpha_1 = 0.22, \alpha = 0.4, \beta = 1.5, B_r = 1.5, S_T = 0.7, S_H = 0.5$	103
7.14	Variation of frictional force for α_2 when $Z = 0.23, \epsilon = 0.01, \alpha_1 = 0.22, \alpha = 0.4, \beta = 1.5, B_r = 1.5, S_T = 0.7, S_H = 0.5$	103
7.15	Variation of Pressure rise for β when $Z = 0.23, \epsilon = 0.01, \alpha_1 = 0.22, \alpha = 0.4, \alpha_2 = 0.5, B_r = 1.5, S_T = 0.7, S_H = 0.5$	103
7.16	Variation of frictional force for β when $Z = 0.23, \epsilon = 0.01, \alpha_1 = 0.22, \alpha = 0.4, \alpha_2 = 0.5, B_r = 1.5, S_T = 0.7, S_H = 0.5$	104
7.17	Pressure gradient $\frac{dp}{dz}$ for sinusoidal wave when $Z = 0.23, \epsilon = 0.01, \alpha = 0.4, \alpha_2 = 0.5, B_r = 1.5, S_T = 0.7, S_H = 0.5$	104
7.18	Pressure gradient $\frac{dp}{dz}$ for sinusoidal wave when $Z = 0.23, \epsilon = 0.01, \alpha_1 = 0.22, \alpha = 0.4, B_r = 1.5, S_T = 0.7, S_H = 0.5$	104
7.19	Streamlines pattern for sinusoidal wave $Z = 0.23, \epsilon = 0.01, \alpha_1 = 0.22, \alpha = 0.4, \alpha_2 = 0.5, B_r = 1.5, S_T = 0.7, S_H = 0.5$	105
7.20	Streamlines pattern for multisinusoidal wave $Z = 0.23, \epsilon = 0.01, \alpha_1 = 0.22, \alpha = 0.4, \alpha_2 = 0.5, B_r = 1.5, S_T = 0.7, S_H = 0.5$	105
7.21	Streamlines pattern for Trapizoidal $Z = 0.23, \epsilon = 0.01, \alpha_1 = 0.22, \alpha = 0.4, \alpha_2 = 0.5, B_r = 1.5, S_T = 0.7, S_H = 0.5$	105

Symbols

U, V	Velocity components
λ	Wavelength
b	Wave amplitude
c_1	Wave speed
t	Time
p	Pressure
ρ	Density
g	Gravity
α	Thermal diffusivity
B_0	Magnetic field
ϕ	Amplitude ratio
ϵ_1	Relaxation time
ϵ_2	Delay time
τ	Stress tensor
B	Biot number
N_t	Thermospheres parameter
G_r	Grashof number
N_b	Brownian motion number
a_1	Radius of the inner tube
a_2	Radius of the outer tube
C_p	Specific heat
D_B	Brownian diffusion coefficient
M	Hartman number
Q_0	Heat absorption parameter
N_u	Nusselt number

P	Pressure
P_r	Prandtl number
Re	Reynold number
T	Temperature of the fluid
T_0	Temperature of the inner tube
T_1	Temperature of the outer tube
b, c, d	Material constant
E_c	Eckert number
R, Z	Cylindrical coordinates
B_κ	Brinkman number
n	Power law index
S_H	Schmidth number
S_T	Soret number
We	Weissenberg number
Q	Volume flow rate
ξ	length of cilia tips
δ	Eccentricity of path
γ	Ratio
δ	Wave number
$\alpha, \alpha_1, \alpha_2$	Jeffrey six-constant parameter

Acknowledgement

Thanks to Gracious Almighty Allah, who bestowed me with divine privilege and potency to complete this work.

I wish to express my warmest, sincerest thanks and profound gratitude to my supervisor, **Dr. Shafqat Hussain** and co supervisor **Prof. Sohail Nadeem**. It was because of their inspiring guidance, consistent encouragement, sympathetic attitude and dynamics supervision during the entire study programme, that I was able to prepare this work.

I am grateful to respected Head of department of Mathematics **Dr. Muhammad Sagheer** for providing us proper atmosphere to complete the research work.

I would like special thanks to my elder brothers **Shahzad Naveed** and **Nasir Naveed** for their moral support and guidance.

I would like to acknowledge my friends and class fellows **Hina Sadaf, Shugufta Ijaz, Iqra Shahzadi, Muhammad Bilal, Khalid Mehmood , Yasir Mehmood** for their moral support and help during my reasrch work.

It would have been impossible for me to accomplish this study without the incredible support of my parents. My special thanks goes to my sisters **Dr. Nusrat Shaheen, Zile-e-Huma and Dr. Anila Qadir** for being such a nice sisters and for their love and care. I would like special thanks to my caring and loving husband **Dr. Khadim Hussain Rai** for their moral support and guidance.

Aqila Shaheen

Abstract

In this thesis, we have investigated the peristaltic flow of Newtonian and non-Newtonian nanofluid flows in a channel, uniform and non-uniform tube. We have modelled and simplified the governing equations of such a fluid under the assumptions of long wave length and low Reynolds number approximation. The momentum equation is solved by utilizing the homotopy perturbation technique for velocity while the exact solutions are computed for temperature and concentration equations. The analysis depicts the impact of different situations such as endoscopic tube, magnetic field, convective boundary conditions and viscous dissipation in the flow of nanofluids induced by pressure gradient. The effects of different governing parameters on velocity and temperature fields are analyzed graphically for peristaltic waves. The physics of the involved parameters and important features of the modeled problems are discussed and analyzed with the help of streamlines and plots for various quantities.

Chapter 1

Introduction

A process of symmetrical contraction and expansion of progressive waves on the walls of the channel which mix and transport fluid in a channel is termed as peristalsis. In several procedures of physiology and engineering, peristaltic flow concerns are broadly encountered in channel or tube. The applications of peristalsis covers swallowing food through the esophagus, urine transportation from kidney to bladder, assessment of chyme in gastrointestinal tract, ovum movement in the female fallopian tube, vasomotion of narrow blood vessels, movement of spermatozoa in human reproductive tract and water movement from ground to above branches of grown-up trees [1–4].

Peristaltic flows have many biological and industrial applications such as blood pumps in heart, lung machines and transportation of mordant fluids. For the viscous fluids, Lithium and Sharpio [5] presented the earliest theoretical and experimental models for peristaltic transport. Peristalsis during male reproductive system was examined experimentally and numerically by Srivastava [6], Gupta [7], Guha [8] and Batra [9], where a peristaltic flow has been modelled in the vas deferens by considering it to be a non uniform tube. Many modern mechanical procedures have been investigated on the primary of the peristaltic pumping for transporting fluids without internal moving parts, for example, the blood pump in the heart, lung machine and the peristaltic transport of noxious fluid in the nuclear industry. It was also clarified that in the case of hyperthermia, the tissue can be destroyed when heated upto $42^0 - 45^0C$. A mathematical model of peristaltic hydromagnetic flow in a tube for the Johnson-Segalman fluid has been studied by Hayat and Ali [10]. Hydromagnetic flow of fluid in a uniform pipe with

variable thickness was investigated by Hakeem *et al.* [11]. Nadeem and Akbar [12] have studied the peristaltic wave of a non-Newtonian fluid in a non uniform inclined pipe. Peristaltic transportation of a non-Newtonian fluid in an inclined channel was discussed by Vajravelu *et al.* [13].

Another important field of research related to peristalsis is known as Cilia, are microscopic hair-like structures are found in almost all groups of the animal kingdom. The length of single cilium is 1 – 10 micrometers and width is about less than 1 micrometer. There are two types of cilia define as motile and non-motile cilia. A mathematical model for the flow of a Casson fluid due to metachronal beating of cilia in a tube has been presented by Ali *et al.* [14]. Gueron [15] has investigated the movement of the cilia, its modeling and the dynamics of multi tissue connection. Metachronal beating of cilia under the influence of Casson fluid and magnetic field has been analyzed by Akbar *et al.* [16]. Peristaltic flow of Carreau fluid in a rectangular duct through a porous medium was investigated by Ellahi *et al.* [17]. A model for the variation of viscous fluid due to ciliary motion in the ducts diffusive of male propagative tract has been investigated by Lardier and Shack [18]. Physiological breakdown of Carreau fluid due to ciliary motion has been discussed by Nadeem *et al.* [19]. The relations of cilia and its impulsion have achieved to a large extent by engineers and physicists [20, 21]. Numerical simulation of peristaltic flow of a Carreau nanofluid in an asymmetric channel have been discussed by Akbar *et al.* [22]. Further studies relating to the sort of ciliary motion have been found in Refs. [23, 24].

Fluids can be characterized into Newtonian and non-Newtonian fluids, Newtonian fluids are those in which the local stress is linearly proportional to the local strain. Some examples of Newtonian fluids are water, mineral oil, gasoline, alcohol, kerosene, organic solvents, glycerin, etc. The fluids similar to condensed milk, tomato paste, soup, sugar solution and shampoos cannot be distinguished from the Newtons law of viscosity. Such fluids collapse in the class of non-Newtonian fluids. The study of peristaltic flows of non-Newtonian fluids are also important field of research and has attracted the attention of many researchers. The non-Newtonian fluids cannot be examined through one constitutive equation because of their diverse rheological properties. Different models of non-Newtonian fluids have been established, which are named as, Pseudoplastic, Dilatant, Bingham, Casson, Herschel-Bulkley and Jeffrey six-constant models. Viscoelastic

fluids are such fluids that explains limited elastic improvement that lead to the exclusion of a deforming stress. These fluids possess properties of both elastic solids and viscous fluids. Non-Newtonian fluids are classified and introduced on the basis of their rheological properties. Study of peristaltic flow of Newtonian and non-Newtonian fluids with various flow geometries have been reported by many researcher such as [25, 26]. Jeffrey six-constant fluid model [27] is a theoretically complicated non-Newtonian fluid model of differential type which exhibits many properties and applications. More recently, the study of convective heat transfer in nanofluids have great achievement and success due to its wide application in various industrial processes.

The study of endoscope is another useful area of research in peristaltic mechanism. Basically, endoscope is very essential instrument used for determining actual reasons for many problems in human organs in which the fluids are moving by peristaltic pumping such as, stomach, small intestine, etc. Also, there are no differentiation between endoscope and a catheter in a fluid dynamics. Further more, the use of a catheter in an artery causes the change of the flow field and manage the pressure circulation accordingly. Akbar *et al.* [28] ware discussed the endoscopic effects with entropy generation analysis in peristalsis for the thermal conductivity of $H_0 + Cu$ (copper) nanofluids. Effects of an endoscope and generalized Newtonian fluid on peristaltic motion were investigated by Hakeem *et al.* [29]. Mekheimer *et al.* [30] have studied the peristaltic transport of a particle fluid suspension through a uniform and non-uniform annulus. Physiological breakdown of Jeffrey six-constant nanofluid flow in an endoscope with non-uniform wall have been discussed by Nadeem *et al.* [31]. In another study, Nadeem *et al.* [32] have discussed the effects of induced magnetic field on peristaltic flow of Jeffrey six-constant fluid in a vertical symmetric channel .

The rate of heat transfer is dependent on the temperatures of the systems and the properties of the prevailing medium through which the heat is transferred. Different authors have discussed [33, 34] the effect of force on the heat convection and mass transfer. Three different types of heat transfer are conduction, convection and radiation. Convection is defined as the transfer of heat by the movement of molecules of fluid from hot place to cold place or by the bulk motion of fluid. Conduction is the flow of heat through liquids and solids by the collision and vibration of free electronics molecules. In other words, the transfer of heat from one body to another body due to the only

collision of molecules which are in contact is called conduction. Radiation is that process in which heat is transferred directly by electromagnetic radiations. In liquids and gases, convection and radiation play very important role in the transfer of heat but in solids convection is totally absent and radiation is usually negligible. Thus for solid materials conduction play major role in the transfer of heat. Vajravelu *et al.* [35] have analyzed the peristaltic flow and heat transfer in a vertical porous annulus with long wave approximation. The heat transfer over an unsteady stretching surface with variable heat flux in the presence of a heat source or sink has been discussed by Vajravelu *et al.* [36]. Manca [37] numerically analyzed the forced convection flow of nanofluid in a ribbed channel. Akbar *et al.* [38] have analyzed the heat transfer on physiological driven movement with CNT and variable viscosity in the flow of nanofluids. Few recent studies on peristaltic flow through heat transport have been found in Refs. [39, 40].

Study of peristaltic flow in the presence of magnetic field has also achieved a lot of importance in daily life and engineering sciences. Some previous papers dealing with MHD flows of peristaltic are discussed [41–43]. Effects of MHD on the peristaltic flows for different modes of heat transfer like conduction, convection and radiations are reported in the Refs. [44–48]. For other studies regarding MHD flows, are can consult the Refs. [49–51].

Since the first investigation done by the Choi [52], the study of nanofluids have attracted the attention of many researchers due to its tremendous applications in various fields of life such as biomedical devices, treatment of tumor, nuclear reactor, microchips, cooling, radiators and nanomedicines etc. Only few researches are available on the peristaltic flows of nanofluids (see [53–58]).

1.1 Thesis contribution

The present thesis investigates the peristaltic flows of Jeffrey six-constant fluid, Sisko fluid and Carreau fluid for different flow geometries. We have presented the modelling of various non-Newtonian fluids, simplifications and the analytical solutions of the modelled problems. The physical features of various pertinent parameters are also discussed with the help of streamlines and plots for various quantities.

1.2 Scheme of the thesis

This thesis consists of further seven chapters shortly described as:

Chapter 2: In this chapter, we have examined the endoscopic effects of peristaltic flow of Jeffrey six-constant fluid model in the presence of magnetohydrodynamics. The effect of convective heat transfer and nanoparticles are also taken into account. The governing equations of non-Newtonian fluid along with heat and nanoparticles are modelled and simplified by using low Reynolds number and long wavelength assumptions. The velocity equation is solved by utilizing the homotopy perturbation technique while the exact solutions are computed for temperature and concentration equations. The obtained expressions for the velocity, temperature and nanoparticles concentration profiles are plotted and the impact of various physical parameters are investigated for different peristaltic waves. The contents of this chapter are published in the international journal AIP advances.

Chapter 3: This chapter deals with the simulation of mixed convection flow for physiological breakdown of Jeffrey six-constant fluid in an inclined tube. Influence of convective boundary conditions are also examined. The governing equations of non-Newtonian fluid along with heat are modelled and simplified by using low Reynolds number and long wavelength assumptions. The velocity equation is solved by utilizing the homotopy perturbation technique while the exact solutions are computed for temperature equations. The obtained expressions for the velocity and temperature profiles are plotted and the impact of various physical parameters are investigated for different peristaltic waves. The contents of this chapter are published in Bulletin of the polish Academy of Science.

Chapter 4: This chapter deals with the peristaltic flow of sisko fluid with convective boundary conditions in a uniform tube. The effects of viscous dissipation are also taken into account. The governing equations of non-Newtonian fluid along with heat and nanoparticles are modelled and simplified by using low Reynolds number and long wavelength assumptions. The velocity equation is solved by utilizing the homotopy perturbation technique while the exact solutions are computed for temperature and concentration equations. The solutions depend on Brikman number B_κ and magnetohydrodynamics M . The obtained expressions for the velocity, temperature and concentration profiles

are plotted and the impact of various physical parameters are investigated for different peristaltic waves.

Chapter 5: This chapter deals with the physiological flow of Carreau fluid due to ciliary motion inside a symmetric channel. The main purpose of this chapter is to present a mathematical model of ciliary motion in an annulus. In this analysis, the symmetric channel of a non-Newtonian fluid is observed in an annulus with ciliated tips. The governing equations of non-Newtonian fluid are modelled and simplified by using low Reynolds number and long wavelength assumptions. The velocity equation is solved by utilizing the homotopy perturbation technique in terms of a variant of small dimensionless parameter p . The obtained expressions for the velocity profiles are plotted and the impact of different physical parameters are investigated for different peristaltic waves. The contents of this chapter are published in AIP advances.

Chapter 6: In this chapter, deals with the mathematical model of ciliary motion in an annulus. The effect of convective heat transfer and nanoparticle are taken into account. The governing equations of Jeffrey six-constant fluid along with heat and nanoparticle are modelled and then simplified by using long wavelength and low Reynolds number assumptions. The reduced equations are solved with the help of homotopy perturbation method. The obtained expressions for the velocity, temperature and nanoparticles concentration profiles are plotted and the impact of various physical parameters are investigated for different peristaltic waves. Streamlines has also been plotted at the last part of the chapter. The contents of this chapter are sketched for publication in Brazilian society of mechanical science and engineering

Chapter 7: In this chapter deals with the peristaltic motion of non-Newtonian Jeffrey six-constant fluid is observed in an annulus with ciliated tips under the effect of heat and mass transfer. The effects of viscous dissipation are also taken into account. The governing equations of non-Newtonian fluid along with heat and nanoparticles are modelled and simplified by using low Reynolds number and long wavelength assumptions. The velocity equation is solved by utilizing the perturbation technique while the exact solutions are computed for temperature and concentration equations. The solutions depend on birkman number, soret number and schmidth number. The obtained expressions for the velocity, temperature and nanoparticles concentration profiles are

plotted and the impact of various physical parameters are investigated for different peristaltic waves. The contents of this chapter are published in communication in theoretical physics (CTP).

Chapter 8: Here, we summarize the thesis and give the major conclusion occurring from the entire research and recommendations for the future work.

Chapter 2

Physiological breakdown of Jeffrey six-constant nanofluid flow in an endoscope with nonuniform wall

This chapter deals with the physiological breakdown of Jeffrey six-constant nanofluid flow under the effect of endoscopes tube. The effect of convective heat transfer and nanoparticles are also taken into account. The governing equations of non-Newtonian fluid along with heat and nanoparticles are modelled and simplified by using low Reynolds number and long wavelength assumptions. The velocity equation is solved by utilizing the homotopy perturbation technique while the exact solutions are computed for temperature and concentration equations. The solutions depend on thermophoresis number N_t , local nanoparticles Grashof number G_r and Brownian motion number N_b . The obtained expressions for the velocity, temperature and nanoparticles concentration profiles are plotted and the impact of various physical parameters are investigated for different peristaltic waves.

2.1 Problem Formulation

We are taking into account the peristaltic nanofluid flow of an incompressible six-constant Jeffrey fluid in a non-uniform vertical tube. The flow is generated by sinusoidal wave trains propagating with constant speed c_1 along the wall of the tube. Heat transfer along with nanoparticle phenomena has been taken into account. The inner tube is rigid and is maintained at temperature T_0 while the outer tube has a sinusoidal wave traveling down its walls and is maintained at temperature T_1 . The geometry of the wall surfaces is shown in Figure 2.1 and mathematically defined as

$$\bar{R}_1 = a_1, \quad (2.1)$$

$$\bar{R}_2 = a_2 + b \sin \left[\frac{2\pi}{\lambda} (\bar{Z} - c_1 \bar{t}) \right], \quad (2.2)$$

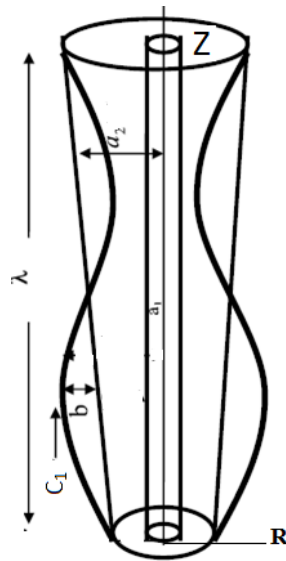


FIGURE 2.1: Geometry of the problem.

where a_1 is the radius of the inner tube, a_2 is the radius of the outer tube at inlet, λ is the wavelength, b is the wave amplitude and c_1 is the wave speed. We consider the cylindrical coordinate system (\bar{R}, \bar{Z}) in such a way that R is taken along the radial direction and \bar{Z} is the axial direction.

The governing equations for a two dimensional and incompressible Jeffrey six-constant

fluid model can be written as

$$\frac{\partial \bar{U}}{\partial \bar{R}} + \frac{\bar{U}}{\bar{R}} + \frac{\partial \bar{W}}{\partial \bar{Z}} = 0, \quad (2.3)$$

$$\rho \left(\frac{\partial}{\partial \bar{t}} + \bar{U} \frac{\partial}{\partial \bar{R}} + \bar{W} \frac{\partial}{\partial \bar{Z}} \right) \bar{U} = -\frac{\partial \bar{P}}{\partial \bar{R}} + \frac{1}{\bar{R}} \frac{\partial}{\partial \bar{R}} (\bar{R} \bar{\tau}_{\bar{R}\bar{R}}) + \frac{\partial}{\partial \bar{Z}} (\bar{\tau}_{\bar{R}\bar{Z}}) + \frac{\bar{\tau}_{\bar{\theta}\bar{\theta}}}{\bar{R}}, \quad (2.4)$$

$$\begin{aligned} \rho \left(\frac{\partial}{\partial \bar{t}} + \bar{U} \frac{\partial}{\partial \bar{R}} + \bar{W} \frac{\partial}{\partial \bar{Z}} \right) \bar{W} &= -\frac{\partial \bar{P}}{\partial \bar{Z}} + \frac{1}{\bar{R}} \frac{\partial}{\partial \bar{R}} (\bar{R} \bar{\tau}_{\bar{R}\bar{Z}}) + \frac{\partial}{\partial \bar{Z}} (\bar{\tau}_{\bar{Z}\bar{Z}}) \\ &+ \rho g \alpha (\bar{T} - \bar{T}_0) + \rho g \alpha (\bar{C} - \bar{C}_0) - \sigma B_0^2 \bar{W}, \end{aligned} \quad (2.5)$$

$$\begin{aligned} \left(\frac{\partial}{\partial \bar{t}} + \bar{U} \frac{\partial}{\partial \bar{R}} + \bar{W} \frac{\partial}{\partial \bar{Z}} \right) \bar{T} &= \alpha \left(\frac{\partial^2 \bar{T}}{\partial \bar{R}^2} + \frac{1}{\bar{R}} \frac{\partial \bar{T}}{\partial \bar{R}} + \frac{\partial^2 \bar{T}}{\partial \bar{Z}^2} \right) \\ &+ \tau \left[D_B \left(\frac{\partial \bar{C}}{\partial \bar{R}} \frac{\partial \bar{T}}{\partial \bar{R}} + \frac{\partial \bar{C}}{\partial \bar{Z}} \frac{\partial \bar{T}}{\partial \bar{Z}} \right) + \frac{D_{\bar{T}}}{\bar{T}_0} \left(\left(\frac{\partial \bar{T}}{\partial \bar{R}} \right)^2 + \left(\frac{\partial \bar{T}}{\partial \bar{Z}} \right)^2 \right) \right], \end{aligned} \quad (2.6)$$

$$\begin{aligned} \left(\frac{\partial}{\partial \bar{t}} + \bar{U} \frac{\partial}{\partial \bar{R}} + \bar{W} \frac{\partial}{\partial \bar{Z}} \right) \bar{C} &= D_B \left(\frac{\partial^2 \bar{C}}{\partial \bar{R}^2} + \frac{1}{\bar{R}} \frac{\partial \bar{C}}{\partial \bar{R}} + \frac{\partial^2 \bar{C}}{\partial \bar{Z}^2} \right) \\ &+ \frac{D_{\bar{T}}}{\bar{T}_0} \left(\frac{\partial^2 \bar{T}}{\partial \bar{R}^2} + \frac{1}{\bar{R}} \frac{\partial \bar{T}}{\partial \bar{R}} + \frac{\partial^2 \bar{T}}{\partial \bar{Z}^2} \right), \end{aligned} \quad (2.7)$$

where $\tau = \frac{(\rho c)_p}{(\rho c)_f}$ is the ratio among the efficient heat capacity of the nanoparticle material and the heat capacity of the fluid. The transformations between the two frames are

$$\bar{r} = \bar{R}, \quad \bar{z} = \bar{Z} - c_1 \bar{t}, \quad (2.8)$$

$$\bar{u} = \bar{U}, \quad \bar{w} = \bar{W} - c_1. \quad (2.9)$$

The corresponding boundary conditions are defined as

$$\bar{w} = -c_1, \quad \bar{T} = \bar{T}_0, \quad \bar{C} = \bar{C}_0, \quad \text{at} \quad \bar{r} = \bar{r}_1, \quad (2.10)$$

$$\bar{w} = -c_1, \quad \bar{T} = \bar{T}_1, \quad \bar{C} = \bar{C}_1, \quad \text{at} \quad \bar{r} = \bar{r}_2 = a_2 + b \sin \left[\frac{2\pi}{\lambda} (\bar{Z} - c_1 \bar{t}) \right]. \quad (2.11)$$

The constitutional equation for a Jeffrey six-constant fluid is defined as [32]

$$\begin{aligned} \tau + \epsilon_1 \left[\frac{d\bar{\tau}}{dt} - W \cdot \bar{\tau} + \bar{\tau} \cdot W + d(\bar{\tau} \cdot D + D \cdot \bar{\tau}) + b\bar{\tau} : DI + cDtr\bar{\tau} \right] \\ = 2\mu \left[D + \epsilon_2 \left(\frac{dD}{dt} - W \cdot D + D \cdot W + 2dD \cdot D + bD : DI \right) \right]. \end{aligned} \quad (2.12)$$

Here

$$\begin{aligned} \text{D(symmetric measurement of velocity gradient)} &= \frac{\nabla\bar{V} + (\nabla\bar{V})^{t_1}}{2}, \\ \text{W(antisymmetric measurement of velocity gradient)} &= \frac{\nabla\bar{V} - (\nabla\bar{V})^{t_1}}{2}. \end{aligned}$$

Introducing the following non-dimensional variables

$$\begin{aligned} R &= \frac{\bar{R}}{a_2}, \quad r = \frac{\bar{r}}{a_2}, \quad r_1 = \frac{\bar{r}_1}{a_2} = \epsilon, \quad Z = \frac{\bar{Z}}{\lambda}, \quad z = \frac{\bar{z}}{\lambda}, \quad W = \frac{\bar{W}}{c_1}, \quad w = \frac{\bar{w}}{c_1}, \quad \tau = \frac{a\bar{\tau}}{c\mu_0}, \\ U &= \frac{\lambda\bar{U}}{a_2c_1}, \quad u = \frac{\lambda\bar{u}}{a_2c_1}, \quad t = \frac{c_1\bar{t}}{\lambda}, \quad p = \frac{a_2^2\bar{p}}{c_1\lambda\mu}, \quad \lambda_1 = \frac{\epsilon_1c_1}{a_2}, \quad \lambda_2 = \frac{\epsilon_2c_1}{a_2}, \\ R_e &= \frac{\rho a_2 c_1}{\mu}, \quad E_c = \frac{c^2}{C_p T_0}, \quad \delta = \frac{a}{\lambda}, \quad r_2 = \frac{\bar{r}_2}{a_2} = 1 + \frac{\lambda k z}{a_2} + \phi \sin 2\pi z, \quad P_r = \frac{\nu}{\alpha}, \\ \theta &= \frac{(\bar{T} - \bar{T}_1)}{(\bar{T}_0 - \bar{T}_1)}, \quad \alpha = \frac{k}{(\rho c)_f}, \quad N_b = \frac{(\rho c)_p D_B (\bar{C}_0 - \bar{C}_1)}{(\rho c)_f}, \quad M = \sqrt{\frac{\sigma}{\mu}} B_0 a^2, \\ B_r &= \frac{g \alpha a_2^3 (\bar{C}_0 - \bar{C}_1)}{\nu^2}, \quad N_t = \frac{(\rho c)_p D_T (\bar{C}_0 - \bar{C}_1)}{(\rho c)_f \alpha}, \quad \sigma = \frac{(\bar{C} - \bar{C}_1)}{(\bar{C}_0 - \bar{C}_1)}. \end{aligned}$$

With the help of Eqs. (2.8) and (2.9), Eqs. (2.3)-(2.7) under the assumption of low Reynolds number and long wavelength $\delta \ll 1$ take the form

$$0 = -\frac{\partial p}{\partial z} + \frac{1}{r} \frac{\partial}{\partial r} (r \tau_{rz}) + G_r \theta + B_r \sigma - M^2 (w + 1), \quad (2.13)$$

$$0 = \frac{\partial p}{\partial r}, \quad (2.14)$$

$$0 = \frac{1}{r} \frac{\partial}{\partial r} \left(r \frac{\partial \theta}{\partial r} \right) + N_b \frac{\partial \theta}{\partial r} \frac{\partial \sigma}{\partial r} + N_t \left(\frac{\partial \theta}{\partial r} \right)^2, \quad (2.15)$$

$$0 = \frac{1}{r} \frac{\partial}{\partial r} \left(r \frac{\partial \sigma}{\partial r} \right) + \frac{N_t}{N_b} \left(\frac{1}{r} \frac{\partial}{\partial r} \left(r \frac{\partial \theta}{\partial r} \right) \right). \quad (2.16)$$

The corresponding boundary conditions are reduced as

$$w = -1, \quad \theta = 1, \quad \sigma = 1, \quad \text{at} \quad r = r_1 = \epsilon,$$

$$w = -1, \quad \theta = 0, \quad \sigma = 0, \quad \text{at} \quad r = r_2 = 1 + \frac{\lambda k z}{a_2} + \phi \sin 2\pi z.$$

With the help of Eqs. (2.8) and (2.9), Eq. (2.12) under the assumption of low Reynolds number and long wavelength $\delta \ll 1$ take the form

$$\tau_{rz} = \frac{\frac{\partial w}{\partial r} \left[1 + \lambda_1 \lambda_2 (1 - d(d+b) - \frac{c}{2}(2d+3b)) \left(\frac{\partial w}{\partial r} \right)^2 \right]}{\left[1 + \lambda_1^2 (1 - d(d+b) - \frac{c}{2}(2d+3b)) \left(\frac{\partial w}{\partial r} \right)^2 \right]}.$$

Finally, in simplified form Eq. (2.13) can be written as

$$\frac{\partial p}{\partial r} = 0, \quad (2.17)$$

$$\begin{aligned} \frac{\partial p}{\partial z} &= \frac{1}{r} \frac{\partial}{\partial r} \left(r \frac{\partial w}{\partial r} \right) + \frac{1}{r} \frac{\partial}{\partial r} \left(\alpha \alpha_1 r \left(\frac{\partial w}{\partial r} \right)^3 \right) \\ &\quad + \frac{1}{r} \frac{\partial}{\partial r} \left(\alpha^2 \alpha_2 r \left(\frac{\partial w}{\partial r} \right)^5 \right) + G_r \theta + B_r \sigma - M^2(w + 1), \end{aligned} \quad (2.18)$$

$$0 = \frac{1}{r} \frac{\partial}{\partial r} \left(r \frac{\partial \theta}{\partial r} \right) + N_b \frac{\partial \theta}{\partial r} \frac{\partial \sigma}{\partial r} + N_t \left(\frac{\partial \theta}{\partial r} \right)^2, \quad (2.19)$$

$$0 = \frac{1}{r} \frac{\partial}{\partial r} \left(r \frac{\partial \sigma}{\partial r} \right) + \frac{N_t}{N_b} \left(\frac{1}{r} \frac{\partial}{\partial r} \left(r \frac{\partial \theta}{\partial r} \right) \right). \quad (2.20)$$

The boundary conditions are reduced as

$$\begin{aligned} w = -1, \quad \theta = 1, \quad \sigma = 1, \quad \text{at} \quad r = r_1 = \epsilon, \\ w = -1, \quad \theta = 0, \quad \sigma = 0, \quad \text{at} \quad r = r_2 = 1 + \frac{\lambda k z}{a_2} + \phi \sin 2\pi z. \end{aligned}$$

2.2 Solution of the problem

2.2.1 Exact Solution

The exact solutions for the temperature and the nanoparticle concentration satisfying the relative boundary conditions are directly written as

$$\theta(r, z) = \frac{g_3(z)}{g_1(z) N_b} + \frac{g_4(z)}{r g_1(z) N_b}, \quad (2.21)$$

$$\sigma(r, z) = -\frac{N_t}{N_b} \left[g_5(z) + g_4(z) r^{-g_1(z) N_b} \right] + g_1(z) \ln r + g_2(z), \quad (2.22)$$

where

$$\begin{aligned}
 g_1 &= \frac{1 + \frac{N_t}{N_b}}{\ln r_1 - \ln r_2}, & g_2 &= \frac{\ln r_2 \left(1 + \frac{N_t}{N_b}\right)}{\ln r_2 - \ln r_1}, \\
 g_3 &= \frac{r_1^{\frac{N_b \left(1 + \frac{N_t}{N_b}\right)}{\ln r_1 - \ln r_2}} (N_b + N_t)}{\left(r_1^{\frac{N_b \left(1 + \frac{N_t}{N_b}\right)}{\ln r_1 - \ln r_2}} - r_2^{\frac{N_b \left(1 + \frac{N_t}{N_b}\right)}{\ln r_1 - \ln r_2}} \right) (\ln r_1 - \ln r_2)}, \\
 g_4 &= -\frac{r_1^{\frac{N_b \left(1 + \frac{N_t}{N_b}\right)}{\ln r_1 - \ln r_2}} r_2^{\frac{N_b \left(1 + \frac{N_t}{N_b}\right)}{\ln r_1 - \ln r_2}}}{\left(r_1^{\frac{N_b \left(1 + \frac{N_t}{N_b}\right)}{\ln r_1 - \ln r_2}} - r_2^{\frac{N_b \left(1 + \frac{N_t}{N_b}\right)}{\ln r_1 - \ln r_2}} \right)}, & g_5 &= \frac{g_3}{g_1 N_b}.
 \end{aligned}$$

2.2.2 Homotopy Perturbation Method

The grouping of the perturbation method and homotopy analysis is called homotopy perturbation method (HPM) (an analytical technique), which eliminates fixed perturbation method while maintaining all their advantages.

We apply the homotopy perturbation method for solving the above problems. To illustrate the basic idea of the method, we consider the following nonlinear differential equation

$$A(u) - f(r) = 0, \quad (2.23)$$

with the boundary condition of

$$B\left(u, \frac{\partial u}{\partial n}\right) = 0, \quad (2.24)$$

where $A(u)$ is defined as follows

$$A(u) = L(u) + N(u). \quad (2.25)$$

Homotopy perturbation structure is given as

$$H(v, p) = L(v) - L(u_0) + pL(u_0) + p[N(v) - f(r)], \quad (2.26)$$

or

$$H(v, p) = (1 - p)[L(v) - L(u_0)] + p[A(v) - f(r)] = 0, \quad (2.27)$$

where

$$v(v, p) : \Omega \times [0, 1] \longrightarrow \mathcal{R}, \quad (2.28)$$

obviously considering Eqs. (2.26) and (2.27) we have

$$H(v, 0) = L(v) - L(u_0) = 0, \quad (2.29)$$

$$H(v, 1) = A(v) - f(r) = 0, \quad (2.30)$$

where $p \in [0, 1]$ is an embedding parameter and u_0 is the first approximation that satisfies the boundary condition.

$$v = v_0 + pv_1 + p^2v_2, \quad (2.31)$$

and the best approximation is $p = 1$

$$v = v_0 + v_1 + v_2. \quad (2.32)$$

We use homotopy perturbation method to solve the Eq. (2.18)

$$\begin{aligned} H(q, w) = & L(w) - L(w_{10}) + qL(w_{10}) + q \left[\frac{1}{r} \frac{\partial}{\partial r} \left(\alpha \alpha_1 r \left(\frac{\partial w}{\partial r} \right)^3 \right) \right. \\ & \left. + \frac{1}{r} \frac{\partial}{\partial r} \left(\alpha^2 \alpha_2 r \left(\frac{\partial w}{\partial r} \right)^5 \right) + G_r \theta + B_r \sigma - M^2(w + 1) - \frac{\partial p}{\partial z} \right]. \end{aligned} \quad (2.33)$$

We take linear operator $L = \frac{1}{r} \frac{\partial}{\partial r} (r \frac{\partial}{\partial r})$ and the following initial guess which satisfy the boundary conditions [27]

$$w_{10}(r, z) = -1 + p_0 \left[A \ln r + \frac{r^2}{4} + B \right]. \quad (2.34)$$

Let us define

$$w(r, q) = w_0 + qw_1 + q^2w_2 + q^3w_3 + \dots$$

Making use of above expression and using the similar procedure as discussed in [20], the expression for velocity profile can be written as

$$\begin{aligned} w = & -1 + \left(A_1 \ln[r] + \frac{r^2}{4} + A_2 \right) p + A_3 \frac{1}{r^4} \ln[r] + A_4 \frac{1}{r^2} \ln[r] \\ & + A_5 (r^5 \ln[r]) + A_6 (r^4 \ln[r]) + A_7 (r^6 \ln[r]) + A_8 (r^3 \ln[r]) \\ & + A_9 (r^2 \ln[r]) + A_{10} \ln[r] + A_{11}. \end{aligned} \quad (2.35)$$

where A_1, A_2, \dots, A_{11} are constants and given in Appendix 4. The expression for pressure gradient can be written as

$$\frac{dp}{dz} = \frac{16[F + A_{13}]}{A_{14}}. \quad (2.36)$$

Flow rate in dimensionless form can be written as

$$F = 2Q - \frac{\phi^2}{2} - 1 + \epsilon^2. \quad (2.37)$$

The expression for pressure rise Δp and friction forces (at the wall) on the inner and outer tubes are $F^{(0)}$ and $F^{(i)}$ in non-dimensional forms are defined as

$$\Delta p = \int_0^1 \left(\frac{dp}{dz} \right) dz, \quad (2.38)$$

$$F^{(0)} = \int_0^1 r_1^2 \left(-\frac{dp}{dz} \right) dz, \quad (2.39)$$

$$F^{(i)} = \int_0^1 r_2^2 \left(-\frac{dp}{dz} \right) dz. \quad (2.40)$$

Velocities streamfunction relation is defined as follow

$$u = -\frac{1}{r} \left(\frac{\partial \psi}{\partial z} \right), \quad w = \frac{1}{r} \left(\frac{\partial \psi}{\partial r} \right).$$

For the flow analysis, we have discussed three waveforms sinusoidal wave, trapezoidal wave and multisinusoidal wave. The dimensionless equations can be written as follows:

1. Sinusoidal wave

$$h(z) = 1 + \frac{\lambda kz}{a_0} + \phi \sin(2\pi z).$$

2. Multisinusoidal wave

$$h(z) = 1 + \frac{\lambda kz}{a_0} + \phi \sin(2m\pi z).$$

3. Trapezoidal wave

$$h(z) = 1 + \frac{\lambda kz}{a_0} + \phi \frac{32}{\pi^2} \sum_{n=1}^{\infty} \frac{\sin \frac{\pi}{8}(2n-1)}{(2n-1)^2} \sin(2\pi(2n-1)z).$$

The coefficient of heat transfer at the wall can be computed with the help of the expression $Z = h_z \theta_r$.

2.3 Results and discussions

In this section, we have discussed the solution for the peristaltic flow of Jeffrey six-constant nanofluid flow in an endoscope with diverging tube. The expressions for temperature, velocity, pressure rise, pressure gradient and streamlines are calculated numerically. Figures 2.2-2.3 show the variation in temperature profile for different values of brownian motion parameter (N_b) and thermophoresis parameter (N_t). Figure 2.2 depicts that the temperature profile increases by increasing the values of brownian motion parameter (N_b), due to increase in the collision between the particles which produces heat. Figure 2.3 depicts the influence of thermophoresis parameter (N_t) on temperature field. An increase in thermophoresis parameter results in the enhancement of temperature field. Physically, the thermophoresis parameter have a direct relation with temperature gradient. So if we increases the thermophoresis parameter (N_t), it means the temperature gradient rises, which is responsible for the resulting increase in temperature field.

Figure 2.4 describes the impact of brownian motion parameter (N_b) on concentration field. As the brownian motion parameter (N_b) is directly proportional to concentration gradient, an increase in brownian motion parameter (N_b) enhances the concentration field. Particles can diffuse under the effect of temperature gradient so increase in thermophoresis parameter (N_t) results in the reduction of concentration field which is exhibited through Figure 2.5. Figure 2.6 show that velocity profile gets increasing function in the region ($0.2 \leq r \leq 0.58$) whereas it get opposite behaviour in the rest of the region. The impact of magnetohydrodynamics (M) on velocity distribution is incorporated in

Figure 2.7. With an increase in magnetohydrodynamics the velocity profile decreases for $(0.2 \leq r \leq 0.58)$ and increases for $(0.6 \leq r \leq 1.0)$. As magnetohydrodynamics cause Lorentz forces, which are resistive forces, so an increase in magnetohydrodynamics leads to more resistance to the fluid resulting in reduction in fluid velocity.

Figures 2.8, 2.11 show the pressure rise (versus flow rate) for diverse values of α, r_1, M . In these figures, it is depicted that by increasing the value of α the pressure rise increases in the region $(Q \in [-3, 0.01])$ whereas reflux occurs in the last. The retrograde pumping region can also be seen in Figures 2.8, 2.11 when $Q < 0$ and $\Delta p > 0$ and free pumping region can be seen when $Q = 0$ and $\Delta p = 0$. Moreover, augmented pumping region can also be seen in figures 2.8, 2.11 when $Q > 0$ and $\Delta p < 0$. Figures 2.9, 2.10, 2.12, 2.13 show the frictional forces (inner and outer tube) for diverse values of α, r_1, M . From these figures, it is depicted that the inner and outer tube frictional forces have an opposite behaviour as compared to pressure rise. It is observed that the outer frictional forces are smaller than the inner frictional forces. Figures 2.14-2.16 describe the behaviour of pressure gradient for three different waveforms: sinusoidal, multisinusoidal, and trapezoidal waves. Figure 2.14 describes that increasing the value of ϕ the pressure gradient decreases in the region $(0 \leq Z \leq 0.5)$ and increases in the region $(0.6 \leq Z \leq 1)$ and reflux occurs in the region $(1.1 \leq Z \leq 1.5)$. Figures 2.15-2.16 show that the behaviour for different values of ϕ by considering the multisinusoidal wave and trapezoidal wave.

Figures 2.17-2.19 illustrate the streamlines for different wave shapes. When we move from sinusoidal wave to multisinusoidal the number of the trapped bolus increases. Figure 2.19 shows the pattern of streamlines for trapezoidal wave.

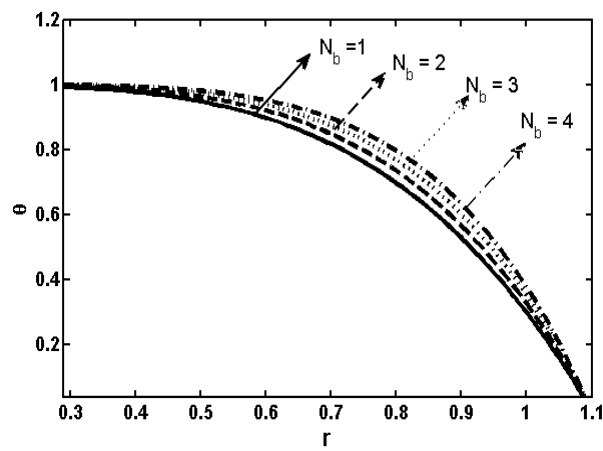


FIGURE 2.2: Variation of temperature for N_b when $N_t = 8$, $Z = 0.2$, $r_1 = 0.1$, $a_0 = 0.01$ and $\lambda = 0.1$, $\phi = 0.02$.

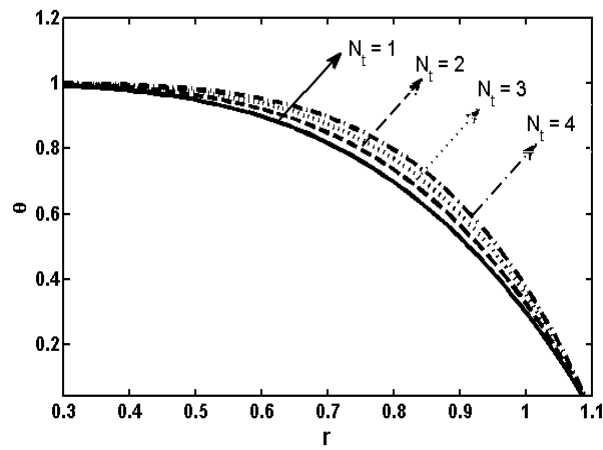


FIGURE 2.3: Variation of temperature for N_t when $N_b = 8$, $Z = 0.2$, $r_1 = 0.1$, $a_0 = 0.01$ and $\lambda = 0.1$, $\phi = 0.02$.

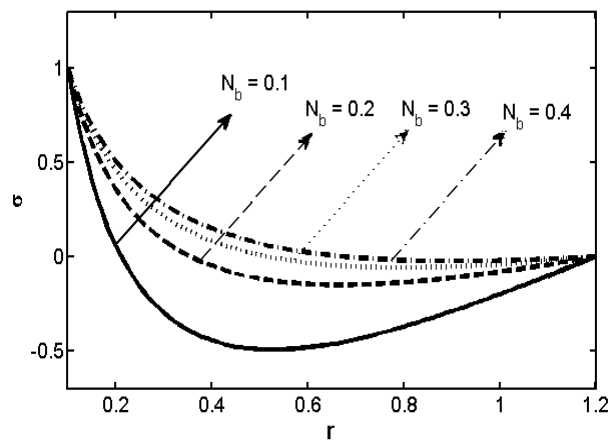


FIGURE 2.4: Variation of concentration for N_b when $N_t = 8$, $Z = 0.2$, $r_1 = 0.1$, $a_0 = 0.01$ and $\lambda = 0.1$, $\phi = 0.02$.

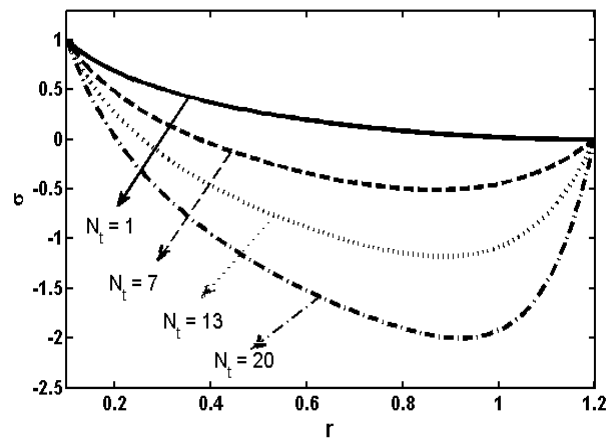


FIGURE 2.5: Variation of concentration for N_t when $N_b = 8$, $Z = 0.2$, $r_1 = 0.1$, $a_0 = 0.01$ and $\lambda = 0.1, \phi = 0.02$.

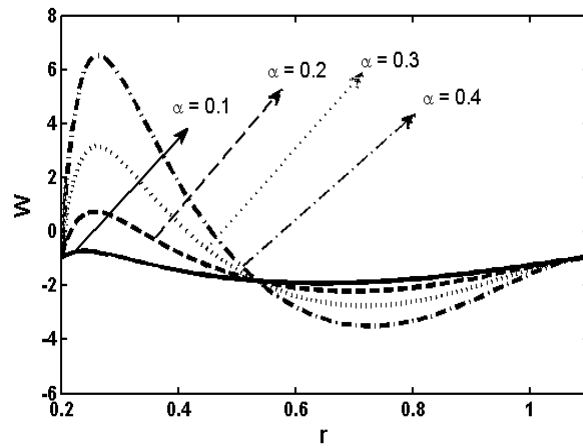


FIGURE 2.6: Variation of velocity for α when $N_t = 8$, $Z = 0.2$, $r_1 = 0.1$, $a_0 = 0.01$ and $\lambda = 0.1, \phi = 0.02$, $N_b = 8$, $\alpha_1 = 8$.

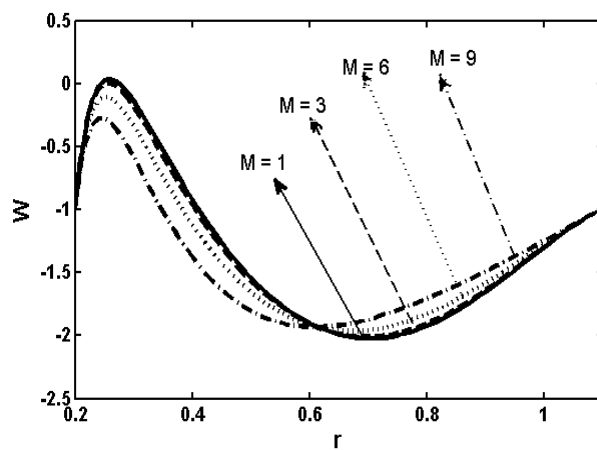


FIGURE 2.7: Variation of velocity for M when $N_t = 8$, $Z = 0.2$, $r_1 = 0.1$, $a_0 = 0.01$ and $\lambda = 0.1$, $\phi = 0.02$, $N_b = 8$, $\alpha_1 = 8$, $\alpha = 0.03$.

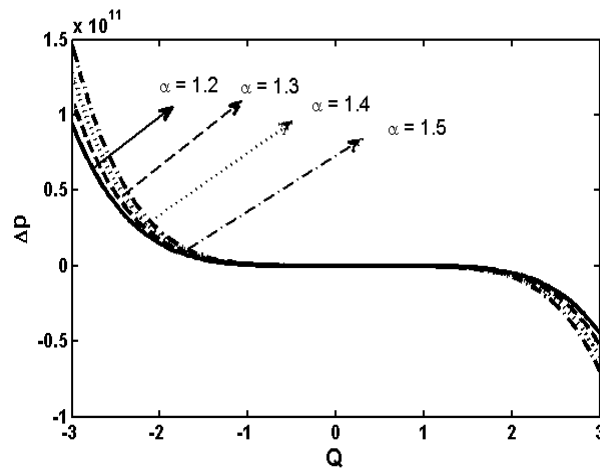


FIGURE 2.8: Variation of pressure rise for α when $N_t = 8$, $Z = 0.2$, $r_1 = 0.1$, $a_0 = 0.01$ and $\lambda = 0.1$, $\phi = 0.02$, $\alpha_1 = 8$, $M = 0.9$.

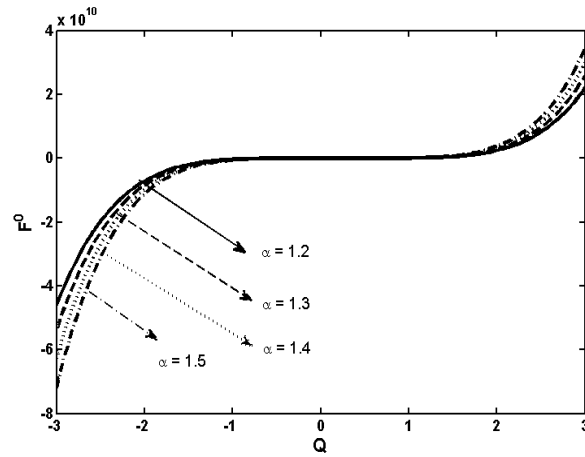


FIGURE 2.9: Variation of frictional force (inner tube) for α when $N_t = 8$, $Z = 0.2$, $r_1 = 0.1$, $a_0 = 0.01$ and $\lambda = 0.1$, $\phi = 0.02$, $\alpha_1 = 8$, $N_b = 0.03$, $M = 0.9$.

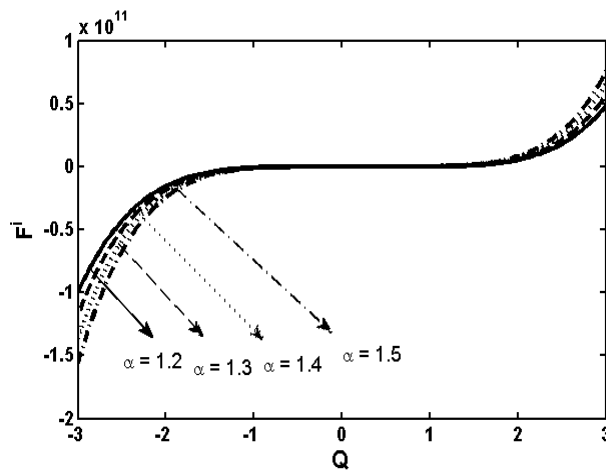


FIGURE 2.10: Variation of frictional force (outer tube) for α when $N_t = 8$, $Z = 0.2$, $r_1 = 0.1$, $a_0 = 0.01$ and $\lambda = 0.1$, $\phi = 0.02$, $\alpha_1 = 8$, $M = 0.9$.

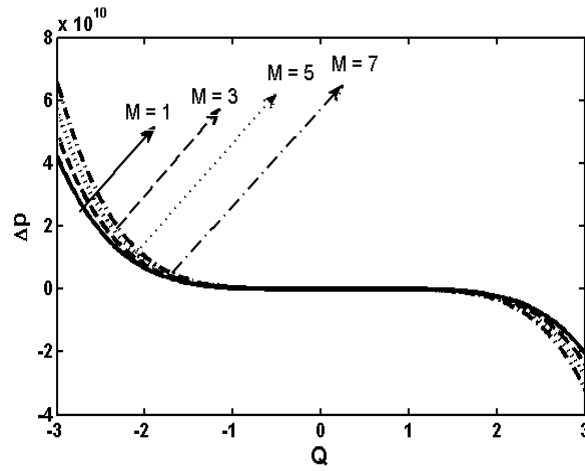


FIGURE 2.11: Variation of pressure rise for M when $N_t = 8$, $Z = 0.2$, $r_1 = 0.1$, $a_0 = 0.01$ and $\lambda = 0.1$, $\phi = 0.02$, $\alpha_1 = 8$, $\alpha = 0.03$, $N_b = 7$.

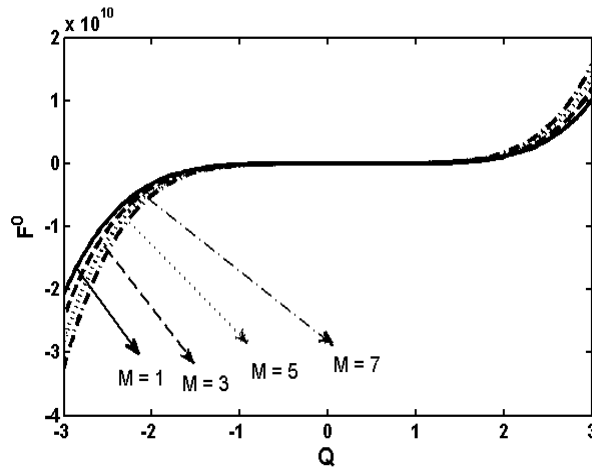


FIGURE 2.12: Variation of frictional force (inner tube) for M when $N_t = 8$, $Z = 0.2$, $r_1 = 0.1$, $a_0 = 0.01$ and $\lambda = 0.1$, $\phi = 0.02$, $\alpha_1 = 8$, $\alpha = 0.03$, $N_b = 7$.

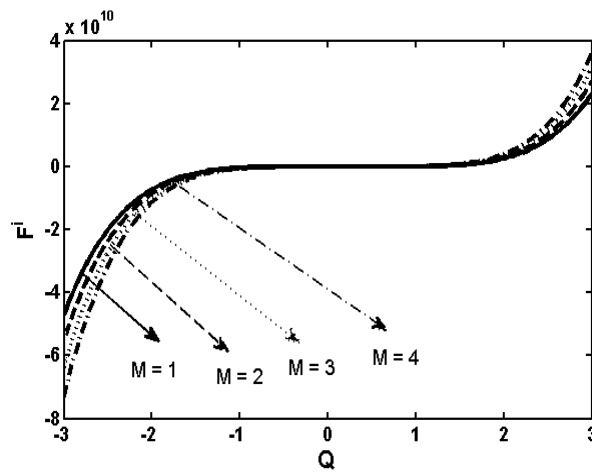


FIGURE 2.13: Variation of frictional force (outer tube) for M when $N_t = 8$, $Z = 0.2$, $r_1 = 0.1$, $a_0 = 0.01$ and $\lambda = 0.1$, $\phi = 0.02$, $\alpha_1 = 8$, $\alpha = 0.03$, $N_b = 7$.

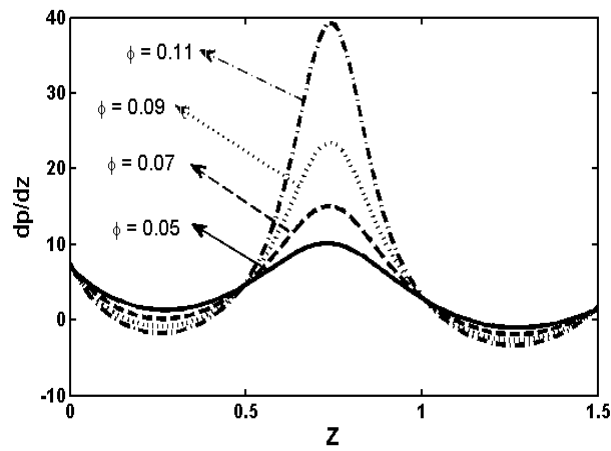


FIGURE 2.14: Pressure gradient $\frac{dp}{dz}$ for sinusoidal wave when $N_t = 8$, $Z = 0.2$, $r_1 = 0.1$, $a_0 = 0.01$ and $\lambda = 0.1$, $N_b = 7$, $\alpha_1 = 8$, $\alpha = 0.03$, $M = 0.9$.

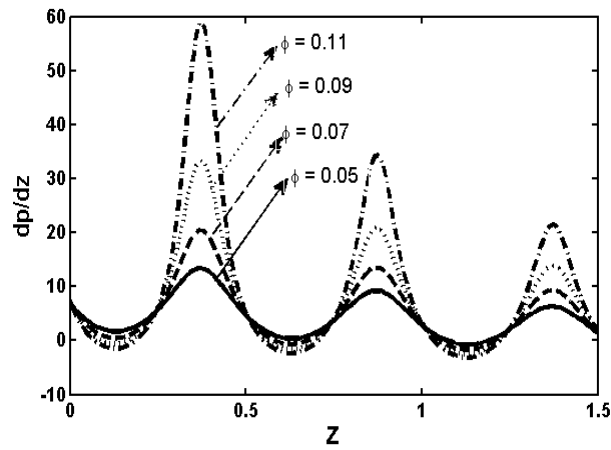


FIGURE 2.15: Pressure gradient $\frac{dp}{dz}$ for multisinusoidal wave when $N_t = 8$, $Z = 0.2$, $r_1 = 0.1$, $a_0 = 0.01$ and $\lambda = 0.1$, $N_b = 7$, $\alpha_1 = 8$, $\alpha = 0.03$, $M = 0.9$.

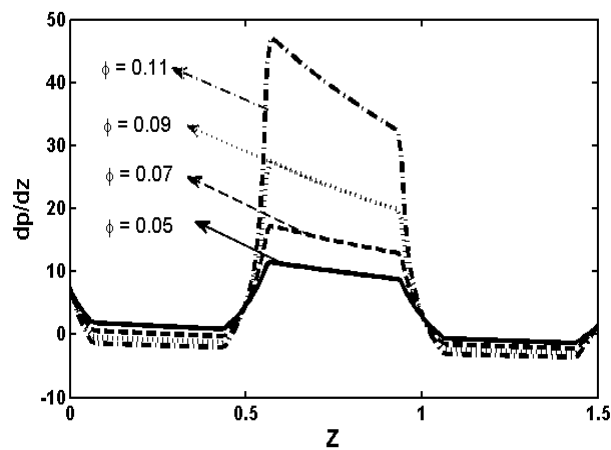


FIGURE 2.16: Pressure gradient $\frac{dp}{dz}$ for Trapezoidal wave when $N_t = 8$, $Z = 0.2$, $r_1 = 0.1$, $a_0 = 0.01$ and $\lambda = 0.1$, $N_b = 7$, $\alpha_1 = 8$, $\alpha = 0.03$, $M = 0.9$.

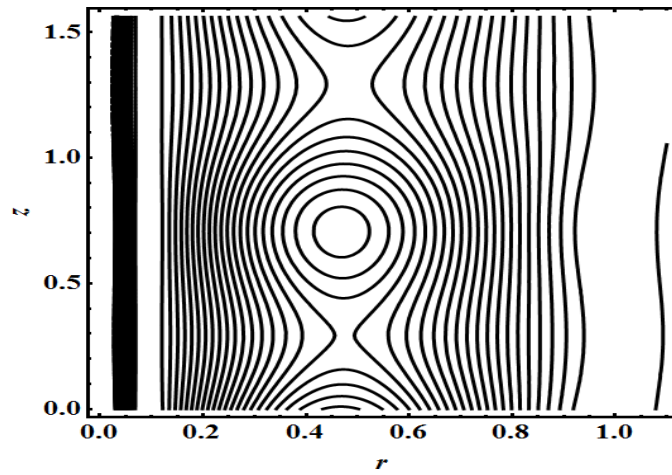


FIGURE 2.17: Streamlines pattern for sinusoidal wave when $N_t = 8$, $Z = 0.2$, $r_1 = 0.1$, $a_0 = 0.01$ and $\lambda = 0.1$, $\phi = 0.02$, $\alpha_1 = 8$, $\alpha = 0.03$, $M = 0.9$.

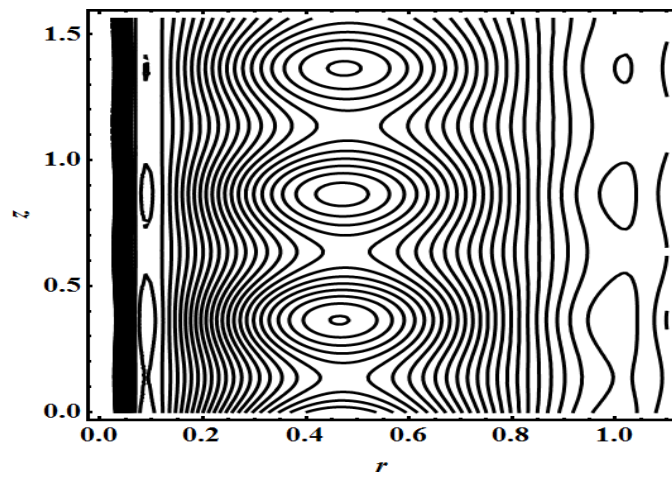


FIGURE 2.18: Streamlines pattern for multisinusoidal wave when $N_t = 8$, $Z = 0.2$, $r_1 = 0.1$, $a_0 = 0.01$ and $\lambda = 0.1$, $\phi = 0.02$, $\alpha_1 = 8$, $\alpha = 0.03$, $M = 0.9$.

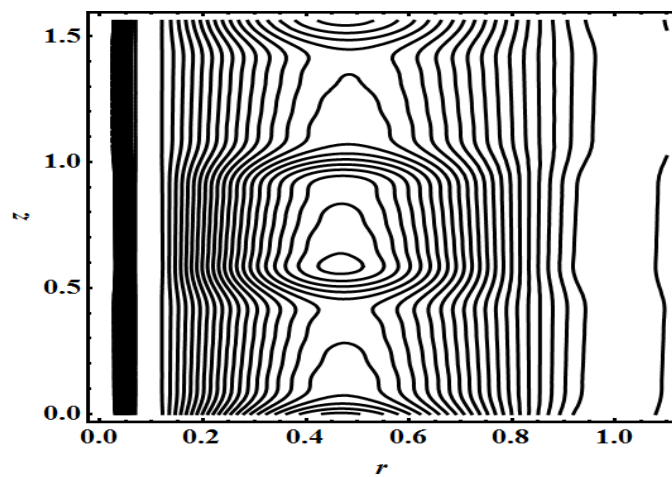


FIGURE 2.19: Streamlines pattern for Trapizoidal wave when $N_t = 8$, $Z = 0.2$, $r_1 = 0.1$, $a_0 = 0.01$ and $\lambda = 0.1$, $\phi = 0.02$, $\alpha_1 = 8$, $\alpha = 0.03$, $M = 0.9$.

2.4 Conclusion

In this chapter, we have analysed the physiological breakdown of Jeffrey six-constant nanofluid flow in an endoscope with diverging tube. The main findings of the present study are as follow:

- The temperature profile is enhanced for the increasing values of parameters N_t and N_b .
- The nanoparticle concentration field is enhanced for the increasing values of thermophoresis N_t and Brownian motion N_b .
- It is clear that frictional forces and pressure rise have an opposite behaviour while compare to each other.
- The pressure gradient increases with the increasing value of ϕ .
- The trapped bolos increases with the increasing value of ϕ .

Chapter 3

Simulation of mixed convection flow for physiological breakdown of Jeffrey six-constant fluid model with convective boundary condition

This chapter deals with the simulation of mixed convection flow for physiological breakdown of Jeffrey six-constant fluid in an inclined tube. Influence of convective boundary conditions is also examined. The governing equations of non-Newtonian fluid along with heat are modelled and simplified by using low Reynolds number and long wavelength assumptions. The momentum equation is solved by utilizing the homotopy perturbation technique for velocity while the exact solutions are computed for temperature equation. The obtained expressions for the velocity and temperature are plotted and the impact of various physical parameters are investigated for different peristaltic waves.

3.1 Problem Formulation

We are taking into account the simulation of mixed convection flow for physiological breakdown of Jeffrey six-constant fluid in an inclined tube. The flow is generated by

sinusoidal wave trains propagating with constant speed c_1 along the walls of the tube.

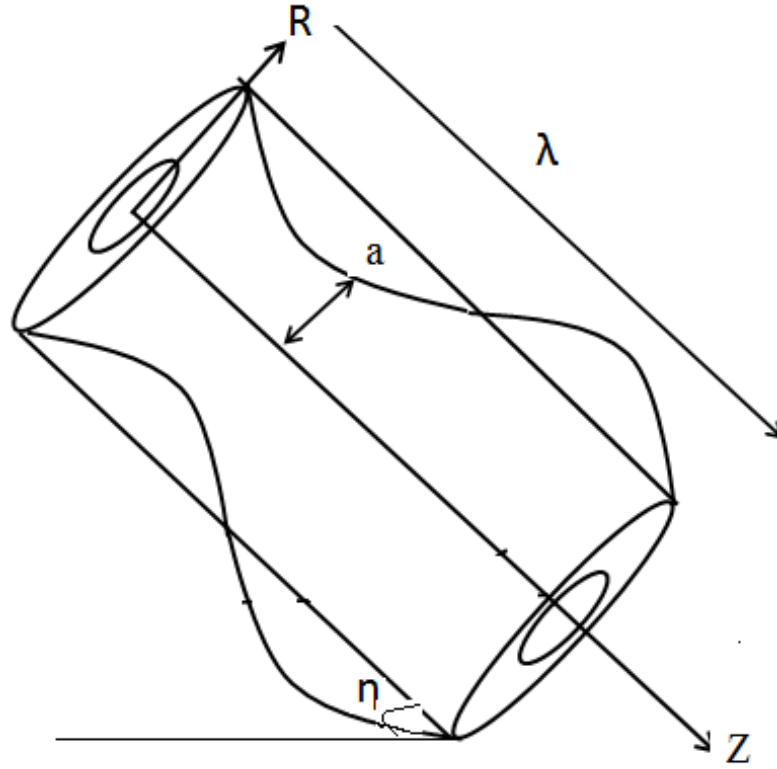


FIGURE 3.1: Geometry of the problem.

The equations for conservation of mass and momentum can be written as

$$\frac{\partial \bar{U}}{\partial \bar{R}} + \frac{\bar{U}}{\bar{R}} + \frac{\partial \bar{W}}{\partial \bar{Z}} = 0, \quad (3.1)$$

$$\begin{aligned} \rho \left(\frac{\partial}{\partial \bar{t}} + \bar{U} \frac{\partial}{\partial \bar{R}} + \bar{W} \frac{\partial}{\partial \bar{Z}} \right) \bar{U} = & -\frac{\partial \bar{P}}{\partial \bar{R}} + \frac{1}{\bar{R}} \frac{\partial}{\partial \bar{R}} (\bar{R} \bar{\tau}_{\bar{R}\bar{R}}) + \frac{\partial}{\partial \bar{Z}} (\bar{\tau}_{\bar{R}\bar{Z}}) - \frac{\bar{\tau}_{\theta\theta}}{\bar{R}} \\ & - \rho \alpha g (\bar{T} - \bar{T}_0) \cos \eta, \end{aligned} \quad (3.2)$$

$$\begin{aligned} \rho \left(\frac{\partial}{\partial \bar{t}} + \bar{U} \frac{\partial}{\partial \bar{R}} + \bar{W} \frac{\partial}{\partial \bar{Z}} \right) \bar{W} = & -\frac{\partial \bar{P}}{\partial \bar{Z}} + \frac{1}{\bar{R}} \frac{\partial}{\partial \bar{R}} (\bar{R} \bar{\tau}_{\bar{R}\bar{Z}}) + \frac{\partial}{\partial \bar{Z}} (\bar{\tau}_{\bar{Z}\bar{Z}}) \\ & + \rho \alpha g (\bar{T} - \bar{T}_0) \sin \eta, \end{aligned} \quad (3.3)$$

$$\rho c_p \left(\frac{\partial}{\partial \bar{t}} + \bar{U} \frac{\partial}{\partial \bar{R}} + \bar{W} \frac{\partial}{\partial \bar{Z}} \right) \bar{T} = \kappa \left(\frac{\partial^2 \bar{T}}{\partial \bar{R}^2} + \frac{1}{\bar{R}} \frac{\partial \bar{T}}{\partial \bar{R}} + \frac{\partial^2 \bar{T}}{\partial \bar{Z}^2} \right) + Q_0, \quad (3.4)$$

where $\tau = \frac{(\rho c)_p}{(\rho c)_f}$ is the ratio among the efficient heat capacity of the nanoparticle material and the heat capacity of the fluid. The transformations between the two frames are

$$\bar{r} = \bar{R}, \quad \bar{z} = \bar{Z} - c_1 \bar{t}, \quad (3.5)$$

$$\bar{u} = \bar{U}, \quad \bar{w} = \bar{W} - c_1. \quad (3.6)$$

The corresponding boundary conditions are defined as

$$\frac{\partial \bar{W}}{\partial \bar{R}} = 0, \quad \frac{\partial \bar{T}}{\partial \bar{R}} = 0, \quad \text{at } \bar{R} = 0, \quad (3.7)$$

$$\bar{W} = 0, \quad K \frac{\partial \bar{T}}{\partial \bar{R}} = -\eta(\bar{T} - \bar{T}_0), \quad \text{at } \bar{R} = \bar{H} = a + b \sin \left[\frac{2\pi}{\lambda} (\bar{Z} - c_1 \bar{t}) \right]. \quad (3.8)$$

The constitutive equation for a Jeffrey six-constant fluid model is defined as [32]

$$\begin{aligned} \tau + \epsilon_1 \left[\frac{d\bar{\tau}}{dt} - W \cdot \bar{\tau} + \bar{\tau} \cdot W + d(\bar{\tau} \cdot D + D \cdot \bar{\tau}) + b \bar{\tau} : DI + c D \text{tr} \bar{\tau} \right] \\ = 2\mu \left[D + \epsilon_2 \left(\frac{dD}{dt} - W \cdot D + D \cdot W + 2dD \cdot D + bD : DI \right) \right]. \end{aligned} \quad (3.9)$$

Here

$$\begin{aligned} D(\text{symmetric part of velocity gradient}) &= \frac{\nabla \bar{V} + (\nabla \bar{V})^t}{2}, \\ W(\text{antisymmetric part of velocity gradient}) &= \frac{\nabla \bar{V} - (\nabla \bar{V})^t}{2}. \end{aligned}$$

Introducing the following non-dimensional variables

$$\begin{aligned} R &= \frac{\bar{R}}{a}, \quad r = \frac{\bar{r}}{a}, \quad Z = \frac{\bar{Z}}{\lambda}, \quad z = \frac{\bar{z}}{\lambda}, \quad W = \frac{\bar{W}}{c_1}, \quad w = \frac{\bar{w}}{c_1}, \quad \tau = \frac{a\bar{\tau}}{c\mu_0}, \\ U &= \frac{\lambda \bar{U}}{ac_1}, \quad u = \frac{\lambda \bar{u}}{ac_1}, \quad t = \frac{c_1 \bar{t}}{\lambda}, \quad \lambda_1 = \frac{\epsilon_1 c_1}{a}, \quad \lambda_2 = \frac{\epsilon_2 c_1}{a}, \\ R_e &= \frac{ac_1 \rho}{\mu_0}, \quad \delta = \frac{a}{\lambda}, \quad h = \frac{\bar{h}}{a} = 1 + \epsilon \sin(2\pi z), \quad P_r = \frac{\mu_0 C_p}{k}, \\ B &= \frac{Q_0 a^2}{k T_0}, \quad \theta = \frac{\bar{T} - \bar{T}_0}{\bar{T}_0}, \quad \alpha = \frac{k}{(\rho c)_f}, \quad G_r = \frac{g \beta \rho a^2 \bar{T}_0}{c \mu}, \quad p = \frac{a^2 \bar{p}}{c_1 \lambda \mu_0}. \end{aligned}$$

Making use of non-dimensional variables Eqs. (3.1) - (3.4), we obtain

$$\frac{\partial u}{\partial r} + \frac{u}{r} + \frac{\partial w}{\partial z} = 0, \quad (3.10)$$

$$\begin{aligned} \delta^3 R_e \left(u \frac{\partial u}{\partial r} + w \frac{\partial u}{\partial z} \right) &= -\frac{\partial p}{\partial r} + \delta^2 \frac{\partial}{\partial z} (\tau_{rz}) + \frac{\delta}{r} \frac{\partial}{\partial r} (r\tau_{rr}) \\ &\quad - \frac{\delta}{r} \tau_{\theta\theta} - \delta G_r (\cos \eta) \theta, \end{aligned} \quad (3.11)$$

$$\begin{aligned} \delta R_e \left(u \frac{\partial w}{\partial r} + w \frac{\partial w}{\partial z} \right) &= -\frac{\partial P}{\partial z} + \frac{1}{r} \frac{\partial}{\partial r} (r\tau_{rz}) + \delta \frac{\partial}{\partial z} (\tau_{zz}) \\ &\quad + G_r (\sin \eta) \theta, \end{aligned} \quad (3.12)$$

$$\delta R_e P_r \left(u \frac{\partial \theta}{\partial r} + w \frac{\partial \theta}{\partial z} \right) = \left[\frac{1}{r} \frac{\partial \theta}{\partial r} + \frac{\partial^2 \theta}{\partial r^2} \right] + B. \quad (3.13)$$

The corresponding boundary conditions are reduced as

$$\frac{\partial w}{\partial r} = 0, \quad \frac{\partial \theta}{\partial r} = 0, \quad \text{at } r = 0, \quad (3.14)$$

$$w = -1, \quad \frac{\partial \theta}{\partial r} + \kappa \theta = 0, \quad \text{at } r = h = 1 + \epsilon \sin(2\pi z). \quad (3.15)$$

With the help of Eqs. (3.5) and (3.6), Eqs. (3.10) - (3.13) under the assumption of low Reynolds number and long wavelength $\delta \ll 1$ take the form

$$0 = -\frac{\partial p}{\partial z} + \frac{1}{r} \frac{\partial}{\partial r} (r\tau_{rz}) + G_r (\sin \eta) \theta, \quad (3.16)$$

$$0 = \frac{\partial p}{\partial r}, \quad (3.17)$$

$$0 = \left[\frac{1}{r} \frac{\partial \theta}{\partial r} + \frac{\partial^2 \theta}{\partial r^2} \right] + B. \quad (3.18)$$

The boundary conditions are reduced as

$$\frac{\partial w}{\partial r} = 0, \quad \frac{\partial \theta}{\partial r} = 0, \quad \text{at } r = 0,$$

$$w = -1, \quad \frac{\partial \theta}{\partial r} + \kappa \theta = 0, \quad \text{at } r = h = 1 + \epsilon \sin(2\pi z).$$

Finally, the Eq. (3.16) can be written as

$$0 = \frac{\partial p}{\partial r}, \quad (3.19)$$

$$\begin{aligned} \frac{\partial p}{\partial z} &= \frac{1}{r} \frac{\partial}{\partial r} \left(r \frac{\partial w}{\partial r} \right) + \frac{1}{r} \frac{\partial}{\partial r} \left(\alpha \alpha_1 r \left(\frac{\partial w}{\partial r} \right)^3 \right) \\ &\quad + \frac{1}{r} \frac{\partial}{\partial r} \left(\alpha^2 \alpha_2 r \left(\frac{\partial w}{\partial r} \right)^5 \right) + G_r (\sin \eta) \theta, \end{aligned} \quad (3.20)$$

$$0 = \left[\frac{1}{r} \frac{\partial \theta}{\partial r} + \frac{\partial^2 \theta}{\partial r^2} \right] + B. \quad (3.21)$$

The boundary conditions are reduced as

$$\begin{aligned} \frac{\partial w}{\partial r} = 0, \quad \frac{\partial \theta}{\partial r} = 0, & \quad \text{at } r = 0, \\ w = -1, \quad \frac{\partial \theta}{\partial r} + \kappa \theta = 0, & \quad \text{at } r = h = 1 + \epsilon \sin(2\pi z). \end{aligned}$$

3.2 Solution of the problem

3.2.1 Exact Solution

The exact solutions for the temperature satisfying the relative boundary conditions are directly written as:

$$\theta = -B \frac{r^2}{4} + \frac{1}{\kappa} \left(\frac{Bh}{2} + \frac{B\kappa h^2}{4} \right). \quad (3.22)$$

3.2.2 Homotopy Perturbation Method

We use homotopy perturbation method to solve the Eq. (3.20)

$$\begin{aligned} H(q, w) &= L(w) - L(w_{10}) + qL(w_{10}) + q \left[\frac{1}{r} \frac{\partial}{\partial r} \left(\alpha \alpha_1 r \left(\frac{\partial w}{\partial r} \right)^3 \right) \right. \\ &\quad \left. + \frac{1}{r} \frac{\partial}{\partial r} \left(\alpha^2 \alpha_2 r \left(\frac{\partial w}{\partial r} \right)^5 \right) + G_r \sin \eta \theta - \frac{\partial p}{\partial z} \right]. \end{aligned} \quad (3.23)$$

We take linear operator $L = \frac{1}{r} \frac{\partial}{\partial r} (r \frac{\partial}{\partial r})$ and the following initial guess which satisfy the boundary conditions [27]

$$w_{10}(r, z) = -1 + p_0 \left[\frac{r^2 - h^2}{4} \right]. \quad (3.24)$$

Let us define

$$w(r, q) = w_0 + qw_1 + q^2w_2 + q^3w_3 + \dots$$

Making use of above expression and using the similar procedure as discussed in [20], the expression for velocity profile can be written as

$$\begin{aligned} w = & -1 + \left(\frac{r^2 - h^2}{4} \right) \frac{dp}{dz} + m_5(r^2 - h^2) + m_6(r^4 - h^4) + m_7(r^6 - h^6) + m_8(r^8 - h^8) \\ & + m_9(r^{10} - h^{10}) + m_{10}(r^{12} - h^{12}) + m_{11}(r^{14} - h^{14}) + m_{12}(r^{16} - h^{16}) \\ & + m_{13}(r^{18} - h^{18}) + m_{14}(r^{20} - h^{20}) + m_{15}(r^{22} - h^{22}) + m_{16}(r^{24} - h^{24}), \end{aligned} \quad (3.25)$$

where m_5, m_6, \dots, m_{17} are constants and given in Appendix 4. The expression for pressure gradient is defined as

$$\frac{dp}{dz} = \frac{16}{-h^4} [F + m_{17}]. \quad (3.26)$$

Flow rate in the dimensionless form can be written as

$$F = Q - \frac{1}{2} \left(1 + \frac{\epsilon^2}{2} \right). \quad (3.27)$$

The pressure rise Δp can be written as

$$\Delta p = \int_0^1 \left(\frac{dp}{dz} \right) dz. \quad (3.28)$$

Velocities in terms of streamfunctions are defined as

$$u = -\frac{1}{r} \left(\frac{\partial \psi}{\partial z} \right), \quad w = \frac{1}{r} \left(\frac{\partial \psi}{\partial r} \right).$$

3.3 Results and discussions

In this section, we have discussed the simulation of mixed convection flow for physiological breakdown of Jeffrey six-constant fluid model with convective boundary condition. We examined the behaviour for different parameters on velocity, temperature, pressure gradient, pressure rise, and streamlines. Figures 3.2 show the temperature profile for different values of Biot number (κ) on temperature profile and heat source or sink parameter (B) respectively. Figure 3.2 shows that with the increase in heat source or sink parameter (B) temperature profile increases. From figure 3.3 it is seen that with the increase in Biot number (κ) temperature profile decreases. Increased in Brinkman number means greater viscous dissipation, thus by increasing Brinkman number, the collision in the flow causes an enhancement in the internal energy of the fluid, which is responsible for the resulting enhancement in the temperature field. Figures 3.4-3.7 show the impact of Jeffrey six-constant parameter (α), heat source or sink parameter (B), Biot number (κ), Grashof number (G_r) on the velocity profile. Figures 3.4-3.5 illustrate that with an increase in the value of α and κ the velocity profile in the centre of the tube decreases whereas it gets opposite behaviour near the tube or near the peristaltic wave. In Figures 3.6-3.7 it is depicted that, at the centre of the tube, the velocity profile is minimum whereas it gets opposite behaviour near the tube or near the peristaltic wave. Figures 3.8-3.13 show the pressure rise for diverse values of α , λ_1 , λ_2 (fluid parameters). In these figures, it is depicted that by increasing value of λ_1 pressure rise increases in the region ($Q \in [-2, -0.5]$) whereas reflux occur in the last. Three different regions can be recognized from this figure.

The retrograde pumping region can also be seen in Figures 3.8, 3.10, 3.12 when $Q < 0$ and $\Delta p > 0$ and free pumping region can be seen when $Q = 0$ and $\Delta p = 0$. Moreover, augmented pumping region can also be seen in figures 3.8, 3.10, 3.12 when $Q > 0$ and $\Delta p < 0$. Figures 3.9, 3.11, 3.13 show the forces have an opposite behaviour as well as the pressure rise. Figures 3.14-3.16 describe the behaviour of pressure gradient for different waveforms like Sinusoidal, Multisinusoidal, and trapizoidal wave. Figure 3.14 describe that increasing value of ϵ the pressure gradient decreases in the region ($0 \leq Z \leq 0.5$) and increases in the region ($0.6 \leq Z \leq 1$) and reflux occur in the region ($1.1 \leq Z \leq 1.5$). Figures 3.15-3.16 show that the behaviour for different values of ϵ by considering the multisinusoidal wave and trapizoidal wave.

Figures 3.17-3.18 illustrate the streamlines for different wave shapes. When we move

from sinusoidal wave to multisinusoidal the number of the trapped bolus increase. Figure 3.18 show the pattern of streamlines for trapizoidal wave.

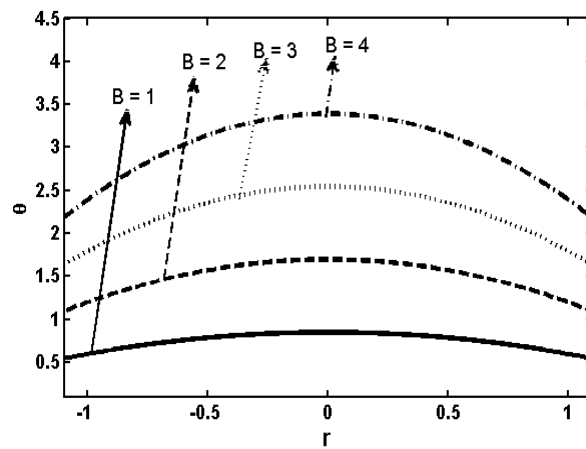


FIGURE 3.2: Variation of temperature for B when $Z = 0.23$, $\epsilon = 0.22$, $\kappa = 2.55$.

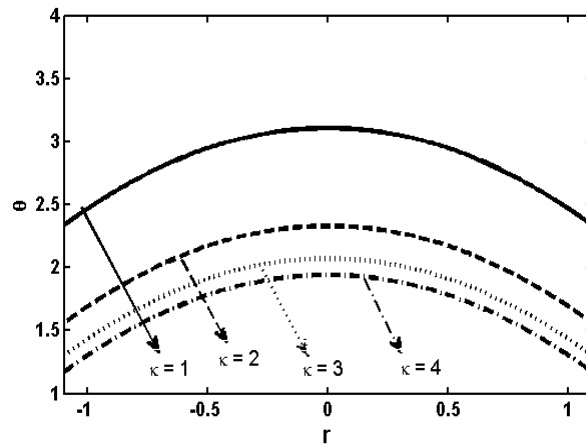


FIGURE 3.3: Variation of temperature for κ when $Z = 0.23$, $\epsilon = 0.22$, $B = 2.55$.

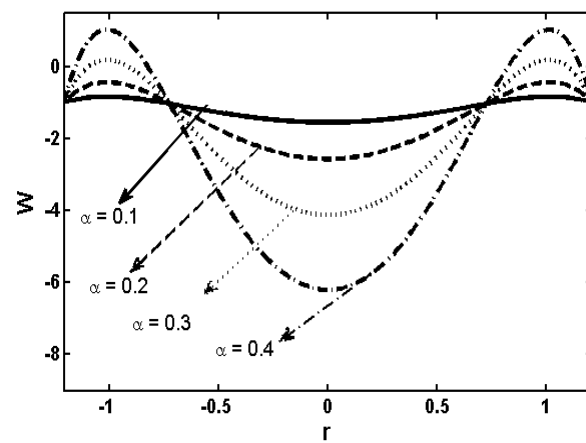


FIGURE 3.4: Variation of velocity for α when $Z = 0.23$, $\epsilon = 0.22$, $\kappa = 2.55$, $\eta = \frac{\pi}{4}$, $B = 0.22$, $G_r = 1.5$, $\alpha_1 = 0.4$, $\alpha_2 = 0.6$.

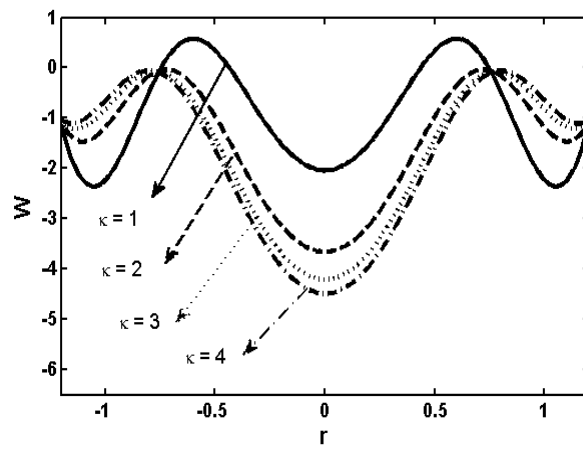


FIGURE 3.5: Variation of velocity for κ when $Z = 0.23$, $\epsilon = 0.22$, $\alpha = 0.22$, $\eta = \frac{\pi}{4}$, $B = 0.22$, $\alpha_1 = 0.22$, $\alpha_2 = 0.4$, $G_r = 1.5$.

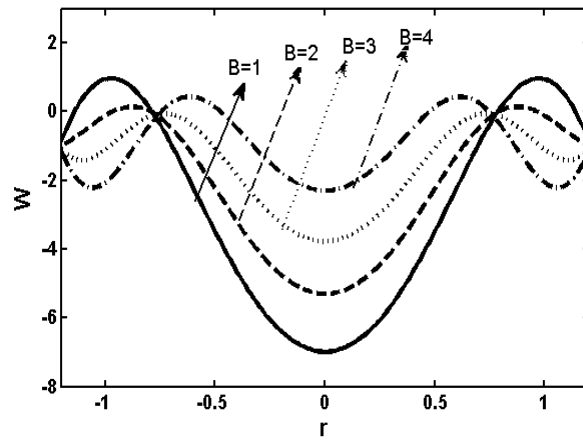


FIGURE 3.6: Variation of velocity for B when $Z = 0.23$, $\epsilon = 0.22$, $\kappa = 2.55$, $\eta = \frac{\pi}{4}$, $\alpha = 0.22$, $\alpha_1 = 0.22$, $\alpha_2 = 0.4$, $G_r = 1.5$.

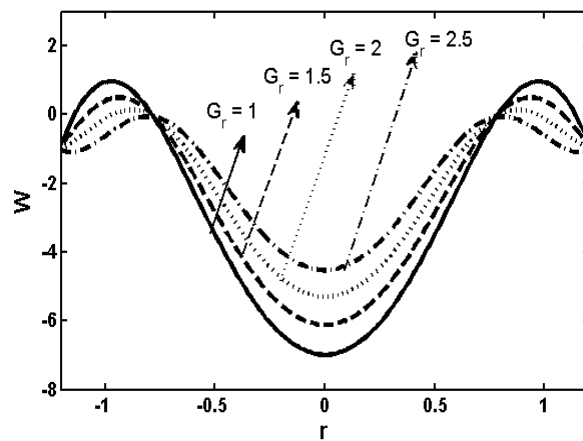


FIGURE 3.7: Variation of velocity for G_r when $Z = 0.23$, $\epsilon = 0.22$, $\eta = \frac{\pi}{4}$, $\alpha = 0.22$, $\alpha_1 = 0.22$, $\alpha_2 = 0.4$, $B = 0.22$.

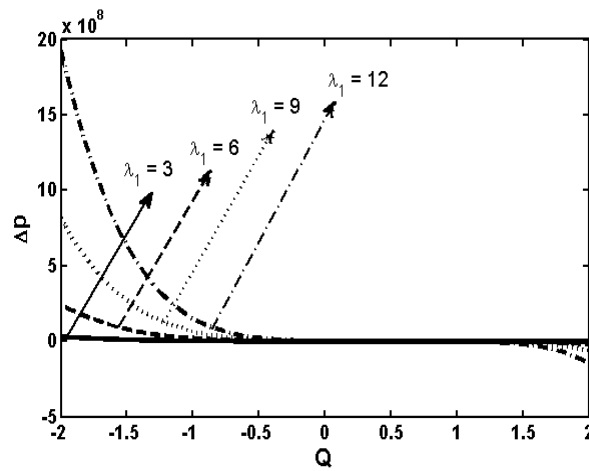


FIGURE 3.8: Variation of pressure rise for λ_1 when $Z = 0.23$, $\epsilon = 0.01$, $\eta = \frac{\pi}{4}$, $\alpha_1 = 0.22$, $\alpha_2 = 0.4$, $G_r = 1.5$, $B = 1.5$.

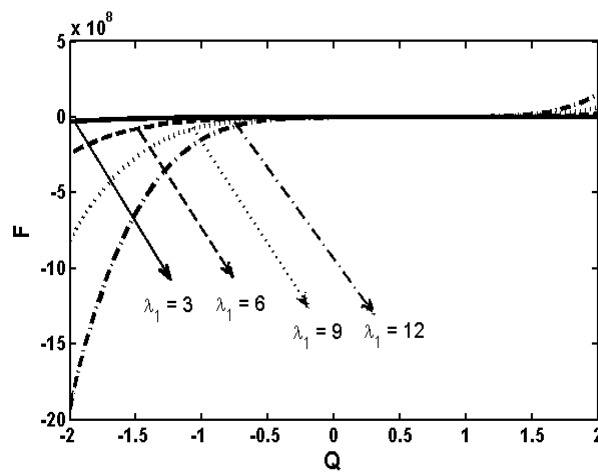


FIGURE 3.9: Variation of frictional forces for λ_1 when $Z = 0.23$, $\epsilon = 0.01$, $\eta = \frac{\pi}{4}$, $\alpha_1 = 0.22$, $\alpha_2 = 0.4$, $G_r = 1.5$, $B = 1.5$.

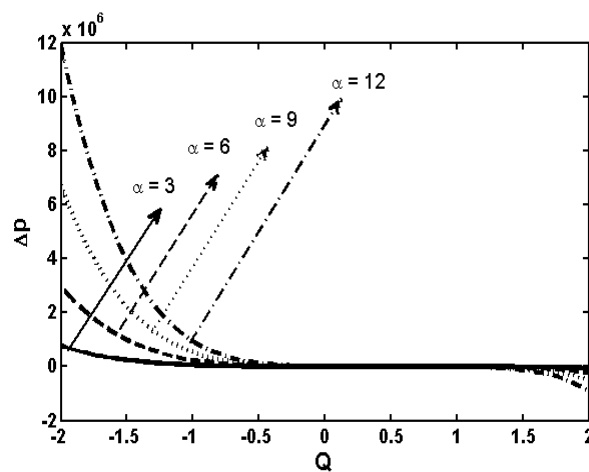


FIGURE 3.10: Variation of pressure rise for α when $Z = 0.23$, $\epsilon = 0.01$, $\eta = \frac{\pi}{4}$, $\alpha_1 = 0.22$, $\alpha_2 = 0.4$, $G_r = 1.5$, $B = 1.5$.

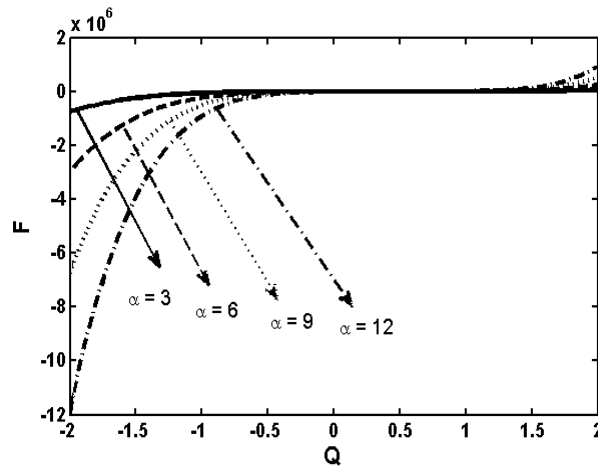


FIGURE 3.11: Variation of frictional forces for α when $Z = 0.23$, $\epsilon = 0.01$, $\eta = \frac{\pi}{4}$, $\alpha_1 = 0.22$, $\alpha_2 = 0.4$, $G_r = 1.5$, $B = 1.5$.

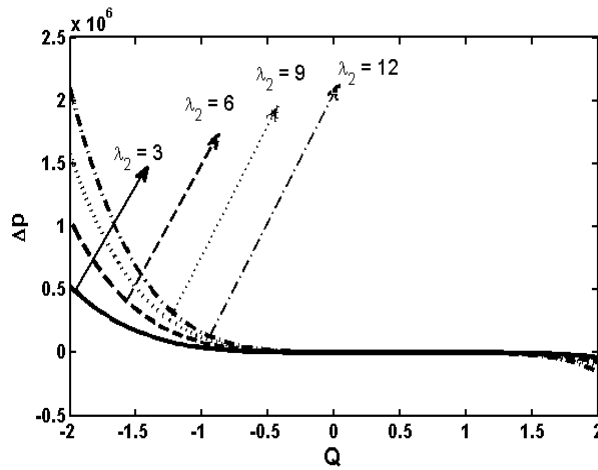


FIGURE 3.12: Variation of pressure rise for λ_2 when $Z = 0.23$, $\epsilon = 0.01$, $\eta = \frac{\pi}{4}$, $\alpha_1 = 0.22$, $\alpha_2 = 0.4$, $G_r = 1.5$, $B = 1.5$.

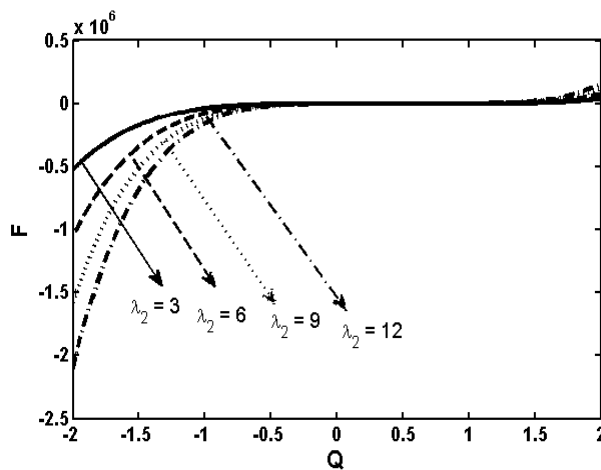


FIGURE 3.13: Variation of frictional forces for λ_2 when $Z = 0.23$, $\epsilon = 0.01$, $\eta = \frac{\pi}{4}$, $\alpha_1 = 0.22$, $\alpha_2 = 0.4$, $G_r = 1.5$, $B = 1.5$.

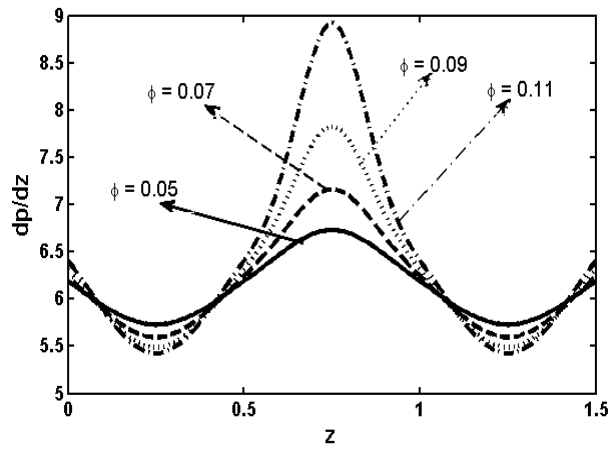


FIGURE 3.14: Pressure gradient $\frac{dp}{dz}$ for sinusoidal wave when $Z = 0.23$, $\eta = \frac{\pi}{4}$, $\alpha_1 = 0.22$, $\alpha_2 = 0.4$, $G_r = 1.5$, $B = 1.5$.

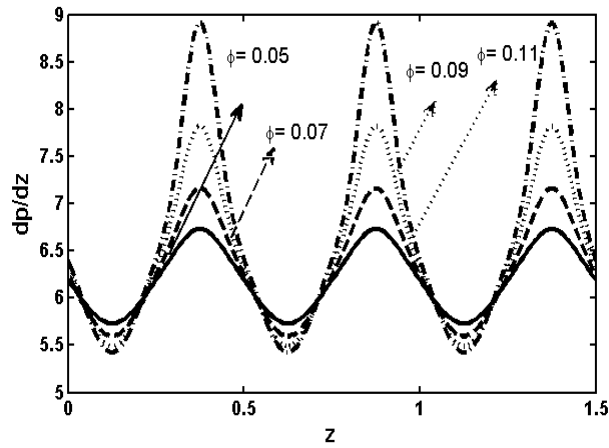


FIGURE 3.15: Pressure gradient $\frac{dp}{dz}$ for multisinusoidal wave when $Z = 0.23$, $\eta = \frac{\pi}{4}$, $\alpha_1 = 0.22$, $\alpha_2 = 0.4$, $G_r = 1.5$, $B = 1.5$.

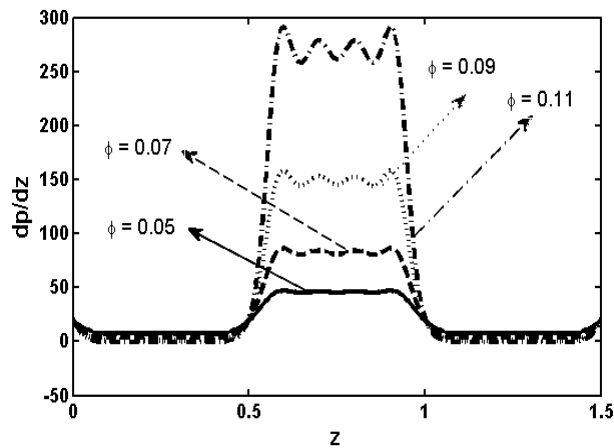


FIGURE 3.16: Pressure gradient $\frac{dp}{dz}$ for trapezoidal wave when $Z = 0.23$, $\eta = \frac{\pi}{4}$, $\alpha_1 = 0.22$, $\alpha_2 = 0.4$, $G_r = 1.5$, $B = 1.5$.

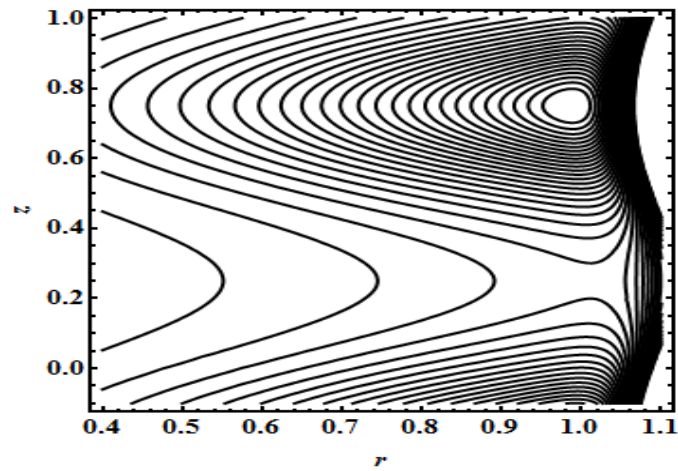


FIGURE 3.17: Streamlines pattern for sinusoidal wave $Z = 0.23$, $\epsilon = 0.01$, $\eta = \frac{\pi}{4}$, $\alpha_1 = 0.22$, $\alpha_2 = 0.4$, $G_r = 1.5$, $B = 1.5$.

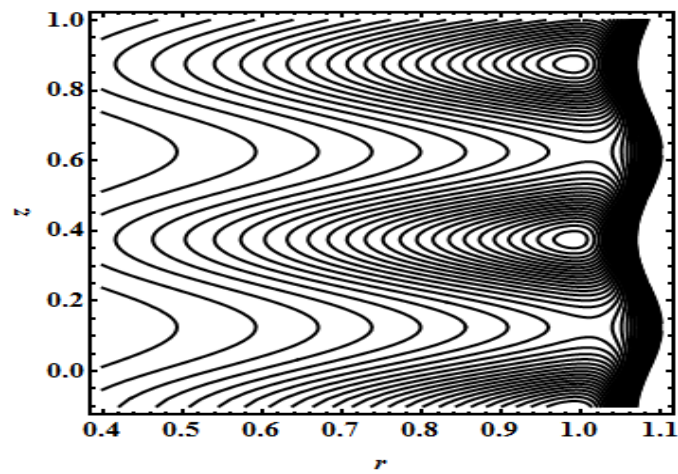


FIGURE 3.18: Streamlines pattern for multisinusoidal wave $Z = 0.23$, $\epsilon = 0.01$, $\eta = \frac{\pi}{4}$, $\alpha_1 = 0.22$, $\alpha_2 = 0.4$, $G_r = 1.5$, $B = 1.5$.

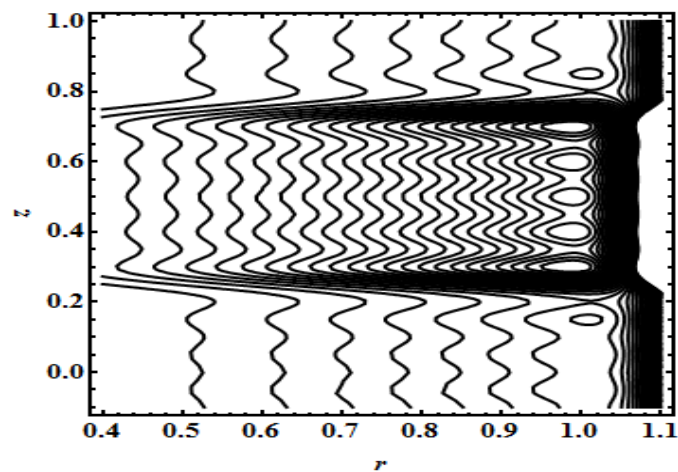


FIGURE 3.19: Streamlines pattern for trapezoidal $Z = 0.23$, $\epsilon = 0.01$, $\eta = \frac{\pi}{4}$, $\alpha_1 = 0.22$, $\alpha_2 = 0.4$, $G_r = 1.5$, $B = 1.5$.

3.4 Conclusion

In this chapter, we have analyzed the simulation of mixed convection flow for physiological breakdown of Jeffrey six-constant fluid model with convective boundary condition in an inclined tube. The main findings of the present study are as follows:

- Temperature profile decreases for increasing values of the Biot number.
- It is clear that frictional forces and pressure rise have an opposite behaviour while compare to each other.
- The pressure gradient increases with the increasing value of ϵ .
- Streamlines bolas take the form of the shape of the geometry.

Chapter 4

Physiological breakdown of Sisko fluid with convective boundary condition in a uniform tube

This chapter deals with the peristaltic flow of Sisko fluid with convective boundary conditions in a uniform tube. The effects of viscous dissipation are also taken into account. The governing equations of non-Newtonian fluid along with heat and nanoparticles are modelled and simplified by using low Reynolds number and long wavelength assumptions. The velocity equation is solved by utilizing the homotopy perturbation technique while the exact solutions are computed for temperature and concentration equations. The solutions depend on Brinkman number (B_κ) and Magnetohydrodynamics (M). The obtained expressions for the velocity, temperature and concentration profiles are plotted and the impact of various physical parameters are investigated for different peristaltic waves

4.1 Mathematical Formulation

We are taking into account the peristaltic flow of Sisko fluid with convective boundary conditions in a uniform tube. The flow is generated by sinusoidal wave trains propagating with constant speed c_1 along the wall of the tube. Viscous dissipation effects are also taken into account. The geometry of the wall surfaces is shown in Figure 4.1 and

mathematically defined as

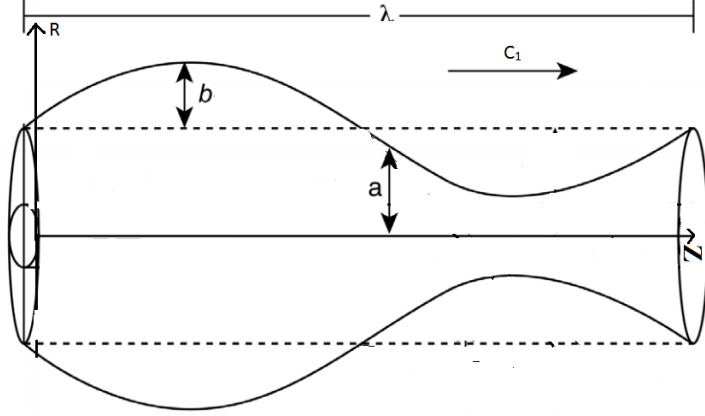


FIGURE 4.1: A physical sketch of the problem.

$$\bar{H} = a + b \sin \left[\frac{2\pi}{\lambda} (\bar{Z} - c_1 \bar{t}) \right], \quad (4.1)$$

where a is the radius of the tube, b is the wave amplitude, λ represent the wavelength, c_1 is the propagation speed and \bar{t} is the time.

For an incompressible fluid the law of conservation of mass and momentum in the absence of body forces can be written as

$$\frac{\partial \bar{U}}{\partial \bar{R}} + \frac{\bar{U}}{\bar{R}} + \frac{\partial \bar{W}}{\partial \bar{Z}} = 0, \quad (4.2)$$

$$\rho \left(\frac{\partial}{\partial \bar{t}} + \bar{U} \frac{\partial}{\partial \bar{R}} + \bar{W} \frac{\partial}{\partial \bar{Z}} \right) \bar{U} = -\frac{\partial \bar{P}}{\partial \bar{R}} + \frac{1}{\bar{R}} \frac{\partial}{\partial \bar{R}} (\bar{R} \bar{S}_{RR}) + \frac{\partial}{\partial \bar{Z}} (\bar{S}_{RZ}) - \frac{\bar{S}_{\theta\theta}}{\bar{R}}, \quad (4.3)$$

$$\rho \left(\frac{\partial}{\partial \bar{t}} + \bar{U} \frac{\partial}{\partial \bar{R}} + \bar{W} \frac{\partial}{\partial \bar{Z}} \right) \bar{W} = -\frac{\partial \bar{P}}{\partial \bar{Z}} + \frac{1}{\bar{R}} \frac{\partial}{\partial \bar{R}} (\bar{R} \bar{S}_{RZ}) + \frac{\partial}{\partial \bar{Z}} (\bar{S}_{ZZ}) - \sigma B_0^2 \bar{W}, \quad (4.4)$$

$$\begin{aligned} \rho C_p \left(\frac{\partial}{\partial \bar{t}} + \bar{U} \frac{\partial}{\partial \bar{R}} + \bar{W} \frac{\partial}{\partial \bar{Z}} \right) \bar{T} = & \bar{S}_{RR} \frac{\partial \bar{U}}{\partial \bar{R}} + \bar{S}_{RZ} \frac{\partial \bar{W}}{\partial \bar{R}} + \bar{S}_{RZ} \frac{\partial \bar{U}}{\partial \bar{Z}} + \bar{S}_{ZZ} \frac{\partial \bar{U}}{\partial \bar{R}} \\ & + \bar{S}_{\theta\theta} \frac{\bar{U}}{\bar{R}} + \bar{K} \left(\frac{\partial^2 \bar{T}}{\partial \bar{R}^2} + \frac{1}{\bar{R}} \frac{\partial \bar{T}}{\partial \bar{R}} + \frac{\partial^2 \bar{T}}{\partial \bar{Z}^2} \right), \end{aligned} \quad (4.5)$$

$$\begin{aligned} \left(\frac{\partial}{\partial \bar{t}} + \bar{U} \frac{\partial}{\partial \bar{R}} + \bar{W} \frac{\partial}{\partial \bar{Z}} \right) \bar{C} = & D \left(\frac{\partial^2 \bar{C}}{\partial \bar{R}^2} + \frac{1}{\bar{R}} \frac{\partial \bar{C}}{\partial \bar{R}} + \frac{\partial^2 \bar{C}}{\partial \bar{Z}^2} \right) \\ & + \frac{D \bar{k}_T}{\bar{T}_0} \left(\frac{\partial^2 \bar{T}}{\partial \bar{R}^2} + \frac{1}{\bar{R}} \frac{\partial \bar{T}}{\partial \bar{R}} + \frac{\partial^2 \bar{T}}{\partial \bar{Z}^2} \right). \end{aligned} \quad (4.6)$$

The transformation relation between the two frames are

$$\begin{aligned}\bar{r} &= \bar{R}, & \bar{z} &= \bar{Z} - c_1 \bar{t}, \\ \bar{u} &= \bar{U}, & \bar{w} &= \bar{W} - c_1.\end{aligned}$$

The corresponding boundary conditions are defined as

$$\begin{aligned}\frac{\partial \bar{W}}{\partial \bar{R}} = 0, & \quad \frac{\partial \bar{T}}{\partial \bar{R}} = 0, & \quad \frac{\partial \bar{C}}{\partial \bar{R}} = 0, & \quad \text{at } \bar{R} = 0, \\ \bar{W} = 0, & \quad K \frac{\partial \bar{T}}{\partial \bar{R}} = -\eta(\bar{T} - \bar{T}_0), & \quad \bar{C} = \bar{C}_0, & \quad \text{at } \bar{R} = \bar{H} = a + b \sin \left[\frac{2\pi}{\lambda} (\bar{Z} - c\bar{t}) \right].\end{aligned}$$

The constitutive equation for a Sisko fluid model is defined as

$$\begin{aligned}\bar{\mathbf{S}} &= \left[a_1 + b_1 \left(\sqrt{\bar{\Pi}} \right)^{n-1} \right] \bar{A}_1, \\ \bar{A}_1 &= \bar{L} + \bar{L}^T, \quad \bar{L} = \nabla \bar{V}, \quad \bar{\Pi} = \frac{1}{2} \text{tr} \bar{A}_1^2.\end{aligned}$$

The non-dimensional constants are defined as

$$\begin{aligned}R &= \frac{\bar{R}}{a}, & r &= \frac{\bar{r}}{a}, & Z &= \frac{\bar{Z}}{\lambda}, & z &= \frac{\bar{z}}{\lambda}, & W &= \frac{\bar{W}}{c_1}, & w &= \frac{\bar{w}}{c_1}, & S &= \frac{a\bar{S}}{c_1\mu_0}, \\ U &= \frac{\lambda\bar{U}}{ac_1}, & u &= \frac{\lambda\bar{u}}{ac_1}, & t &= \frac{c_1\bar{t}}{\lambda}, & \lambda_1 &= \frac{\epsilon_1 c_1}{a}, & \lambda_2 &= \frac{\epsilon_2 c_1}{a}, \\ Re &= \frac{ac_1\rho}{\mu_0}, & \delta &= \frac{a}{\lambda}, & h &= \frac{\bar{h}}{a} = 1 + \epsilon \sin(2\pi z), & Pr &= \frac{\mu_0 C_p}{k}, \\ Ec &= \frac{c^2}{C_p T_0}, & \theta &= \frac{\bar{T} - \bar{T}_0}{\bar{T}_0}, & \Pi &= \frac{a\bar{\Pi}}{c_1}, & \alpha &= \frac{k}{(\rho c)_f}, & p &= \frac{a^2 \bar{p}}{c_1 \lambda \mu_0}, \\ S_T &= \frac{\rho D k_T \bar{T}_0}{\mu T_0 \bar{C}_0}, & S_H &= \frac{\mu}{D\rho}, & \sigma &= \frac{\bar{C} - \bar{C}_o}{\bar{C}_o}, & M &= \sqrt{\frac{\sigma}{\mu}} B_0 a^2.\end{aligned}$$

With the help of above non-dimensional variables and under the assumption of low Reynolds number $Re \ll 1$ and long wavelength $\delta \ll 1$ approximation, the equations

can be written as

$$0 = \frac{\partial u}{\partial r} + \frac{u}{r} + \frac{\partial w}{\partial z}, \quad (4.7)$$

$$0 = \frac{\partial p}{\partial r}, \quad (4.8)$$

$$0 = -\frac{\partial p}{\partial z} + \frac{1}{r} \frac{\partial}{\partial r} (r S_{rz}) - M^2(w + 1), \quad (4.9)$$

$$0 = \frac{1}{r} \frac{\partial}{\partial r} \left(r \frac{\partial \theta}{\partial r} \right) + B_k \frac{\partial w}{\partial r} (S_{rz}), \quad (4.10)$$

$$0 = \frac{1}{S_H} \frac{1}{r} \frac{\partial}{\partial r} \left(r \frac{\partial \sigma}{\partial r} \right) + S_T \frac{1}{r} \frac{\partial}{\partial r} \left(r \frac{\partial \theta}{\partial r} \right). \quad (4.11)$$

The boundary conditions are reduced as

$$\begin{aligned} \frac{\partial w}{\partial r} = 0, \quad \frac{\partial \theta}{\partial r} = 0, \quad \frac{\partial \sigma}{\partial r} = 0, & \quad \text{at } r = 0, \\ w = -1, \quad \frac{\partial \theta}{\partial r} + \kappa \theta = 0, \quad \sigma = 0, & \quad \text{at } r = h = 1 + \epsilon \sin(2\pi z). \end{aligned}$$

The stress tensor can be defined as

$$\begin{aligned} S_{rr} &= 2\delta \left[1 + b \left(\frac{\partial w}{\partial r} \right)^{n-1} \right] \frac{\partial u}{\partial r}, \\ S_{rz} &= \left[1 + b \left(\frac{\partial w}{\partial r} \right)^{n-1} \right] \left(\frac{\partial u}{\partial z} \delta^2 + \frac{\partial w}{\partial r} \right), \\ S_{zz} &= 2\delta \left[1 + b \left(\frac{\partial w}{\partial r} \right)^{n-1} \right] \frac{\partial w}{\partial z}. \end{aligned}$$

Finally, in simplified form Eqs. (4.7)-(4.11) can be written as

$$\frac{\partial p}{\partial r} = 0, \quad (4.12)$$

$$\frac{\partial p}{\partial z} = \frac{1}{r} \frac{\partial}{\partial r} \left(r \left[1 + b \left(\frac{\partial w}{\partial r} \right)^{n-1} \right] \frac{\partial w}{\partial r} \right) - M^2(w + 1), \quad (4.13)$$

$$\frac{1}{r} \frac{\partial}{\partial r} \left(r \frac{\partial \theta}{\partial r} \right) + B_k \frac{\partial w}{\partial r} (S_{rz}) = 0, \quad (4.14)$$

$$\frac{1}{S_H} \frac{1}{r} \frac{\partial}{\partial r} \left(r \frac{\partial \sigma}{\partial r} \right) + S_T \frac{1}{r} \frac{\partial}{\partial r} \left(r \frac{\partial \theta}{\partial r} \right) = 0. \quad (4.15)$$

The boundary conditions are reduced as

$$\begin{aligned} \frac{\partial w}{\partial r} = 0, \quad \frac{\partial \theta}{\partial r} = 0, \quad \frac{\partial \sigma}{\partial r} = 0, & \quad \text{at } r = 0, \\ w = -1, \quad \frac{\partial \theta}{\partial r} + \kappa \theta = 0, \quad \sigma = 0, & \quad \text{at } r = h = 1 + \epsilon \sin(2\pi z). \end{aligned}$$

4.2 Solution Methodology

We use homotopy perturbation method to solve the Eq. (4.13)

$$\begin{aligned} H(q, w) = L(w) - L(w_{10}) + qL(w_{10}) + q \left[\frac{b}{r} \left(\frac{\partial w}{\partial r} \right)^n + nb \left(\frac{\partial w}{\partial r} \right)^{n-1} \left(\frac{\partial^2 w}{\partial r^2} \right) \right. \\ \left. + -M^2(w + 1) - \frac{\partial p}{\partial z} \right]. \end{aligned} \quad (4.16)$$

We choose linear operator $L = \frac{1}{r} \frac{\partial}{\partial r} \left(r \frac{\partial}{\partial r} \right)$ and initial guess which satisfy the required boundary conditions are

$$w_{10}(r, z) = -1 + p_0 \left[\frac{r^2 - h^2}{4} \right]. \quad (4.17)$$

$H(q, w)$ for case 1 ($n = 0$, shear thinning fluid)

$$H(q, w) = L(w) - L(w_{10}) + qL(w_{10}) + q \left[\frac{b}{r} - M^2(w + 1) - \frac{\partial p}{\partial z} \right]. \quad (4.18)$$

$H(q, w)$ for case 2 ($n = 1$, $b = 0$, Newtonian fluid)

$$H(q, w) = L(w) - L(w_{10}) + qL(w_{10}) + q \left[-M^2(w + 1) - \frac{\partial p}{\partial z} \right]. \quad (4.19)$$

$H(q, w)$ for case 3 ($n = 2$, shear thickening fluid)

$$\begin{aligned} H(q, w) = L(w) - L(w_{10}) + qL(w_{10}) + q \left[\frac{b}{r} \left(\frac{\partial w}{\partial r} \right)^2 + 2b \left(\frac{\partial w}{\partial r} \right) \left(\frac{\partial^2 w}{\partial r^2} \right) \right. \\ \left. + -M^2(w + 1) - \frac{\partial p}{\partial z} \right]. \end{aligned} \quad (4.20)$$

According to HPM, we solve for case 3 ($n = 2$, shear thickening fluid)

$$w(r, q) = w_0 + qw_1 + q^2w_2 + q^3w_3 + \dots$$

$$p(r, q) = p_1 + qp_2 + q^2p_3 + q^3p_4 + \dots$$

The velocity field for $q \rightarrow 1$ takes the form

$$\begin{aligned} w = -1 + \left(\frac{r^2 - h^2}{4} \right) \frac{dp}{dz} + A_1(r^2 - h^2) + A_2(r^3 - h^3) + A_3(r^4 - h^4) \\ + A_4(r^5 - h^5) + A_5(r^6 - h^6) + A_6(r^7 - h^7) + A_7(r^9 - h^9). \end{aligned} \quad (4.21)$$

The exact solutions for the temperature satisfying the relative boundary conditions are directly written as

$$\begin{aligned} \theta = \frac{1}{\kappa} \left(\frac{-B_\kappa h^3}{16} - \frac{1}{40} b B_\kappa h^4 + \frac{1}{48} M B_\kappa h^5 + \frac{27}{2240} b B_\kappa h^6 M p_0 + \frac{1}{20} b B_\kappa h^4 p_0^2 \right) \\ + \frac{1}{\kappa} \left(\frac{11}{6144} M^2 B_\kappa h^7 p_0^2 - \frac{9}{1120} b B_\kappa h^6 M p_0^3 - \frac{5}{512} b^2 B_\kappa h^7 M p_0^3 - \frac{1}{96} b^2 B_\kappa h^5 p_0^4 \right) \\ + \frac{1}{\kappa} \left(\frac{3}{224} b^3 B_\kappa h^6 p_0^4 + \frac{1}{1280} b^2 B_\kappa h^4 M^2 p_0^4 + \frac{11}{5376} b^3 B_\kappa h^8 M p_0^5 + \frac{1}{512} b^4 B_\kappa h^7 p_0^6 \right). \end{aligned} \quad (4.22)$$

The exact solutions for the concentration equation satisfying the relative boundary conditions are directly written as

$$\begin{aligned} \sigma = \frac{1}{64} B_\kappa S_T S_H P_0^2 (r^4 - h^4) + \frac{1}{32} B_\kappa S_T S_H P_0 p_1 (r^4 - h^4) - \frac{1}{576} B_\kappa S_T S_H P_0^4 (r^6 - h^6) \alpha_1 \\ + \frac{1}{64} B_\kappa S_T S_H P_1^2 (r^4 - h^4) - \frac{1}{32} S_T S_H P_0 p_2 (r^4 - h^4) + \frac{1}{288} S_T S_H P_0^3 p_1 (r^6 - h^6) \alpha_1 \\ + \frac{1}{288} B_\kappa S_T S_H P_0^3 p_1 (r^6 - h^6) - \frac{3}{2048} S_T S_H P_0^4, \end{aligned} \quad (4.23)$$

where A_1, A_2, \dots, A_8 are constants and given in Appendix 4. The expression for pressure gradient can be written as

$$\frac{dp}{dz} = \frac{16}{-h^4} [F + A_8]. \quad (4.24)$$

Flow rate in the dimensionless form can be written as

$$F = Q - \frac{1}{2} \left(1 + \frac{\epsilon^2}{2} \right). \quad (4.25)$$

The pressure rise Δp can be written as

$$\Delta p = \int_0^1 \left(\frac{dp}{dz} \right) dz. \quad (4.26)$$

Velocities in terms of streamfunctions are defined as

$$u = -\frac{1}{r} \left(\frac{\partial \psi}{\partial z} \right), \quad w = \frac{1}{r} \left(\frac{\partial \psi}{\partial r} \right).$$

For the flow analysis, we have considered three waveforms sinusoidal wave, trapezoidal wave and multisinusoidal wave. The dimensionless equations can be written as

1. **Sinusoidal wave**

$$h(z) = 1 + \epsilon \sin(2\pi z).$$

2. **Multisinusoidal wave**

$$h(z) = 1 + \epsilon \sin(2m\pi z).$$

3. **Trapezoidal wave**

$$h(z) = 1 + \epsilon \left[\frac{32}{\pi^2} \sum_{n=1}^{\infty} \frac{\sin \frac{\pi}{8}(2n-1)}{(2n-1)^2} \sin(2\pi(2n-1)z) \right].$$

4.3 Results and discussions

In this section, we have analyzed the physiological breakdown of Sisko fluid model with convective boundary condition in a uniform tube through graphs. We have presented the solution attained by HPM by framing velocity, pressure rise, pressure gradient, temperature, concentration and streamline graphs for diverse values of the parameters power law index (n), fluid parameter b , magnetohydrodynamics (M), Biot number κ , (Brinkman number) (B_k), (Soret number) S_T , (Schmidt number) S_H respectively. Figures 4.2-4.5 show that with the increase in b, B_k, M temperature profile increases. From figure 4.5 it is seen that with the increase in κ temperature profile decreases. Figures 4.6-4.9 show that with the increase in b, B_k, M, S_T concentration profile increases. From figure 4.10 it is seen that with the increase in S_H concentration profile decreases. An increase in Soret number (S_T) enhances the concentration profile. Physically, when we increase the Soret number (S_T), it gives rise to diffuse the nanoparticles in the fluid, due to convection, which leads to increase the concentration profile. An increase in Schmidt number reduces the concentration profile. It is due to the fluid that an increase in Schmidt number (S_H) to reduces the diffusion of nanoparticles in the fluids flow, which is responsible for the reduction of concentration field.

Figure 4.11 shows that increases the value of M while the velocity profile in the centre of the tube decreases as well as it gets opposite behaviour nearest of the tube or near the peristaltic wave. Figures 4.12-4.13 show that shear stress gets increase function in the region $(0.5 \leq r \leq 0)$ whereas it get opposite behaviour in the region $(-1 \leq r \leq -0.49)$. Figures 4.14-4.19 show the pressure rise (versus flow rate) for diverse value of M, b, ϵ . From figure 4.14, it is depicted that by increasing value of M pressure rise increasing in the region $(Q \in [-2, 0.5])$ whereas reflux occur in the last. The retrograde pumping region can also be seen in Figure 4.14 when $Q < 0$ and $\Delta p > 0$ and free pumping region can be seen when $Q = 0$ and $\Delta p = 0$. Moreover, augmented pumping region can also be seen in figure 4.14 when $Q > 0$ and $\Delta p < 0$. From figure 4.16, 4.18 it is seen that with the increase in ϵ pressure rise decreases in the region $(Q \in [-2, -0.4])$ whereas reflux occur in the last. Figures 4.15, 4.17, 4.19 show the friction force for diverse values of M, b, ϵ . From these figures it is depicted that the friction force have an opposite behaviour as compared to pressure rise.

Figures 4.20-4.22 describe the behaviour of pressure gradient for different waveforms like Sinusoidal, Multisinusoidal, trapizoidal. Figure 4.20 describe that increasing value of ϵ the pressure gradient decreases in the region $(0 \leq Z \leq 0.5)$ and increases in the region $(0.6 \leq Z \leq 1)$ and reflux occur in the region $(1.1 \leq Z \leq 1.5)$.

Figures 4.21-4.22 show that the behaviour for different values of ϵ by considering the multisinusoidal wave, trapizoidal. Figures 4.23-4.24, it is depicted that by increasing value of b, M pressure rise increasing. Figures 4.25-4.34 illustrate the streamlines for different wave shapes. It is distinguish that the streamlines of the flow are affected in a related behaviour by increasing the value of ϵ . In fact it is pragmatic that the strength of trapped bolus appear in the wider part of the tube decreases by increasing the value of ϵ .

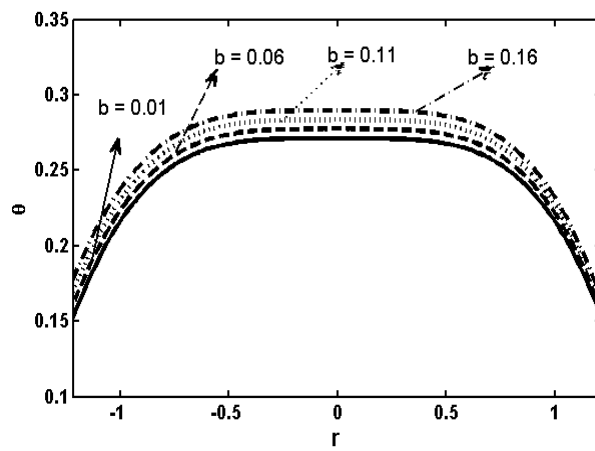


FIGURE 4.2: Variation of temperature for b when $Z = 0.23$, $\epsilon = 0.22$, $\kappa = 2.55$, $M = 0.09$, $B_k = 0.23$.

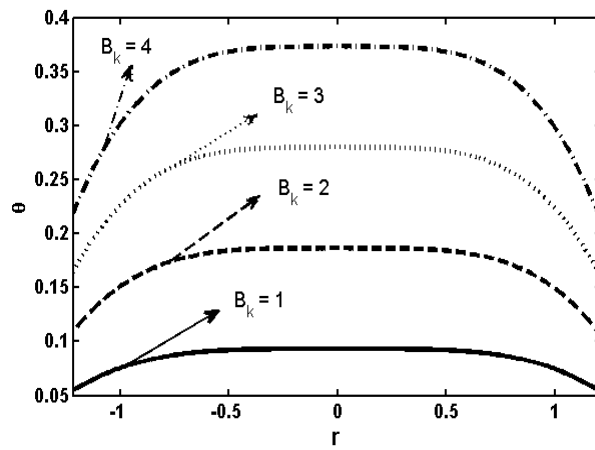


FIGURE 4.3: Variation of temperature for B_k when $Z = 0.23$, $\epsilon = 0.22$, $\kappa = 2.55$, $M = 0.09$, $b = 0.23$.

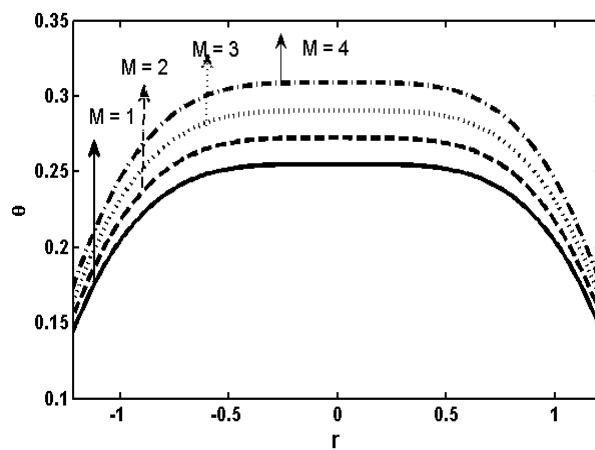


FIGURE 4.4: Variation of temperature for M when $Z = 0.23$, $\epsilon = 0.22$, $\kappa = 2.55$, $b = 0.01$, $B_k = 0.23$.

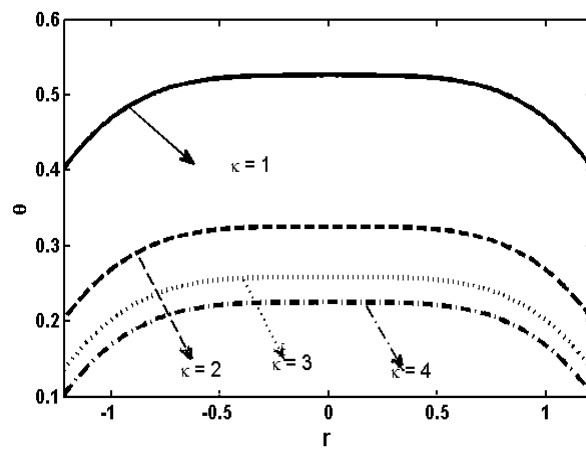


FIGURE 4.5: Variation of temperature graph for κ when $Z = 0.23$, $\epsilon = 0.22$, $b = 0.01$, $M = 0.09$, $B_k = 0.23$.

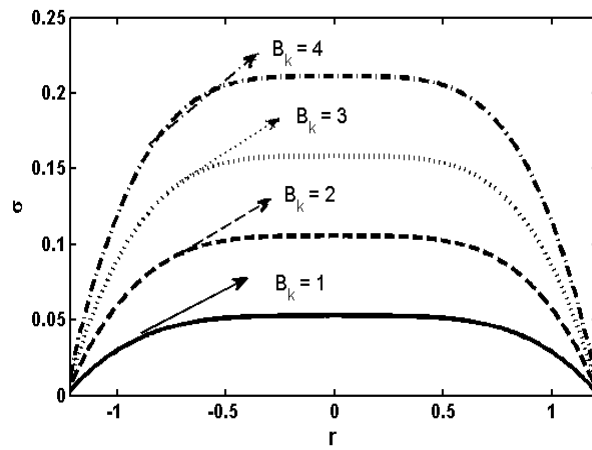


FIGURE 4.6: Variation of nanoparticle concentration graph for B_k when $M = 0.09$, $Z = 0.2$, $S_T = 0.8$, $\lambda = 0.1$, $\epsilon = 0.22$, $S_H = 0.8$.

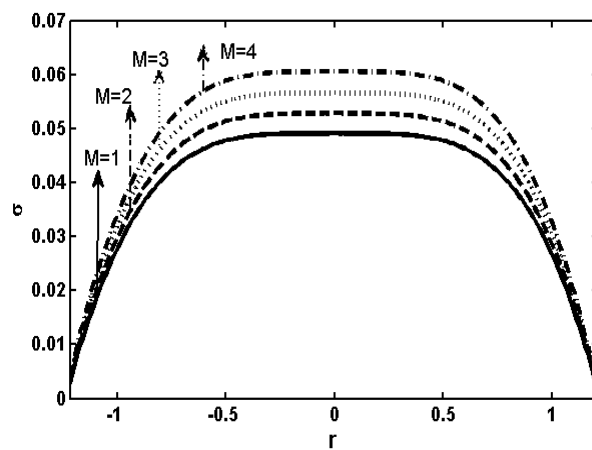


FIGURE 4.7: Variation of nanoparticle concentration graph for M when $B_k = 0.09$, $Z = 0.2$, $S_T = 0.8$, $\lambda = 0.1$, $\epsilon = 0.22$, $S_H = 0.8$.

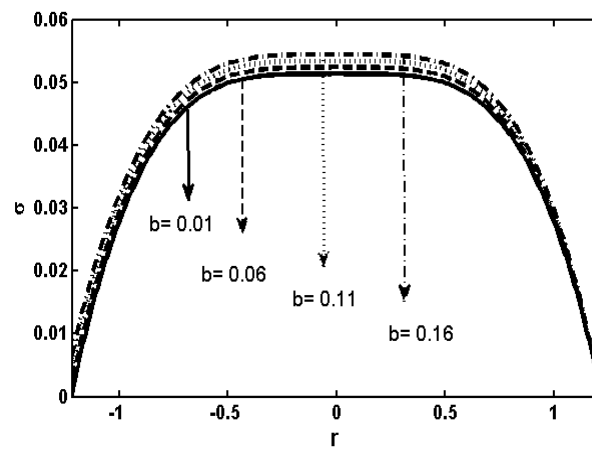


FIGURE 4.8: Variation of nanoparticle concentration graph for b when $M = 0.09$, $Z = 0.2$, $S_T = 0.8$, $\lambda = 0.1$, $\epsilon = 0.22$, $S_H = 0.8$.

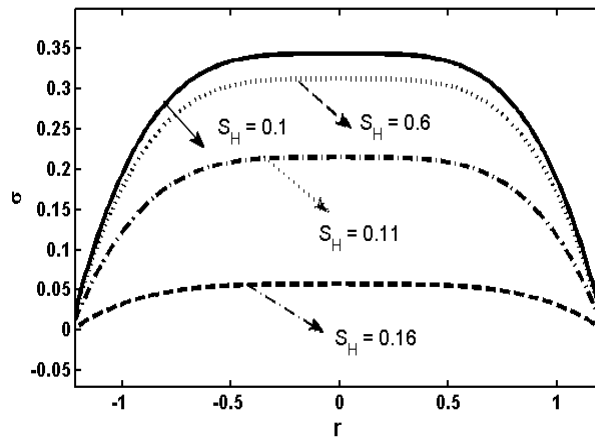


FIGURE 4.9: Variation of nanoparticle concentration graph for S_H when $M = 0.09$, $Z = 0.2$, $S_T = 0.8$, $\lambda = 0.1$, $\epsilon = 0.22$, $b = 0.01$.

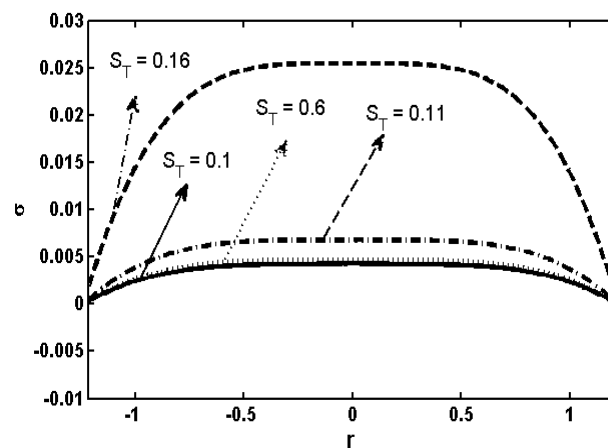


FIGURE 4.10: Variation of nanoparticle concentration graph for S_T when $M = 0.09$, $Z = 0.2$, $b = 0.01$, $\lambda = 0.1$, $\epsilon = 0.22$, $S_H = 0.8$.

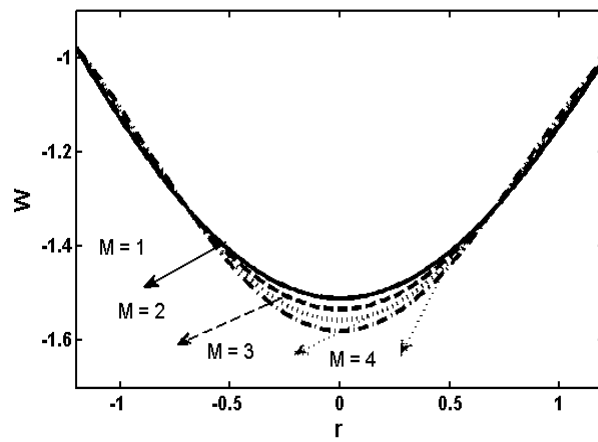


FIGURE 4.11: Variation of velocity graph for M when $b = 0.01$, $Z = 0.2$, $S_T = 0.8$, $\lambda = 0.1$, $\epsilon = 0.22$, $S_H = 0.8$.

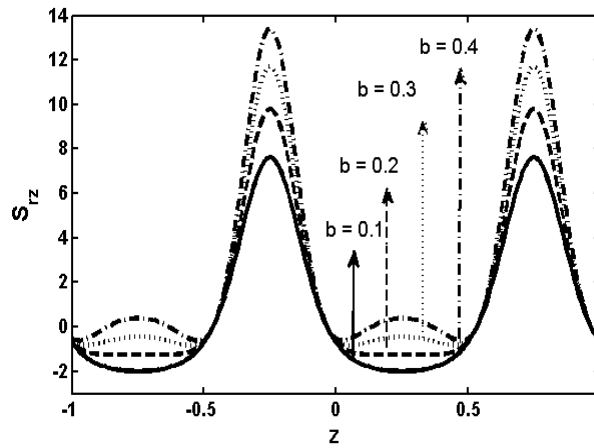


FIGURE 4.12: Variation of shear stress graph for b when $M = 0.09$, $Z = 0.2$, $S_T = 0.8$, $\lambda = 0.1$, $\epsilon = 0.22$, $S_H = 0.8$.

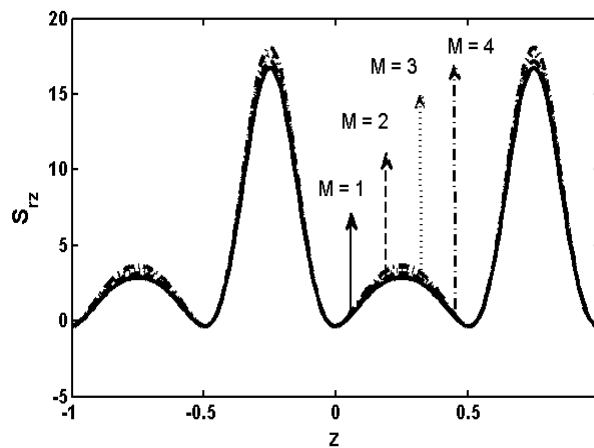


FIGURE 4.13: Variation of shear stress graph for M when $b = 0.01$, $Z = 0.2$, $S_T = 0.8$, $\lambda = 0.1$, $\epsilon = 0.22$, $S_H = 0.8$.

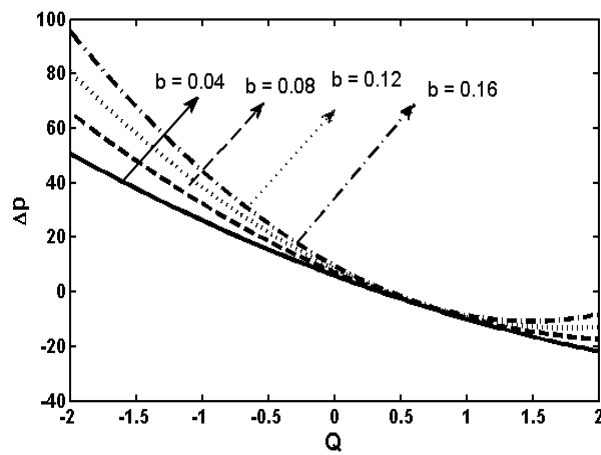


FIGURE 4.14: Variation of pressure rise graph for b when $M = 0.09$, $Z = 0.2$, $S_T = 0.8$, $\lambda = 0.1$, $\epsilon = 0.22$, $S_H = 0.8$.

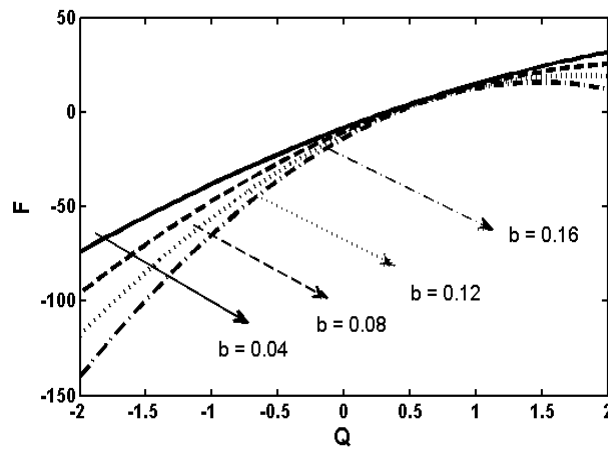


FIGURE 4.15: Variation of frictional forces graph for b when $M = 0.09$, $Z = 0.2$, $S_T = 0.8$, $\lambda = 0.1$, $\epsilon = 0.22$, $S_H = 0.8$.

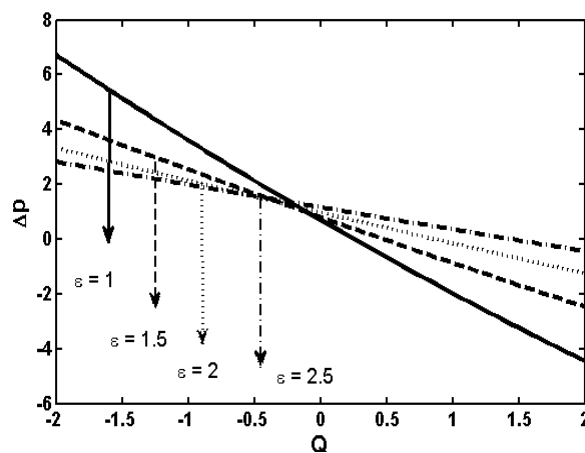


FIGURE 4.16: Variation of pressure rise graph for ϵ when $M = 0.09$, $Z = 0.2$, $S_T = 0.8$, $\lambda = 0.1$, $b = 0.01$, $S_H = 0.8$.

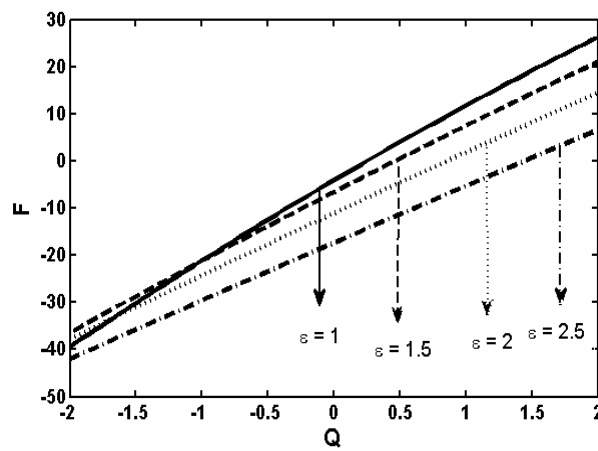


FIGURE 4.17: Variation of frictional forces graph for ϵ when $M = 0.09$, $Z = 0.2$, $S_T = 0.8$, $\lambda = 0.1$, $b = 0.01$, $S_H = 0.8$.

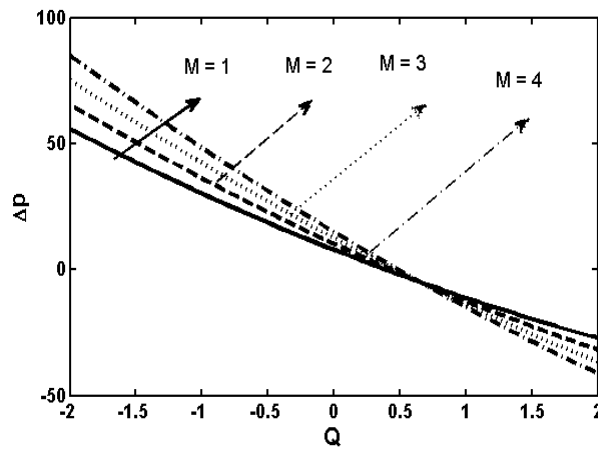


FIGURE 4.18: Variation of pressure rise for M when $b = 0.01$, $Z = 0.2$, $S_T = 0.8$, $\lambda = 0.1$, $\epsilon = 0.22$, $S_H = 0.8$.

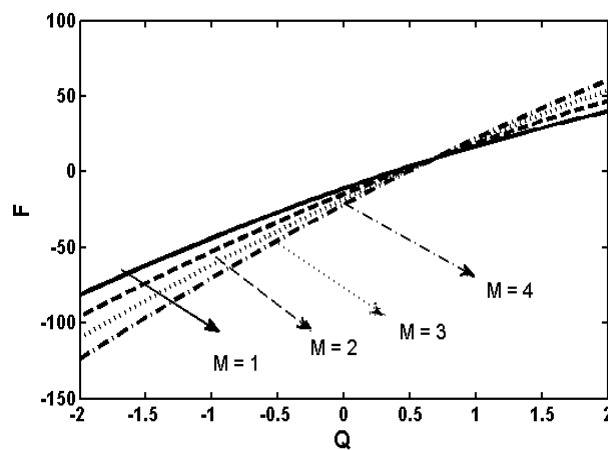


FIGURE 4.19: Variation of frictional forces for M when $b = 0.01$, $Z = 0.2$, $S_T = 0.8$, $\lambda = 0.1$, $\epsilon = 0.22$, $S_H = 0.8$.

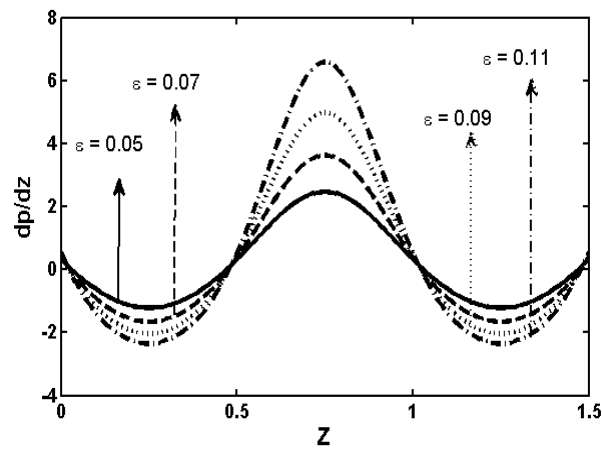


FIGURE 4.20: Pressure gradient $\frac{dp}{dz}$ for sinusoidal wave when $M = 0.09$, $Z = 0.2$, $S_T = 0.8$, $\lambda = 0.1$, $b = 0.01$, $S_H = 0.8$.

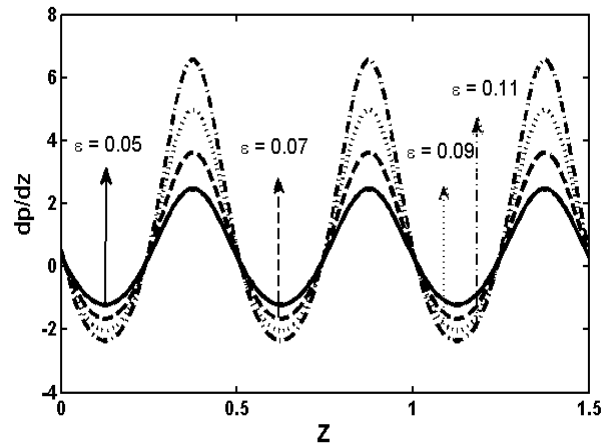


FIGURE 4.21: Pressure gradient $\frac{dp}{dz}$ for multisinusoidal wave when $M = 0.09$, $Z = 0.2$, $S_T = 0.8$, $\lambda = 0.1$, $b = 0.01$, $S_H = 0.8$.

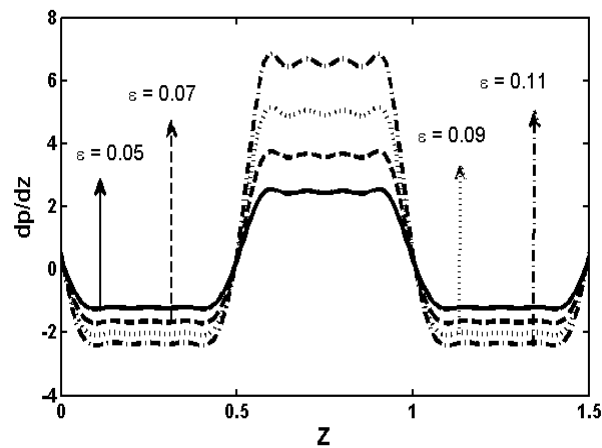


FIGURE 4.22: Pressure gradient $\frac{dp}{dz}$ for Trapezoidal wave when $M = 0.09$, $Z = 0.2$, $S_T = 0.8$, $\lambda = 0.1$, $b = 0.01$, $S_H = 0.8$.

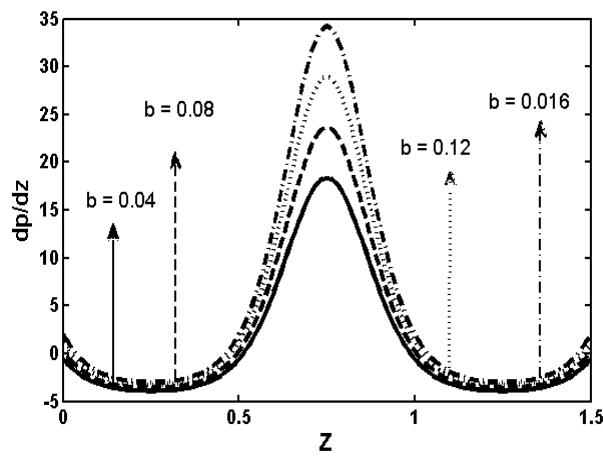


FIGURE 4.23: Pressure gradient $\frac{dp}{dz}$ for b when $M = 0.09$, $Z = 0.2$, $S_T = 0.8$, $\lambda = 0.1$, $\epsilon = 0.01$, $S_H = 0.8$.

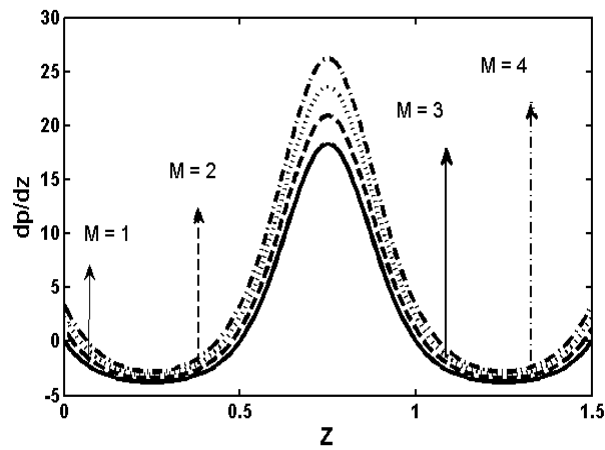


FIGURE 4.24: Pressure gradient $\frac{dp}{dz}$ for M when $\epsilon = 0.22$, $Z = 0.2$, $S_T = 0.8$, $\lambda = 0.1$, $b = 0.01$, $S_H = 0.8$.

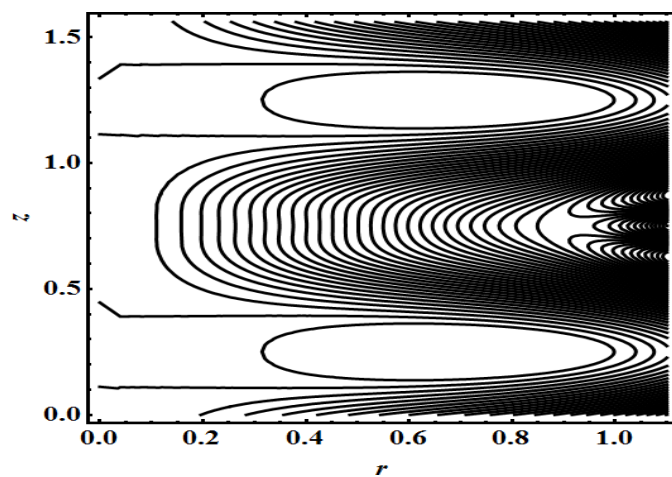


FIGURE 4.25: Streamlines pattern for sinusoidal wave $M = 0.09$, $Z = 0.2$, $S_T = 0.8$, $\lambda = 0.1$, $b = 0.01$, $S_H = 0.8$.

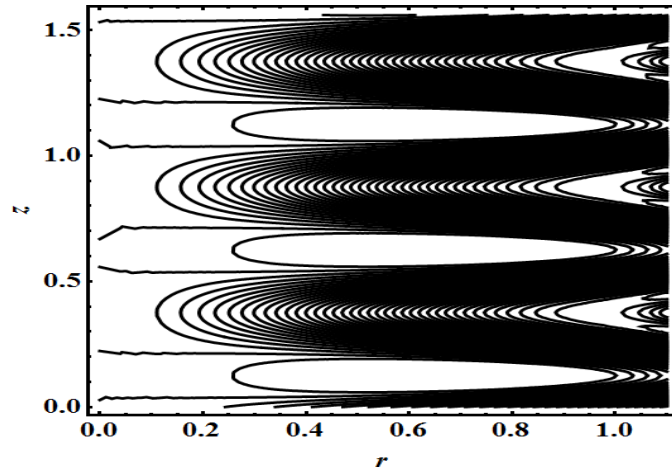


FIGURE 4.26: Streamlines pattern for multisinusoidal wave $M = 0.09$, $Z = 0.2$, $S_T = 0.8$, $\lambda = 0.1$, $b = 0.01$, $S_H = 0.8$.

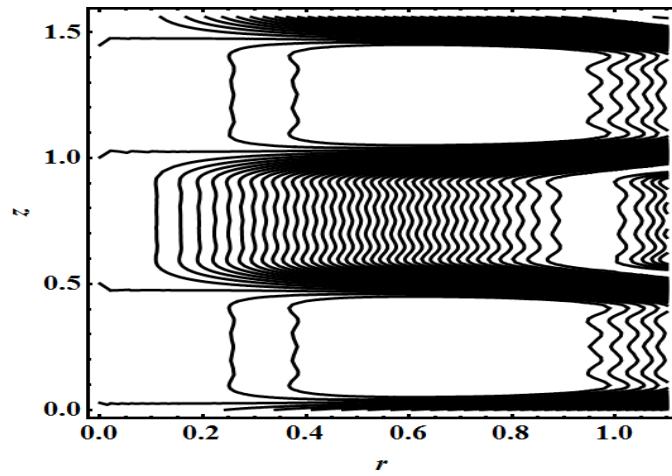


FIGURE 4.27: Streamlines pattern for Trapezoidal wave $M = 0.09$, $Z = 0.2$, $S_T = 0.8$, $\lambda = 0.1$, $b = 0.01$, $S_H = 0.8$.

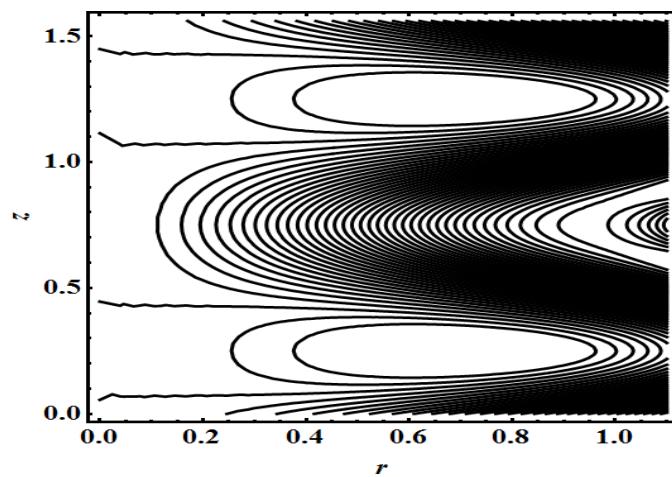


FIGURE 4.28: Streamlines pattern for $b = 0.01$ when $M = 0.09$, $Z = 0.2$, $S_T = 0.8$, $\lambda = 0.1$, $\epsilon = 0.01$, $S_H = 0.8$.

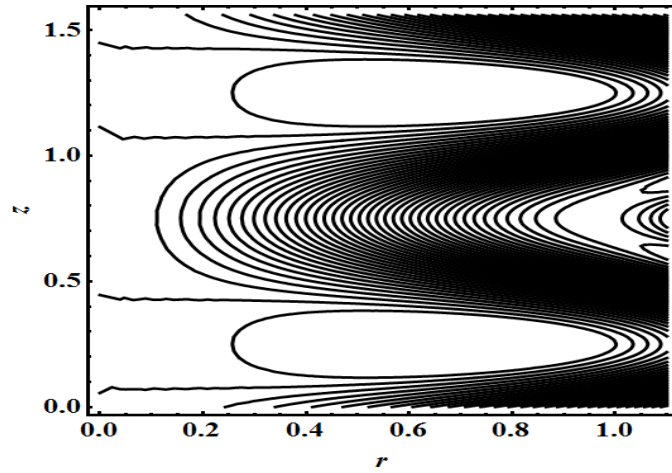


FIGURE 4.29: Streamlines pattern for $b = 0.02$ when $M = 0.09$, $Z = 0.2$, $S_T = 0.8$, $\lambda = 0.1$, $\epsilon = 0.01$, $S_H = 0.8$.

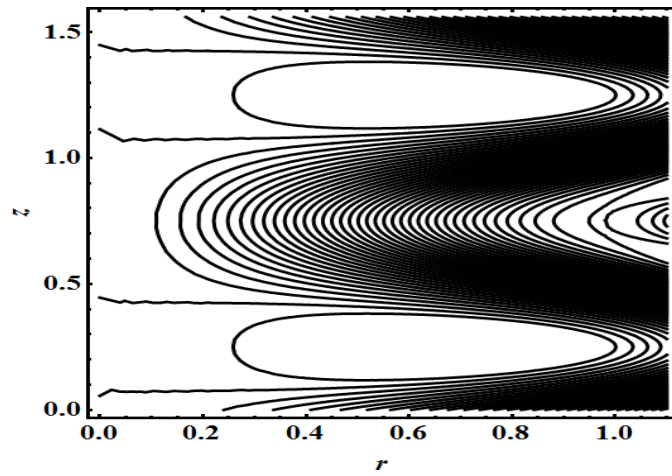


FIGURE 4.30: Streamlines pattern for $b = 0.03$ when $M = 0.09$, $Z = 0.2$, $S_T = 0.8$, $\lambda = 0.1$, $\epsilon = 0.01$, $S_H = 0.8$.

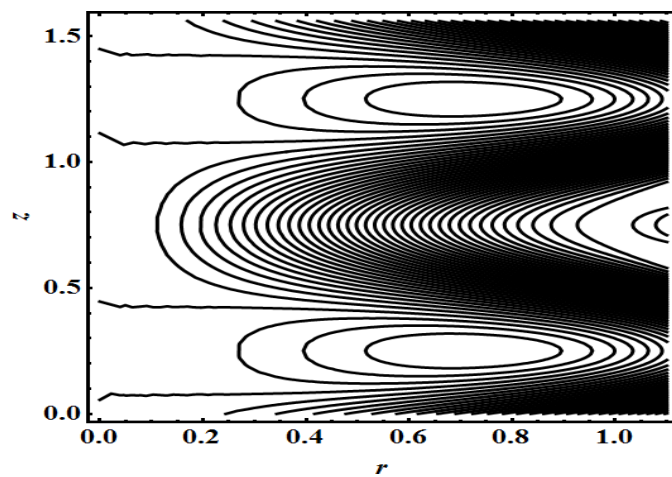


FIGURE 4.31: Streamlines pattern for $b = 0.04$ when $M = 0.09$, $Z = 0.2$, $S_T = 0.8$, $\lambda = 0.1$, $\epsilon = 0.01$, $S_H = 0.8$.

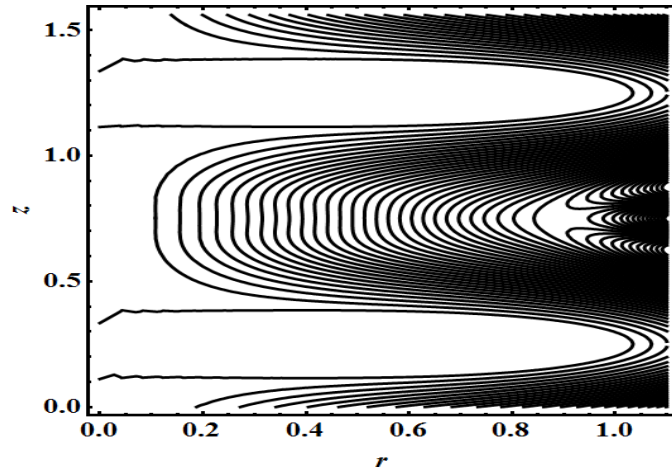


FIGURE 4.32: Streamlines pattern for $M = 1$ when $\epsilon = 0.09$, $Z = 0.2$, $S_T = 0.8$, $\lambda = 0.1$, $b = 0.01$, $S_H = 0.8$.

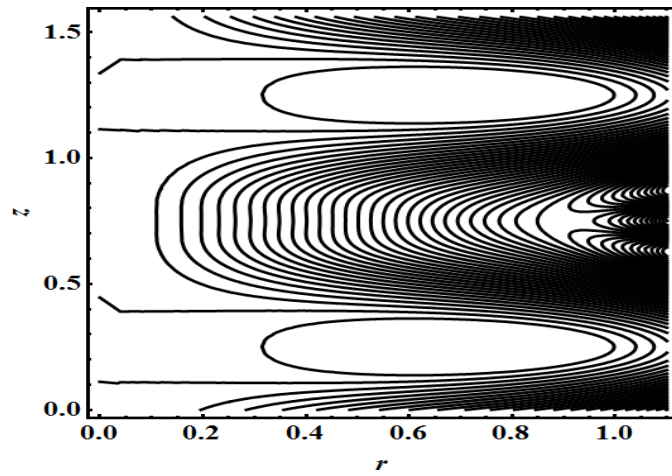


FIGURE 4.33: Streamlines pattern for $M = 2$ when $\epsilon = 0.09$, $Z = 0.2$, $S_T = 0.8$, $\lambda = 0.1$, $b = 0.01$, $S_H = 0.8$.

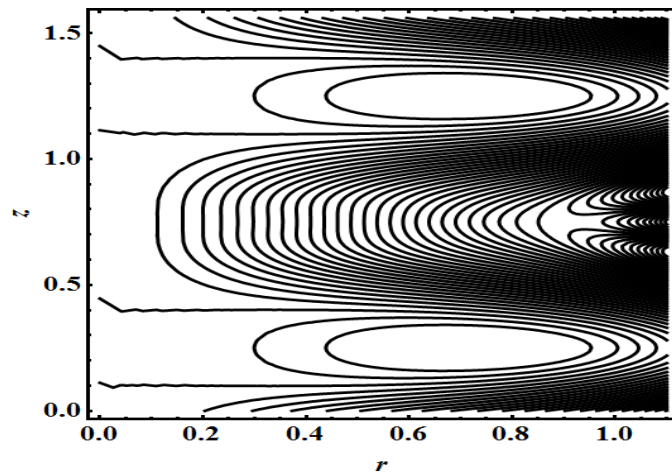


FIGURE 4.34: Streamlines pattern for $M = 3$ when $\epsilon = 0.09$, $Z = 0.2$, $S_T = 0.8$, $\lambda = 0.1$, $b = 0.01$, $S_H = 0.8$.

4.4 Conclusion

In this chapter, we have analysed the peristaltic flow of non-Newtonian fluid with convective boundary conditions in a uniform tube. The viscous dissipation effects are also taken into account. The main findings of the present study are as follow:

- The temperature profile is enhanced for the increasing values of sisko fluid parameter (b), Magnetohydrodynamics (M) and Brinkman number (B_k) and decreases by increasing the values of κ .
- The concentration field is increases by increasing the values of b, M, B_k and decreases by increasing the values of S_H .
- The pressure gradient increases with the increasing value of b, M .
- There is an opposite behavior between pressure rise and the frictional forces.
- The velocity profile decreases with the increasing value of M .
- Streamlines bolas take the form of the shape of the geometry.

Chapter 5

Physiological flow of Carreau fluid due to ciliary motion

This chapter deals with the physiological flow of Carreau fluid due to ciliary motion inside a symmetric channel. The main purpose of this chapter is to present a mathematical model of ciliary motion in an annulus. In this analysis, the symmetric channel of a non-Newtonian fluid is observed in an annulus with ciliated tips. The governing equations of non-Newtonian fluid are modelled and simplified by using low Reynolds number and long wavelength assumptions. The velocity equation is solved by utilizing the homotopy perturbation technique in terms of a variant of small dimensionless parameter p . The obtained expressions for the velocity profiles are plotted and the impact of different physical parameters are investigated for different peristaltic waves.

5.1 Model of the Problem

We have considered the ciliary motion phenomenon for the two dimensional flow of an incompressible fluid in an annulus. A metachronal wave is travelling with a constant velocity c_1 that is generated due to collective beating of cilia along the walls of the channel whose inner surfaces are ciliated. We are considering the cartesian coordinates X, Y . Here X-axis is taken along the center of the body and Y-axis is the normal direction. The geometry of the problem is shown in Figure [6.1](#).

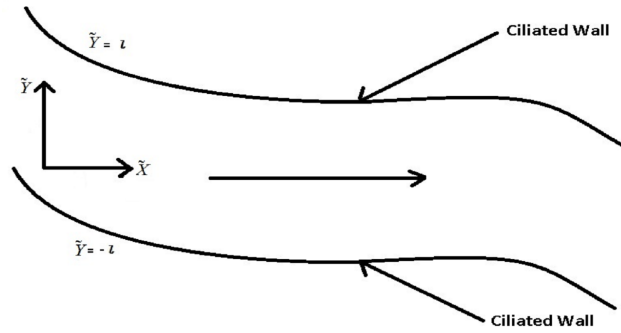


FIGURE 5.1: A physical sketch of the problem

The fundamental equations of continuity, momentum in the absence of body forces can be written as

$$\frac{\partial \bar{U}}{\partial \bar{X}} + \frac{\partial \bar{V}}{\partial \bar{Y}} = 0, \quad (5.1)$$

$$\rho \left[\frac{\partial \bar{U}}{\partial \bar{t}} + \bar{U} \frac{\partial \bar{U}}{\partial \bar{X}} + \bar{V} \frac{\partial \bar{U}}{\partial \bar{Y}} \right] = -\frac{\partial \bar{P}}{\partial \bar{X}} + \frac{\partial \bar{\tau}_{xx}}{\partial \bar{X}} + \frac{\partial \bar{\tau}_{xy}}{\partial \bar{Y}} + \frac{\partial \bar{\tau}_{xz}}{\partial \bar{Z}}, \quad (5.2)$$

$$\rho \left[\frac{\partial \bar{V}}{\partial \bar{t}} + \bar{U} \frac{\partial \bar{V}}{\partial \bar{X}} + \bar{V} \frac{\partial \bar{V}}{\partial \bar{Y}} \right] = -\frac{\partial \bar{P}}{\partial \bar{Y}} + \frac{\partial \bar{\tau}_{yx}}{\partial \bar{X}} + \frac{\partial \bar{\tau}_{yy}}{\partial \bar{Y}} + \frac{\partial \bar{\tau}_{yz}}{\partial \bar{Z}}, \quad (5.3)$$

where \bar{P} represents the pressure and \bar{U}, \bar{V} represents the velocity components. The constitutional equation for a Carreau fluids defined as

$$\boldsymbol{\tau} = [\mu_\infty + (\mu_0 - \mu_\infty)] [1 + (\Gamma\boldsymbol{\gamma})^2]^{\frac{n-1}{2}} \boldsymbol{\gamma}, \quad (5.4)$$

$$\boldsymbol{\gamma} = \sqrt{\frac{1}{2} \sum \sum \boldsymbol{\gamma}_{ij} \boldsymbol{\gamma}_{ij}} = \sqrt{\frac{1}{2} \Pi \boldsymbol{\gamma}_{ij}}, \quad (5.5)$$

where Π is the second invariant of the strain tensor $\boldsymbol{\gamma}_{ij}$. We examine the constitutive equations in the case when $\mu_\infty = 0$ and $\Gamma\boldsymbol{\gamma} \ll 1$. Therefore, we write the extra stress component as

$$\boldsymbol{\tau} = \mu_0 \left[1 + \left(\frac{n-1}{2} \right) \Gamma^2 \boldsymbol{\gamma}^2 \right] \boldsymbol{\gamma}, \quad (5.6)$$

where

$$\mathbf{\Upsilon}_{ij} = \bar{\mathbf{T}} = (\nabla \cdot \mathbf{V}) + (\nabla \cdot \mathbf{V})^t. \quad (5.7)$$

The envelops of the cilia tips can be expressed mathematically as

$$\bar{Y} = j(\bar{X}, \bar{t}) = \pm \left[d + d\epsilon \cos\left(\frac{2\pi}{\lambda}\right)(\bar{X} - c\bar{t}) \right] = \pm l, \quad (5.8)$$

$$\bar{X} = k(\bar{X}, \bar{t}) = \bar{X}_0 + \epsilon\alpha d \sin\left(\frac{2\pi}{\lambda}\right)(\bar{X} - c\bar{t}) = \pm l, \quad (5.9)$$

The horizontal velocities of the cilia are

$$\bar{U}_0 = -\frac{\left(\frac{2\pi}{\lambda}\right)(\epsilon\alpha d c \cos\left(\frac{2\pi}{\lambda}\right)(\bar{X} - c\bar{t}))}{1 - \left(\frac{2\pi}{\lambda}\right)(\epsilon\alpha d c \cos\left(\frac{2\pi}{\lambda}\right)(\bar{X} - c\bar{t}))}, \quad (5.10)$$

$$\bar{V}_0 = -\frac{\left(\frac{2\pi}{\lambda}\right)(\epsilon\alpha d c \sin\left(\frac{2\pi}{\lambda}\right)(\bar{X} - c\bar{t}))}{1 - \left(\frac{2\pi}{\lambda}\right)(\epsilon\alpha d c \cos\left(\frac{2\pi}{\lambda}\right)(\bar{X} - c\bar{t}))}. \quad (5.11)$$

The non-dimensional variables are stated as

$$\begin{aligned} X &= \frac{\bar{X}}{\lambda}, & Y &= \frac{\bar{Y}}{d}, & h &= \frac{l}{d}, & \gamma &= \frac{d}{\lambda}, \\ t &= \frac{c\bar{t}}{\lambda}, & V &= \frac{\bar{V}}{\gamma c}, & V_0 &= \frac{\bar{V}_0}{\gamma c}, & p &= \frac{d^2 \bar{p}}{c\lambda\mu_0}, \\ U &= \frac{\bar{U}}{c}, & U_0 &= \frac{\bar{U}_0}{c}, & R_e &= \frac{\rho c d}{\mu_0}, & \mathbf{\Upsilon} &= \frac{d\bar{\mathbf{\Upsilon}}}{c}, \\ W_e &= \frac{\Gamma c}{d}, & \tau_{xx} &= \frac{d}{\mu_0 c} \bar{\tau}_{xx}, & \tau_{xy} &= \frac{d}{\mu_0 c} \bar{\tau}_{xy}, \\ \tau_{yx} &= \frac{d}{\mu_0 c} \bar{\tau}_{yx}, & \tau_{yy} &= \frac{d}{\mu_0 c} \bar{\tau}_{yy}. \end{aligned}$$

The transformation between two frames are

$$X = x + t, \quad Y = y,$$

$$U = u + 1, \quad V = v.$$

Under the assumption of low Reynolds number and long wavelength $\gamma \ll 1$ are estimated

$$\frac{\partial u}{\partial x} + \frac{\partial v}{\partial y} = 0, \quad (5.12)$$

$$R_e \gamma \left[u \frac{\partial u}{\partial x} + v \frac{\partial u}{\partial y} \right] = -\frac{\partial p}{\partial x} + \gamma \frac{\partial \tau_{xx}}{\partial x} + \frac{\partial \tau_{xy}}{\partial y}, \quad (5.13)$$

$$R_e \gamma^3 \left[u \frac{\partial v}{\partial x} + v \frac{\partial v}{\partial y} \right] = -\frac{\partial p}{\partial y} + \gamma^2 \frac{\partial \tau_{yx}}{\partial x} + \gamma^2 \frac{\partial \tau_{yy}}{\partial y}. \quad (5.14)$$

The extra stress tensor can be written as

$$\begin{aligned} \tau_{xx} &= 2\gamma \left[1 + \left(\frac{n-1}{2} \right) W_e^2 \gamma^2 \right] \left(\frac{\partial u}{\partial x} \right), \\ \tau_{xy} &= \tau_{yx} = \left[1 + \left(\frac{n-1}{2} \right) W_e^2 \gamma^2 \right] \left(\frac{\partial u}{\partial y} + \gamma^2 \frac{\partial v}{\partial x} \right), \\ \tau_{yy} &= 2\gamma \left[1 + \left(\frac{n-1}{2} \right) W_e^2 \gamma^2 \right] \left(\frac{\partial v}{\partial y} \right). \end{aligned}$$

The boundary conditions are reduced as

$$u_0 = -1 - \frac{2\xi\pi\gamma\delta \cos(2\pi x)}{1 - 2\pi\xi\delta\gamma \cos(2\pi x)}, \quad (5.15)$$

$$v_0 = \frac{2\pi\xi\delta\gamma \sin(2\pi x)}{1 - 2\pi\xi\delta\gamma \cos(2\pi x)}, \text{ at } y = \pm h = \pm [1 + \xi \cos(2\pi x)], \quad (5.16)$$

where ξ represents the length of cilia, δ is eccentricity of path and γ is ratio.

5.2 Solution Methodology

We use the homotopy perturbation method to solve the Eq. (5.13)

$$-\frac{dP}{dx} + \frac{\partial \tau_{xy}}{\partial y} = 0, \quad (5.17)$$

$$-\frac{dP}{dx} + \frac{\partial^2 u}{\partial y^2} + \frac{3(n-1)W_e^2}{2} \left(\frac{\partial u}{\partial y} \right)^2 \frac{\partial^2 u}{\partial y^2} = 0. \quad (5.18)$$

The boundary conditions are reduced as

$$\begin{aligned} \frac{\partial u}{\partial y} &= 0, & \text{at } y &= 0, \\ u_0 &= -1 - 2\xi\pi\gamma\delta \cos(2\pi x), & \text{at } y &= h = 1 + \epsilon \cos(2\pi x), \end{aligned}$$

since the above boundary value problem is non-linear. Thus it is appropriate to solve it analytically with the help of homotopy perturbation method. According to HPM, we determine L is the linear operator and N is the non-linear operator as

$$L = \frac{\partial^2(\cdot)}{\partial y^2}, \quad (5.19)$$

$$N = -\frac{dP}{dx} + \frac{\partial^2(\cdot)}{\partial y^2} + \frac{3(n-1)W_e^2}{2} \left(\frac{\partial(\cdot)}{\partial y} \right)^2 \frac{\partial^2(\cdot)}{\partial y^2}. \quad (5.20)$$

We construct a homotopy $v(r, p) : \Omega \times [0, 1] \rightarrow \mathcal{R}$ which satisfy

$$H(v, p) = (1-p)[L(v) - L(w_0)] + p[L(v) + N(v) - g(r)] = 0. \quad (5.21)$$

Thus it is appropriate to solve it analytically with the help of Homotopy perturbation method (HPM)

$$(1-p) \left[\frac{\partial^2 v}{\partial y^2} - \frac{\partial^2 w_0}{\partial y^2} \right] + p \left[-\frac{dP}{dx} + \frac{\partial^2(v)}{\partial y^2} + \frac{3(n-1)W_e^2}{2} \left(\frac{\partial(v)}{\partial y} \right)^2 \frac{\partial^2(v)}{\partial y^2} \right] = 0. \quad (5.22)$$

The corresponding boundary conditions are defined as

$$\begin{aligned} \frac{\partial u}{\partial y} &= 0, & \text{at } y &= 0, \\ u_0 &= -1 - 2\xi\pi\gamma\delta \cos(2\pi x), & \text{at } y &= h = 1 + \epsilon \cos(2\pi x). \end{aligned}$$

Let us define

$$\begin{aligned} v &= v_0 + pv_1 + p^2v_2 + \dots \\ P &= P_1 + pP_2 + p^2P_3 + \dots \\ q &= q_0 + pq_1 + p^2q_2 + \dots \end{aligned}$$

We take the initial guess which is satisfy the boundary conditions

$$w_0 = u_0 + \left(\frac{y^2 - h^2}{2} \right) \frac{dP_0}{dx}. \quad (5.23)$$

The solutions for the velocity satisfying the relative boundary condition are directly written as

$$u = u_0 + \left(\frac{y^2 - h^2}{2} \right) \frac{dP}{dx} + \frac{(n-1)W_e^2(y^4 - h^4) \left(\frac{dp_0}{dx} \right)^3}{4} \quad (5.24)$$

$$- \frac{3}{8}(n-1)W_e^2(y^4 - h^4) \left(\frac{dp_0}{dx} \right)^2 \frac{dp_1}{dx} + \frac{1}{8}(n-1)^2W_e^4(y^6 - h^6) \left(\frac{dp_0}{dx} \right)^5.$$

Volume of the flow rate in dimensionless form is defined as

$$q = \int_0^h u dy. \quad (5.25)$$

The expression for volume flow rate is defined as

$$q = u_0 h - \frac{h^3}{3} \left(\frac{dp}{dx} \right) + \frac{2(n-1)W_e^2 h^4 \left(\frac{dp_0}{dx} \right)^3}{5} + \frac{3}{10}(n-1)W_e^2 h^5 \left(\frac{dp_0}{dx} \right)^2 \frac{dp_1}{dx} \quad (5.26)$$

$$- \frac{3}{28}(n-1)^2 W_e^4 h^7 \left(\frac{dp_0}{dx} \right)^5.$$

The expression for pressure gradient is defined as

$$\frac{dp}{dx} = \frac{3}{h^3} \left[-Q + u_0 h - \frac{h^3}{3} \left(\frac{dp}{dx} \right) + \frac{2(n-1)W_e^2 h^4 \left(\frac{dp_0}{dx} \right)^3}{5} \right] \quad (5.27)$$

$$+ \left[\frac{3}{10}(n-1)W_e^2 h^5 \left(\frac{dp_0}{dx} \right)^2 \frac{dp_1}{dx} - \frac{3}{28}(n-1)^2 W_e^4 h^7 \left(\frac{dp_0}{dx} \right)^5 \right].$$

The Δp is defined as

$$\Delta p = \int_0^1 \frac{dP}{dx} dx. \quad (5.28)$$

Velocities in terms of streamfunction are defined as

$$\frac{\partial \Psi}{\partial x} = -v, \quad \frac{\partial \Psi}{\partial y} = u. \quad (5.29)$$

The streamfunction is defined as

$$\begin{aligned} \Psi = u_0 y + \left(\frac{y^3}{6} - \frac{y h^2}{2} \right) \frac{dP}{dx} + \frac{(n-1) W_e^2 \left(\frac{y^5}{5} - h^4 y \right) \left(\frac{dp_0}{dx} \right)^3}{4} \\ - \frac{3}{8} (n-1) W_e^2 \left(\frac{y^5}{5} - h^4 y \right) \left(\frac{dp_0}{dx} \right)^2 \frac{dp_1}{dx}. \end{aligned} \quad (5.30)$$

5.3 Results and discussions

In this section, we have discussed the solution for Physiological flow of Carreau fluid due to ciliary motion. The expression for velocity, pressure rise, pressure gradient and streamlines are calculated numerically. Figures 5.2-5.5 show the velocity profile for diverse values of n (power law index), W_e (Weissenberg number), Q , ξ , δ and γ . Figures 5.2-5.3 show that with the increase in n (power law index), W_e (Weissenberg number) velocity profile decreases. Figure 5.4 show that velocity profile gets increasing function in the region $(-1 \leq y \leq -0.5, 0.5 \leq y \leq 1.0)$ whereas it get opposite behaviour in the region $(-0.6 \leq y \leq 0.6)$. From figure 5.5 it is seen that with the increase in Q velocity profile also increases. Figures 5.6-5.8 show the pressure gradient for different values of Q, n . It is depicted that with the increase in n and Q pressure gradient decreases. From figure 5.9 it is seen that pressure gradient gets decreasing function in the region $(-0.7 \leq x \leq -0.3, 0.3 \leq y \leq 0.7)$ whereas it get opposite behaviour in the region $(-0.2 \leq x \leq 0.2)$. Figures 5.10-5.11 it is depicted that at the centre of the channel pressure gradient decreases whereas it get opposite behaviour nearest of the channel. Figures 5.12-5.15 show the pressure rise for diverse values of n (power law index), W_e (Weissenberg number), Q , ξ , δ and γ . It is depicted that with the increase in n, W_e, γ, δ pressure rise increases. From figure 5.16 it is depicted that by increasing value of ξ (length of cilia tips) pressure rise increases in the region $(Q \in [-1.5, 0.01])$ whereas reflux occur in the last.

The retrograde pumping region can also be seen in Figure 5.16 when $Q < 0$ and $\Delta p > 0$ and free pumping region can be seen when $Q = 0$ and $\Delta p = 0$. Moreover, augmented pumping region can also be seen in figure 5.16 when $Q > 0$ and $\Delta p < 0$. Figures 5.17-5.28 illustrate the streamlines for different value of ξ, Q, W_e . It is distinguish that the streamlines of the flow are affected in a related behaviour by increasing the value of W_e .

In fact it is pragmatic that the strength of trapped bolus appear in the wider part of the tube increases by increasing the value of W_e .

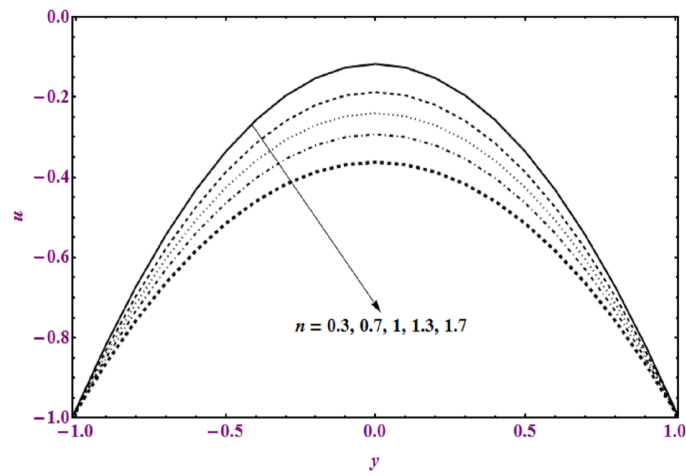


FIGURE 5.2: Variation of velocity for n when $Q = 0.3$, $\xi = 0.7$, $\delta = 0.8$, $\gamma = 0.7$, $W_e = 0.9$.

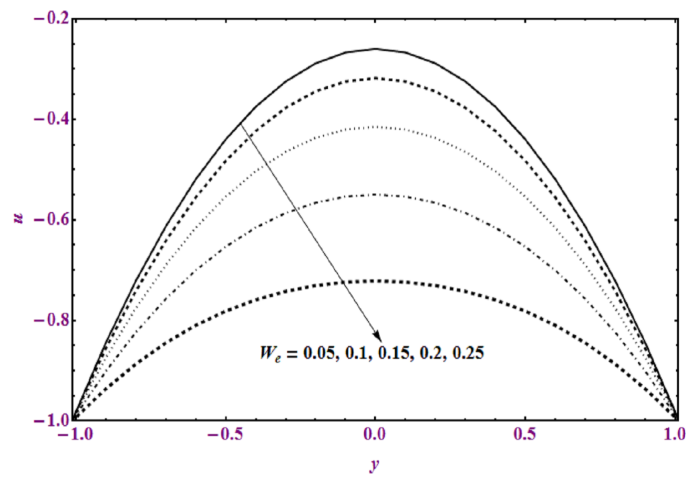


FIGURE 5.3: Variation of velocity for W_e when $\delta = 0.3$, $\xi = 0.7$, $\gamma = 0.8$, $Q = 0.7$, $W_e = 0.9$.

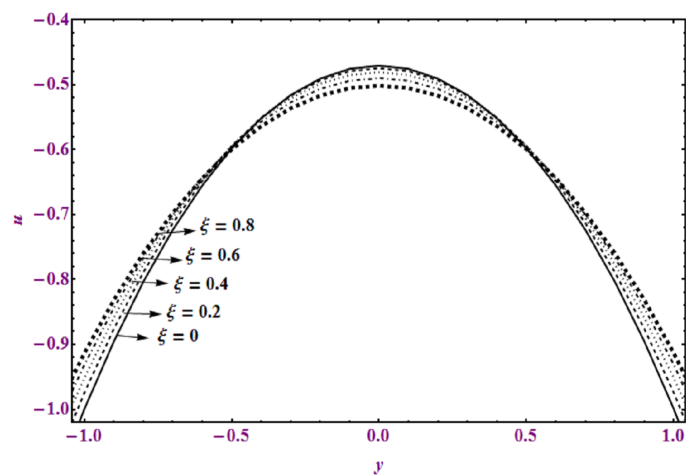


FIGURE 5.4: Variation of velocity for ξ when $\delta = 0.3$, $n = 0.7$, $\gamma = 0.8$, $Q = 0.7$, $W_e = 0.9$.

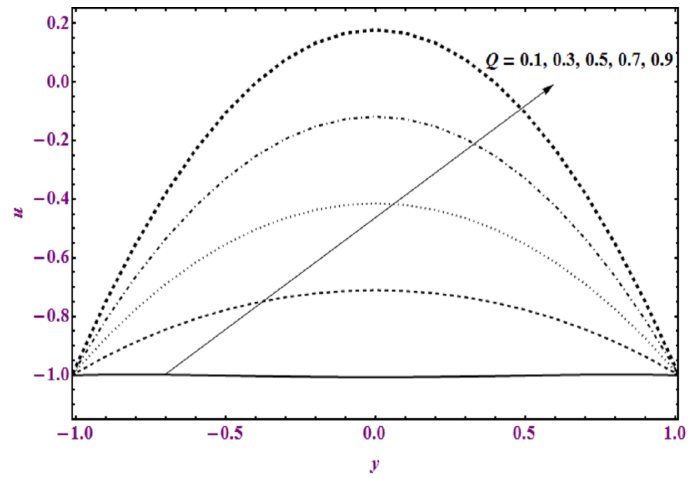


FIGURE 5.5: Variation of velocity for Q when $\delta = 0.3, \xi = 0.6, \gamma = 0.8, n = 0.2, W_e = 0.9$.

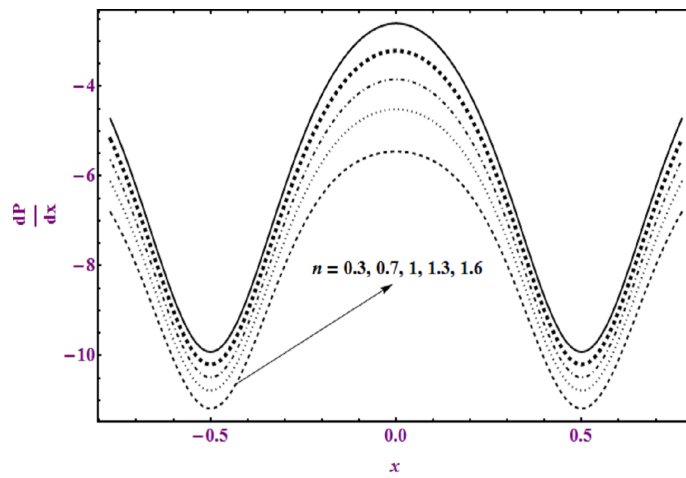


FIGURE 5.6: Variation of pressure gradient for n when $\delta = 0.3, \xi = 0.6, \gamma = 0.8, Q = 0.7, W_e = 0.9$.

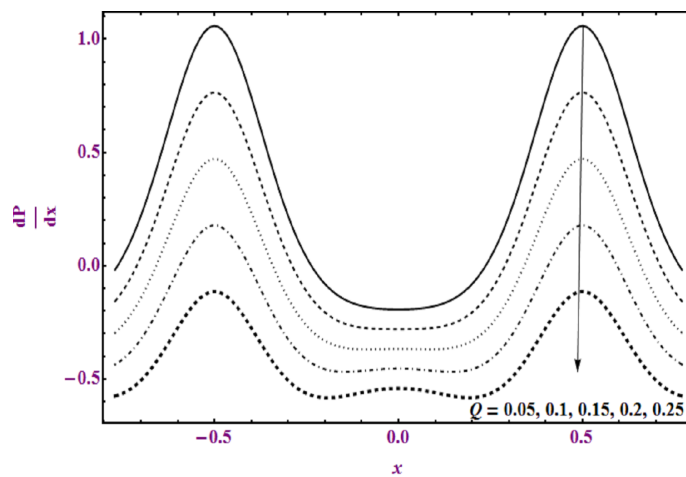


FIGURE 5.7: Variation of pressure gradient for Q when $\delta = 0.3, \xi = 0.6, \gamma = 0.8, n = 0.6, W_e = 0.9$.

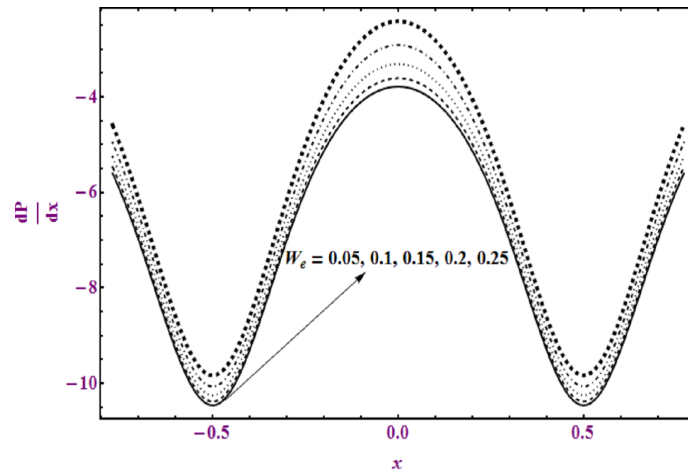


FIGURE 5.8: Variation of pressure gradient for W_e when $\gamma = 0.3, Q = 0.6, n = 0.8, \delta = 0.5, \xi = 0.6$.

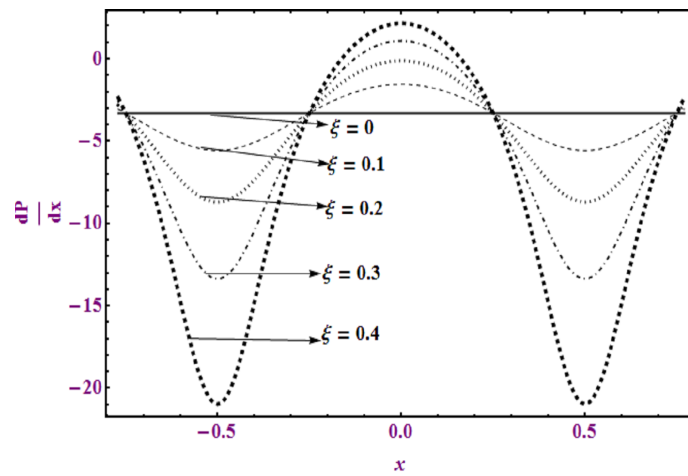


FIGURE 5.9: Variation of pressure gradient for ξ when $\gamma = 0.3, Q = 0.6, n = 0.8, W_e = 0.5, \delta = 0.9$.

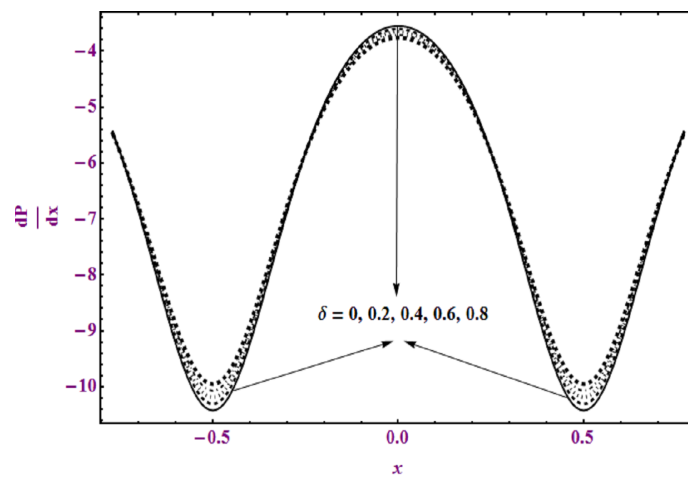


FIGURE 5.10: Variation of pressure gradient for δ when $\gamma = 0.6, Q = 0.5, \xi = 0.8, n = 0.5, W_e = 0.9$.

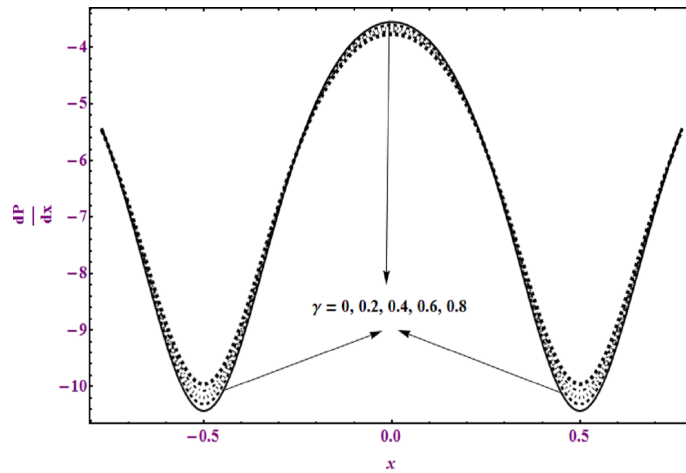


FIGURE 5.11: Variation of pressure gradient for γ when $\xi = 0.1, \delta = 0.1, Q = 0.1, W_e = 0.5, n = 0.3$.

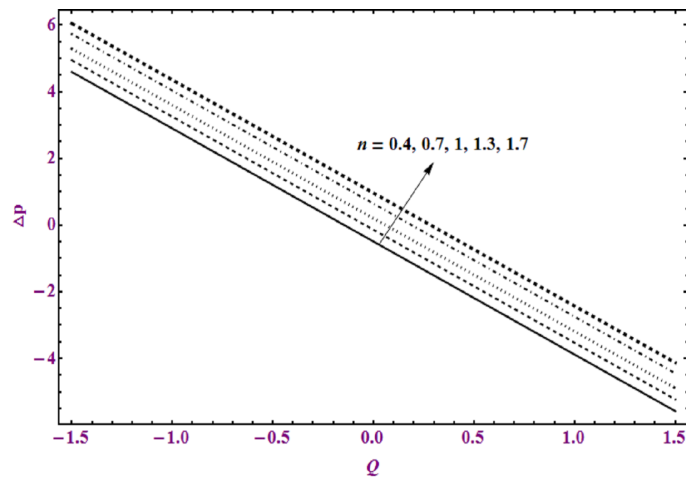


FIGURE 5.12: Variation of pressure gradient for n when $Q = 0.1, W_e = 0.1, \gamma = 0.1, \xi = 0.5, \delta = 0.3$.

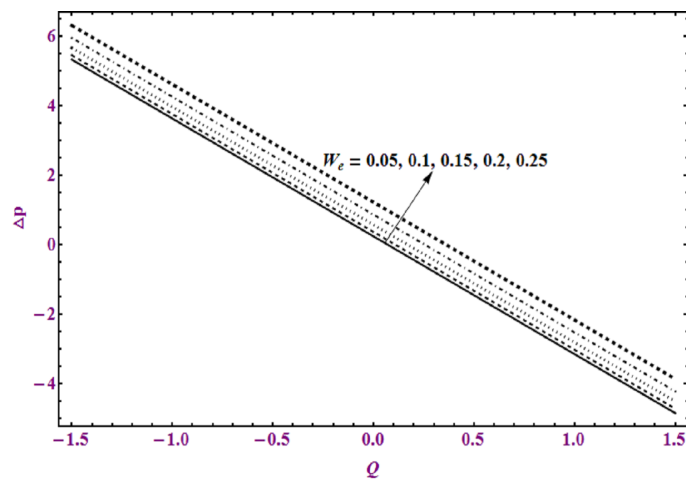


FIGURE 5.13: Variation of pressure rise for W_e when $Q = 0.1, n = 0.1, \xi = 0.1, \delta = 0.5, b = 0.3$.

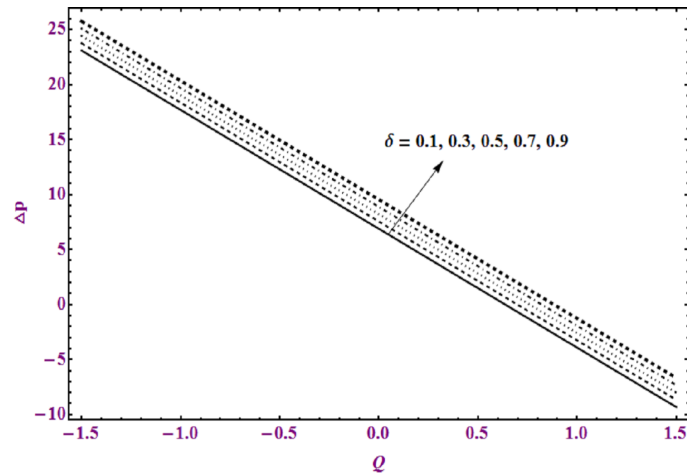


FIGURE 5.14: Variation of pressure rise for δ when $Q = 0.1, n = 0.1, \xi = 0.1, \gamma = 0.5, b = 0.3$.

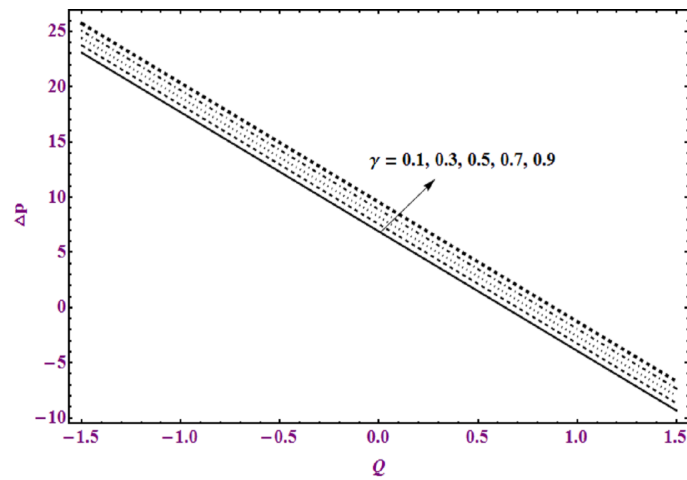


FIGURE 5.15: Variation of pressure rise for γ when $Q = 0.1, \xi = 0.1, b = 0.1, n = 0.5, W_e = 0.3$.

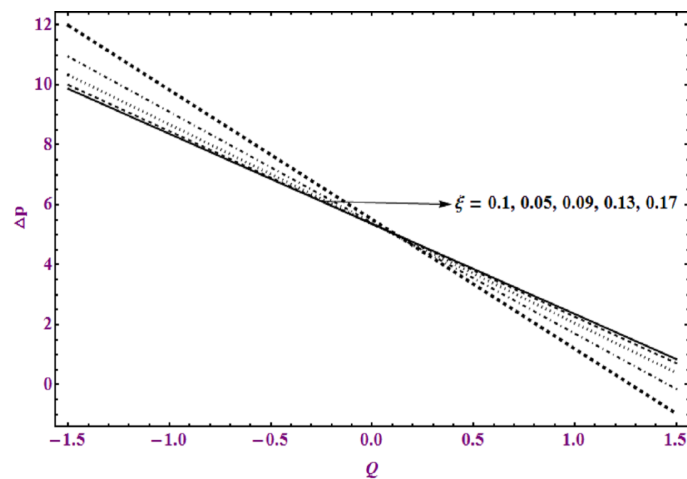


FIGURE 5.16: Variation of pressure rise for ξ when $Q = 0.1, b = 0.1, W_e = 0.1, n = 0.5, \gamma = 0.3$.

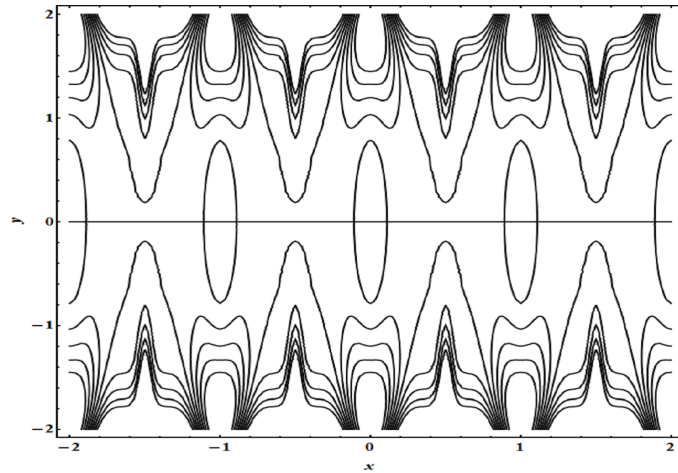


FIGURE 5.17: Streamlines for different value of $Q = 0.1, \xi = 0.1n = 0.1, W_e = 0.1, Q = 0.5, \gamma = 0.3$.

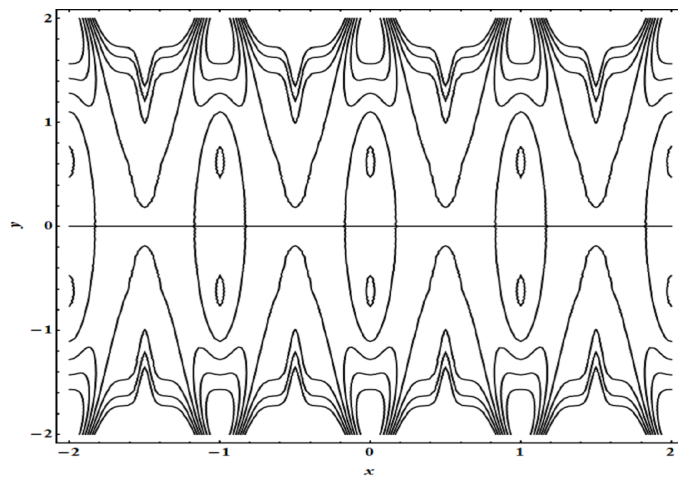


FIGURE 5.18: Streamlines for different value of $Q = 0.1, W_e = 0.1n = 0.1, \gamma = 0.1, \delta = 0.5, \xi = 0.3$.

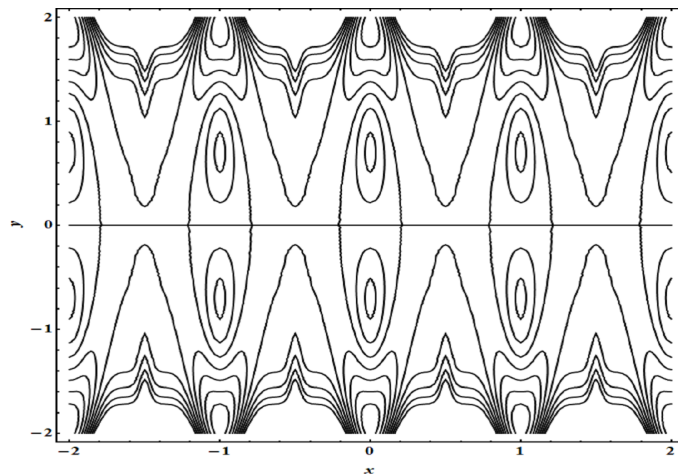


FIGURE 5.19: Streamlines for different value of $Q = 0.1, W_e = 0.1n = 0.1, \gamma = 0.1, \delta = 0.5, \xi = 0.3$.

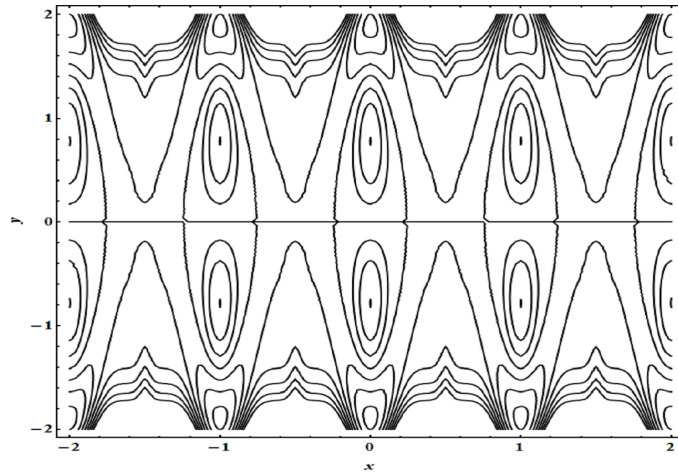


FIGURE 5.20: Streamlines for different value of $Q = 0.1, W_e = 0.1n = 0.1, \gamma = 0.1, \delta = 0.5, \xi = 0.3$.

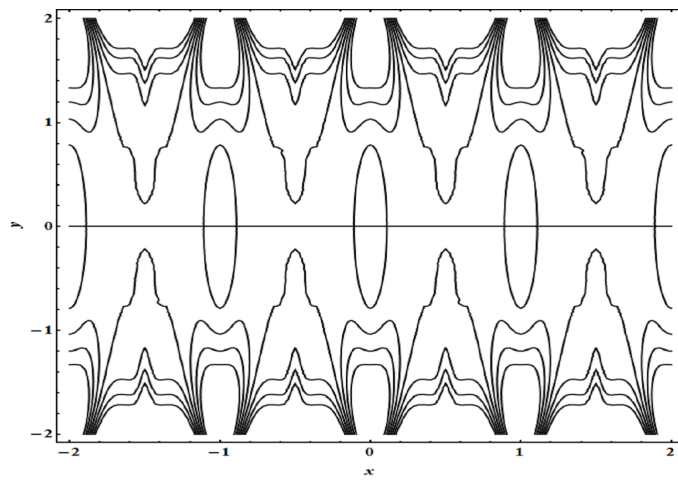


FIGURE 5.21: Streamlines for different value of $Q = 0.1, W_e = 0.1n = 0.1, \gamma = 0.1, \delta = 0.5, \xi = 0.3$.

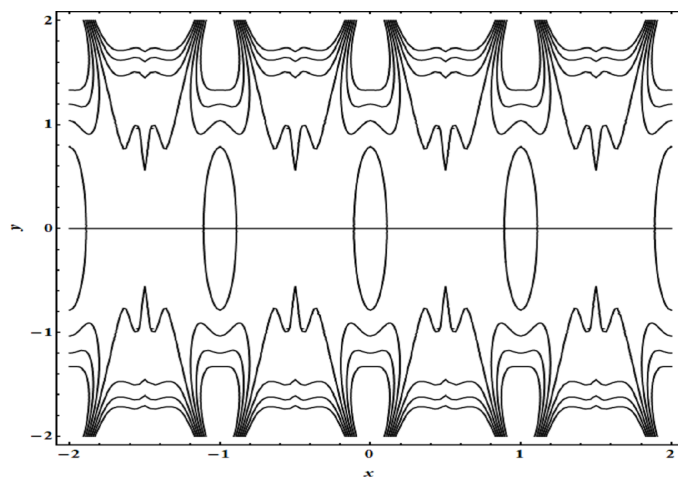


FIGURE 5.22: Streamlines for different value of $Q = 0.1, W_e = 0.1n = 0.1, \gamma = 0.1, \delta = 0.5, \xi = 0.3$.

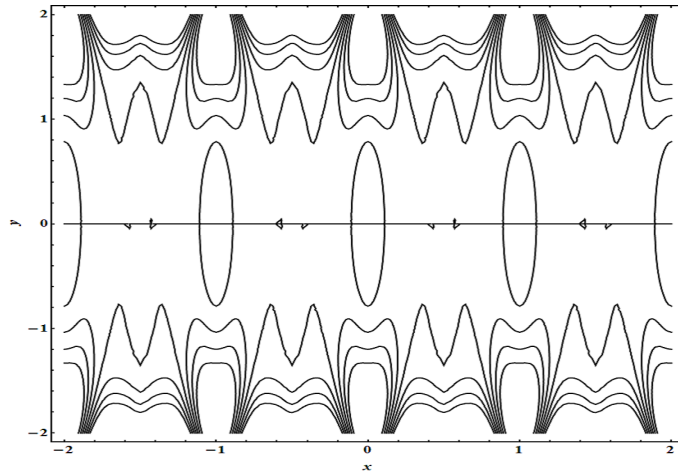


FIGURE 5.23: Streamlines for different value of $Q = 0.1, W_e = 0.1n = 0.1, \gamma = 0.1, \delta = 0.5, \xi = 0.3$.

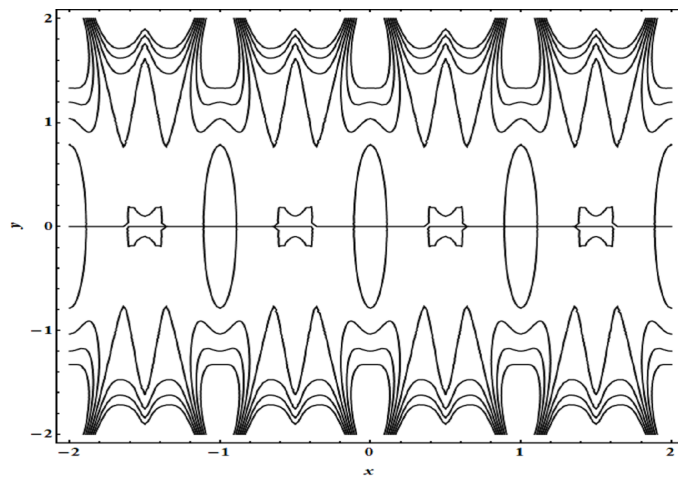


FIGURE 5.24: Streamlines for different value of $Q = 0.1, W_e = 0.1n = 0.1, \gamma = 0.1, \delta = 0.5, \xi = 0.3$.

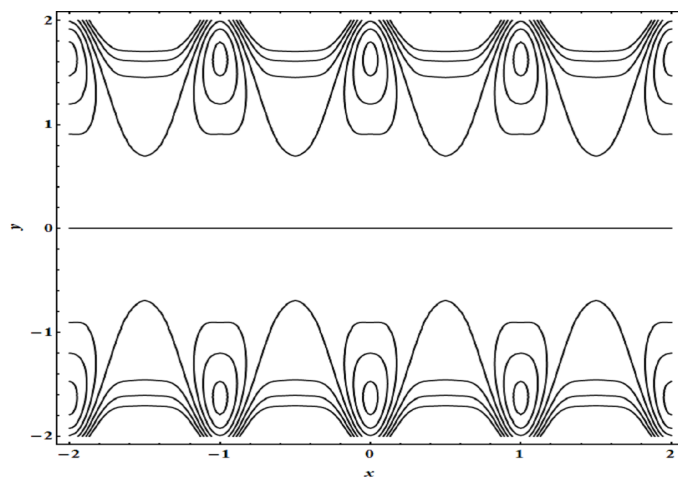


FIGURE 5.25: Streamlines for different value of $Q = 0.1, W_e = 0.1n = 0.1, \gamma = 0.1, \delta = 0.5, \xi = 0.3$.

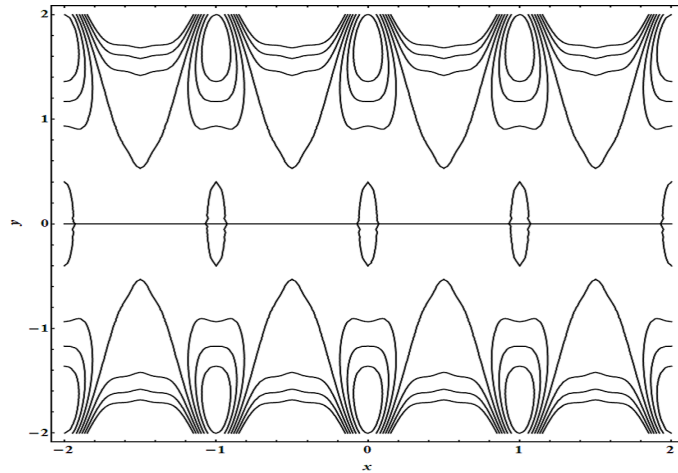


FIGURE 5.26: Streamlines for different value of $Q = 0.1, W_e = 0.1n = 0.1, \gamma = 0.1, \delta = 0.5, \xi = 0.3$.

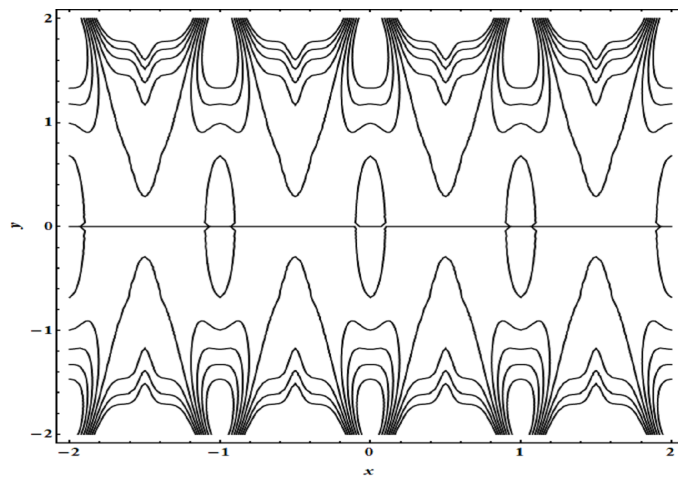


FIGURE 5.27: Streamlines for different value of $Q = 0.1, W_e = 0.1n = 0.1, \gamma = 0.1, \delta = 0.5, \xi = 0.3$.

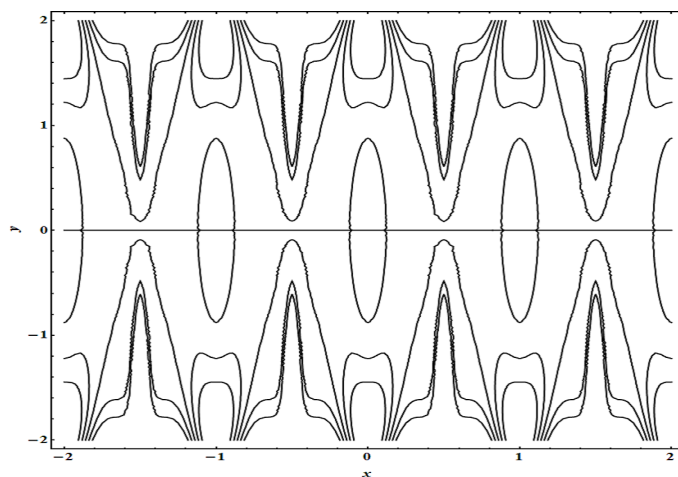


FIGURE 5.28: Streamlines for different value of $Q = 0.1, W_e = 0.1n = 0.1, \gamma = 0.1, \delta = 0.5, \xi = 0.3$.

5.4 Conclusion

In this chapter, we have analysed the Physiological flow Carreau fluid inner a symmetric metachronal wave due to cillary motion. The main findings of the present study are as follow:

- Velocity profile in the centre of the channel decreases as well as it gets opposite behaviour nearest of the channel.
- By increasing value of ξ pressure rise increases in the region ($Q \in [-1.5, 0.01]$) whereas reflux occur in the last.
- Pressure gradient decreases with the increasing value of Q, n .
- Streamlines bolas take the form of the shape of the geometry.

Chapter 6

Metachronal wave analysis for Non-Newtonian fluid under thermophoresis and brownian motion effects

6.1 Introduction

The main purpose of this chapter is to present a mathematical model of ciliary motion in an annulus. The effect of convective heat transfer and nanoparticle are taken into account. The governing equations of Jeffrey six-constant fluid along with heat and nanoparticle are modelled and then simplified by using long wavelength and low Reynolds number assumptions. The reduced equations are solved with the help of homotopy perturbation method. The obtained expressions for the velocity, temperature and nanoparticles concentration profiles are plotted and the impact of various physical parameters are investigated for different peristaltic waves.

6.2 Model of the Problem

We have considered the ciliary motion phenomenon for the two dimensional flow of an incompressible fluid in an annulus. We are considering the cylindrical coordinates

system (R, Z) . The geometry of the problem is shown in Figure 6.1.

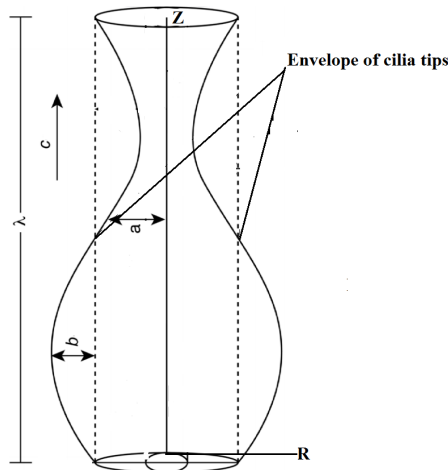


FIGURE 6.1: A physical sketch of the problem

The fundamental equations of continuity, momentum and nanoparticle concentration are

$$\frac{\partial \bar{U}}{\partial \bar{R}} + \frac{\bar{U}}{\bar{R}} + \frac{\partial \bar{W}}{\partial \bar{Z}} = 0, \quad (6.1)$$

$$\rho \left(\frac{\partial}{\partial \bar{t}} + \bar{U} \frac{\partial}{\partial \bar{R}} + \bar{W} \frac{\partial}{\partial \bar{Z}} \right) \bar{U} = -\frac{\partial \bar{P}}{\partial \bar{R}} + \frac{1}{\bar{R}} \frac{\partial}{\partial \bar{R}} (\bar{R} \bar{\tau}_{\bar{R}\bar{R}}) + \frac{\partial}{\partial \bar{Z}} (\bar{\tau}_{\bar{R}\bar{Z}}) + \frac{\bar{\tau}_{\theta\theta}}{\bar{R}}, \quad (6.2)$$

$$\begin{aligned} \rho \left(\frac{\partial}{\partial \bar{t}} + \bar{U} \frac{\partial}{\partial \bar{R}} + \bar{W} \frac{\partial}{\partial \bar{Z}} \right) \bar{W} = & -\frac{\partial \bar{P}}{\partial \bar{Z}} + \frac{1}{\bar{R}} \frac{\partial}{\partial \bar{R}} (\bar{R} \bar{\tau}_{\bar{R}\bar{Z}}) + \frac{\partial}{\partial \bar{Z}} (\bar{\tau}_{\bar{Z}\bar{Z}}) \\ & + \rho g \alpha (\bar{T} - \bar{T}_0) + \rho g \alpha (\bar{C} - \bar{C}_0) - \sigma B_0^2 \bar{W}, \end{aligned} \quad (6.3)$$

$$\begin{aligned} \left(\frac{\partial}{\partial \bar{t}} + \bar{U} \frac{\partial}{\partial \bar{R}} + \bar{W} \frac{\partial}{\partial \bar{Z}} \right) \bar{T} = & \alpha \left(\frac{\partial^2 \bar{T}}{\partial \bar{R}^2} + \frac{1}{\bar{R}} \frac{\partial \bar{T}}{\partial \bar{R}} + \frac{\partial^2 \bar{T}}{\partial \bar{Z}^2} \right) \\ & + \tau \left[D_B \left(\frac{\partial \bar{C}}{\partial \bar{R}} \frac{\partial \bar{T}}{\partial \bar{R}} + \frac{\partial \bar{C}}{\partial \bar{Z}} \frac{\partial \bar{T}}{\partial \bar{Z}} \right) + \frac{D_{\bar{T}}}{\bar{T}_0} \left(\left(\frac{\partial \bar{T}}{\partial \bar{R}} \right)^2 + \left(\frac{\partial \bar{T}}{\partial \bar{Z}} \right)^2 \right) \right], \end{aligned} \quad (6.4)$$

$$\begin{aligned} \left(\frac{\partial}{\partial \bar{t}} + \bar{U} \frac{\partial}{\partial \bar{R}} + \bar{W} \frac{\partial}{\partial \bar{Z}} \right) \bar{C} = & D_B \left(\frac{\partial^2 \bar{C}}{\partial \bar{R}^2} + \frac{1}{\bar{R}} \frac{\partial \bar{C}}{\partial \bar{R}} + \frac{\partial^2 \bar{C}}{\partial \bar{Z}^2} \right) \\ & + \frac{D_{\bar{T}}}{\bar{T}_0} \left(\frac{\partial^2 \bar{T}}{\partial \bar{R}^2} + \frac{1}{\bar{R}} \frac{\partial \bar{T}}{\partial \bar{R}} + \frac{\partial^2 \bar{T}}{\partial \bar{Z}^2} \right), \end{aligned} \quad (6.5)$$

where $\tau = \frac{(\rho c)_p}{(\rho c)_f}$ is the ratio among the heat capacity of the nanoparticle material and the heat capacity of the nanofluid.

The constitutional equation for a Jeffrey six-constant fluid is defined as [32]

$$\begin{aligned} \tau + \epsilon_1 \left[\frac{d\bar{\tau}}{dt} - W.\bar{\tau} + \bar{\tau}.W + d(\bar{\tau}.D + D.\bar{\tau}) + b\bar{\tau} : DI + cDtr\bar{\tau} \right] \\ = 2\mu \left[D + \epsilon_2 \left(\frac{dD}{dt} - W.D + D.W + 2dD.D + bD : DI \right) \right]. \end{aligned} \quad (6.6)$$

Here

$$\begin{aligned} D(\text{symmetric measurement of velocity gradient}) &= \frac{\nabla\bar{V} + (\nabla\bar{V})^{t_1}}{2}, \\ W(\text{antisymmetric measurement of velocity gradient}) &= \frac{\nabla\bar{V} - (\nabla\bar{V})^{t_1}}{2}. \end{aligned}$$

Let us examine that the envelops of the cilia tips can be denoted mathematically as

$$\bar{R} = \bar{H} = \bar{f}(\bar{Z}, \bar{t}) = \left[a + \epsilon a \cos\left(\frac{2\pi}{\lambda}\right) (\bar{Z} - c_1\bar{t}) \right], \quad (6.7)$$

$$\bar{Z} = \bar{g}(\bar{Z}, \bar{Z}_0, \bar{t}) = \bar{Z}_0 + \epsilon\alpha a \sin\left(\frac{2\pi}{\lambda}\right) (\bar{Z} - c_1\bar{t}). \quad (6.8)$$

The velocities of the transporting fluid are just those caused by the cilia tips, which can be expressed

$$\bar{W} = \frac{\partial\bar{Z}}{\partial\bar{t}}|_{z_0} = \frac{\partial\bar{g}}{\partial\bar{t}} + \frac{\partial\bar{g}}{\partial\bar{Z}} \cdot \frac{\partial\bar{Z}}{\partial\bar{t}} = \frac{\partial\bar{g}}{\partial\bar{t}} + \frac{\partial\bar{g}}{\partial\bar{X}}\bar{W}, \quad (6.9)$$

$$\bar{U} = \frac{\partial\bar{R}}{\partial\bar{t}}|_{z_0} = \frac{\partial\bar{f}}{\partial\bar{t}} + \frac{\partial\bar{f}}{\partial\bar{Z}} \cdot \frac{\partial\bar{Z}}{\partial\bar{t}} = \frac{\partial\bar{f}}{\partial\bar{t}} + \frac{\partial\bar{f}}{\partial\bar{X}}\bar{W}. \quad (6.10)$$

Using Eqs. (6.7) and (6.8) into the Eqs. (6.9) and (6.10), we obtain as

$$\bar{W} = -\frac{\left(\frac{2\pi}{\lambda}\right)(\epsilon \alpha a c \cos\left(\frac{2\pi}{\lambda}\right)(\bar{Z} - c_1\bar{t}))}{1 - \left(\frac{2\pi}{\lambda}\right)(\epsilon \alpha a \cos\left(\frac{2\pi}{\lambda}\right)(\bar{Z} - c_1\bar{t}))} = \bar{\chi}(\bar{Z}, \bar{t}),$$

$$\bar{U} = \frac{\left(\frac{2\pi}{\lambda}\right)(\epsilon \alpha a c \sin\left(\frac{2\pi}{\lambda}\right)(\bar{Z} - c_1\bar{t}))}{1 - \left(\frac{2\pi}{\lambda}\right)(\epsilon \alpha a \cos\left(\frac{2\pi}{\lambda}\right)(\bar{Z} - c_1\bar{t}))} \quad \text{at} \quad \bar{r} = \bar{h}.$$

The transformations between the two frames are

$$\bar{r} = \bar{R}, \quad \bar{z} = \bar{Z} - c_1 \bar{t},$$

$$\bar{u} = \bar{U}, \quad \bar{w} = \bar{W} - c_1.$$

The boundary conditions are defined as

$$\frac{\partial \bar{W}}{\partial \bar{r}} = 0, \quad \frac{\partial \bar{T}}{\partial \bar{r}} = 0, \quad \frac{\partial \bar{C}}{\partial \bar{r}} = 0, \quad \text{at} \quad \bar{r} = 0, \quad (6.11)$$

$$\bar{W} = \bar{\chi}(\bar{Z}, \bar{t}), \quad \bar{T} = \bar{T}_0, \quad \bar{C} = \bar{C}_0, \quad \text{at} \quad \bar{r} = \bar{h} = a + a \cos \left[\frac{2\pi}{\lambda} (\bar{Z} - c_1 \bar{t}) \right]. \quad (6.12)$$

Introducing the following non-dimensional variables

$$\begin{aligned} R &= \frac{\bar{R}}{a}, \quad r = \frac{\bar{r}}{a}, \quad Z = \frac{\bar{Z}}{\lambda}, \quad z = \frac{\bar{z}}{\lambda}, \quad W = \frac{\bar{W}}{c_1}, \quad w = \frac{\bar{w}}{c_1}, \quad U = \frac{\lambda \bar{U}}{ac}, \\ u &= \frac{\lambda \bar{u}}{ac_1}, \quad t = \frac{c_1 \bar{t}}{\lambda}, \quad \lambda_1 = \frac{\epsilon_1 c_1}{a}, \quad \lambda_2 = \frac{\epsilon_2 c_1}{a}, \quad R_e = \frac{ac_1 \rho}{\mu_0}, \quad \delta = \frac{a}{\lambda}, \\ h &= \frac{\bar{h}}{a} = 1 + \epsilon \cos(2\pi z), \quad P_r = \frac{\mu_0 C_p}{k}, \quad G_r = \frac{g \alpha a^3 \bar{T}_0}{v^2}, \quad \theta = \frac{(\bar{T} - \bar{T}_0)}{\bar{T}_0}, \\ N_b &= \frac{(\rho c)_p D_B(\bar{C}_0)}{(\rho c)_f}, \quad B_r = \frac{g \alpha a^3 \bar{C}_0}{v^2}, \quad N_t = \frac{(\rho c)_p D_T(\bar{C}_0)}{(\rho c)_f \alpha}, \quad \sigma = \frac{(\bar{C} - \bar{C}_0)}{\bar{C}_0}, \\ M &= \sqrt{\frac{\sigma}{\mu}} B_0 a. \end{aligned}$$

The reduced equations can be written as

$$0 = \frac{\partial p}{\partial r}, \quad (6.13)$$

$$0 = -\frac{\partial p}{\partial z} + \frac{1}{r} \frac{\partial}{\partial r} (r \tau_{rz}) + G_r \theta + B_r \sigma - M^2 (w + 1), \quad (6.14)$$

$$0 = \frac{1}{r} \frac{\partial}{\partial r} \left(r \frac{\partial \theta}{\partial r} \right) + N_b \frac{\partial \theta}{\partial r} \frac{\partial \sigma}{\partial r} + N_t \left(\frac{\partial \theta}{\partial r} \right)^2, \quad (6.15)$$

$$0 = \frac{1}{r} \frac{\partial}{\partial r} \left(r \frac{\partial \sigma}{\partial r} \right) + \frac{N_t}{N_b} \left(\frac{1}{r} \frac{\partial}{\partial r} \left(r \frac{\partial \theta}{\partial r} \right) \right). \quad (6.16)$$

The corresponding boundary conditions are reduced as

$$\frac{\partial w}{\partial r} = 0, \quad \frac{\partial \theta}{\partial r} = 0, \quad \frac{\partial \sigma}{\partial r} = 0, \quad \text{at} \quad r = 0,$$

$$w = -1 - 2\pi \epsilon \delta \alpha \cos(2\pi z), \quad \theta = 0, \quad \sigma = 0, \quad \text{at} \quad r = h = 1 + \epsilon \cos(2\pi z).$$

The extra stress tensor can be defined as

$$\begin{aligned}\tau_{rz} &= \frac{\frac{\partial w}{\partial r} \left[1 + \lambda_1 \lambda_2 (1 - d(d+b) - \frac{c}{2}(2d+3b)) \left(\frac{\partial w}{\partial r} \right)^2 \right]}{\left[1 + \lambda_1^2 (1 - d(d+b) - \frac{c}{2}(2d+3b)) \left(\frac{\partial w}{\partial r} \right)^2 \right]}, \\ \tau_{rr} &= \lambda_2 \left(\frac{\partial w}{\partial r} \right)^2 (1+d+b) - \lambda_1 \left(\frac{\partial w}{\partial r} \right) (1+d+b) \tau_{rz}, \\ \tau_{zz} &= \lambda_2 \left(\frac{\partial w}{\partial r} \right)^2 (-1+d+b) - \lambda_1 \left(\frac{\partial w}{\partial r} \right) (-1+d+b) \tau_{rz}, \\ \tau_{\theta\theta} &= \lambda_2 \left(\frac{\partial w}{\partial r} \right)^2 b - \lambda_1 \left(\frac{\partial w}{\partial r} \right) b \tau_{rz},\end{aligned}$$

where

$$\alpha_1 = 1 - d(d+b) - \frac{c}{2}(2d+3b), \quad \alpha_2 = \lambda_1 \lambda_2 - \lambda_1, \quad \alpha_3 = -\lambda_1^3 \lambda_2.$$

Finally, in simplified form Eqs. (6.13)-(6.16) can be written as

$$\frac{\partial p}{\partial r} = 0, \tag{6.17}$$

$$\begin{aligned}\frac{\partial p}{\partial z} &= \frac{1}{r} \frac{\partial}{\partial r} \left(r \frac{\partial w}{\partial r} \right) + \frac{1}{r} \frac{\partial}{\partial r} \left(\alpha_1 \alpha_2 r \left(\frac{\partial w}{\partial r} \right)^3 \right) \\ &+ \frac{1}{r} \frac{\partial}{\partial r} \left(\alpha_1^2 \alpha_3 r \left(\frac{\partial w}{\partial r} \right)^5 \right) - M^2(w+1),\end{aligned} \tag{6.18}$$

$$0 = \frac{1}{r} \frac{\partial}{\partial r} \left(r \frac{\partial \theta}{\partial r} \right) + N_b \frac{\partial \theta}{\partial r} \frac{\partial \sigma}{\partial r} + N_t \left(\frac{\partial \theta}{\partial r} \right)^2, \tag{6.19}$$

$$0 = \frac{1}{r} \frac{\partial}{\partial r} \left(r \frac{\partial \sigma}{\partial r} \right) + \frac{N_t}{N_b} \left(\frac{1}{r} \frac{\partial}{\partial r} \left(r \frac{\partial \theta}{\partial r} \right) \right). \tag{6.20}$$

The corresponding boundary conditions are reduced as

$$\begin{aligned}\frac{\partial w}{\partial r} = 0, \quad \frac{\partial \theta}{\partial r} = 0, \quad \frac{\partial \sigma}{\partial r} = 0, \quad \text{at } r = 0, \\ w = -1 - 2\pi\epsilon\delta\alpha \cos(2\pi z), \quad \theta = 0, \quad \sigma = 0, \quad \text{at } r = h = 1 + \epsilon \cos(2\pi z).\end{aligned}$$

6.3 Solution Methodology

We use homotopy perturbation method to solve the above Eqs. (6.18 - 6.20)

$$H(q, \theta) = L(\theta) - L(\theta_{10}) + qL(\theta_{10}) + q \left[N_b \frac{\partial \theta}{\partial r} \frac{\partial \sigma}{\partial r} + N_t \left(\frac{\partial \theta}{\partial r} \right)^2 \right]. \quad (6.21)$$

$$H(q, \sigma) = L(\sigma) - L(\sigma_{10}) + qL(\sigma_{10}) + q \left[\frac{N_t}{N_b} \left(\frac{1}{r} \frac{\partial}{\partial r} \left(r \frac{\partial \theta}{\partial r} \right) \right) \right]. \quad (6.22)$$

$$\begin{aligned} H(q, w) = & L(w) - L(w_{10}) + qL(w_{10}) + q \left[\frac{1}{r} \frac{\partial}{\partial r} \left(\alpha_1 \alpha_2 r \left(\frac{\partial w}{\partial r} \right)^3 \right) \right. \\ & \left. + \frac{1}{r} \frac{\partial}{\partial r} \left(\alpha_1^2 \alpha_3 r \left(\frac{\partial w}{\partial r} \right)^5 \right) + G_r \theta + B_r \sigma - M^2(w + 1) - \frac{\partial p}{\partial z} \right]. \end{aligned} \quad (6.23)$$

We have taken linear operator $L = \frac{1}{r} \frac{\partial}{\partial r} \left(r \frac{\partial}{\partial r} \right)$ and initial guesses are discussed which satisfy boundary conditions

$$\theta_{10}(r, z) = \left(\frac{r^2 - h^2}{4} \right),$$

$$\sigma_{10}(r, z) = \left(\frac{r^2 - h^2}{4} \right) \frac{N_t}{N_b},$$

$$W_{10}(r, z) = -1 - 2\pi\epsilon\delta\alpha \cos(2\pi z) + \left(\frac{r^2 - h^2}{4} \right) \frac{\partial p_0}{\partial z}.$$

According to HPM, we define

$$\theta(r, q) = \theta_0 + q\theta_1 + q^2\theta_2 + \dots$$

$$\sigma(r, q) = \sigma_0 + q\sigma_1 + q^2\sigma_2 + \dots$$

$$w(r, q) = w_0 + qw_1 + q^2w_2 + \dots$$

The solutions for velocity, temperature and nanoparticle phenomena can be written as for $q \rightarrow 1$

$$\begin{aligned}
w = & -1 - 2\pi\epsilon\delta\alpha \cos(2\pi z) + \left(\frac{r^4 - h^4}{4}\right) \left(\frac{dp}{dz}\right) - \frac{1}{32}\alpha_2 \left(\frac{\partial p_0}{\partial z}\right)^3 (r^4 - h^4) \\
& - \frac{1}{192}\alpha_1^2\alpha_3 \left(\frac{\partial p_0}{\partial z}\right)^5 (r^6 - h^6) + \frac{1}{16}G_r h^2 (r^2 - h^2) - \frac{1}{64}G_r (r^4 - h^4) \\
& + \frac{1}{16}B_r h^2 (r^2 - h^2) \frac{N_t}{N_b} - \frac{1}{64}B_r (r^4 - h^4) \frac{N_t}{N_b} - \frac{1}{16}h^2 M^2 (r^2 - h^2) \left(\frac{\partial p_0}{\partial z}\right) \\
& + \frac{1}{64}M^2 (r^4 - h^4) \left(\frac{\partial p_0}{\partial z}\right) - \frac{1}{2}M^2 (r^2 - h^2) \pi\epsilon\delta\alpha \cos(2\pi z). \tag{6.24}
\end{aligned}$$

$$\begin{aligned}
\theta = & \left(\frac{r^2 - h^2}{4}\right) - \left(\frac{r^4 - h^4}{32}\right) N_t + \left(\frac{r^4 - h^4}{64}\right) N_t + \left(\frac{h^2 - r^2}{4}\right) + \left(\frac{r^6 - h^6}{576}\right) (N_t)^2 \\
& + \left(\frac{r^4 - h^4}{16}\right) N_t + \left(\frac{r^6 - h^6}{288}\right) (N_t)^2. \tag{6.25}
\end{aligned}$$

$$\sigma = \left(\frac{r^2 - h^2}{4}\right) \frac{N_t}{N_b} + \left(\frac{h^2 - r^2}{2}\right) \frac{N_t}{N_b} - \left(\frac{h^2 - r^2}{4}\right) \frac{N_t}{N_b} + \left(\frac{r^2 - h^2}{32}\right) (N_t)^2. \tag{6.26}$$

$$\frac{dp}{dz} = \frac{16}{-h^4} [F + A1]. \tag{6.27}$$

Where

$$\begin{aligned}
A1 = & \frac{h^2}{2} + h^2 \pi\epsilon\delta\alpha \cos(2\pi z) - \frac{1}{96}h^6 G_r - \frac{1}{16}h^4 \left(\frac{\partial p_0}{\partial z}\right) - \frac{1}{96}h^6 M^2 \left(\frac{\partial p_0}{\partial z}\right) \\
& - \frac{1}{8}h^4 M^2 \pi\epsilon\delta\alpha \cos(2\pi z) + \frac{1}{96}B_r h^6 \frac{N_t}{N_b} - \frac{1}{96}h^6 \alpha_1 \alpha_2 \left(\frac{\partial p_0}{\partial z}\right)^3. \tag{6.28}
\end{aligned}$$

Flow rate in the dimensionless form can be written as

$$F = Q - \frac{1}{2} \left(1 + \frac{\epsilon^2}{2}\right). \tag{6.29}$$

The pressure rise Δp can be written as

$$\Delta p = \int_0^1 \left(\frac{dp}{dz}\right) dz. \tag{6.30}$$

Velocities in terms of streamfunctions are defined as

$$u = -\frac{1}{r} \left(\frac{\partial \psi}{\partial z}\right), \quad w = \frac{1}{r} \left(\frac{\partial \psi}{\partial r}\right).$$

6.4 Results and discussions

In this section, we have discussed the solution for the peristaltic flow of Jeffrey six-constant nanofluid flow due to ciliary motion. The expression for temperature, concentration, velocity, pressure rise, pressure gradient and streamlines are calculated numerically. Figures 6.2-6.4 show the velocity profile for diverse values of fluid parameters (α_1) magnetohydrodynamics (M) and amplitude ratio (ϵ). Figure 6.2 shows that velocity profile gets decreasing function in the region ($-0.6 \leq r \leq 0.6$) whereas it get opposite behaviour in the rest of the region. Figures 6.3-6.4, it is depicted that velocity profile gets increasing function in the region ($-0.6 \leq r \leq 0.6$) whereas it gets opposite behaviour in the rest of the region. Figure 6.5 show the temperature profile for different values of thermophoresis parameter (N_t). It is depicted that with an increase in thermophoresis parameter (N_t) temperature profile decreases. Figures 6.6-6.7 show that with an increase in N_b and N_t concentration profile increases. From figure 6.7, it is seen that with an increase in N_t , concentration profile decreases.

Figures 6.8, 6.10, 6.12 show the pressure rise (versus flow rate) for diverse value of $\alpha_1, \epsilon, \alpha_3$. In these figures, it is depicted that by increasing value of α_1 pressure rise decreasing in the region ($Q \in [-3, -1]$) whereas reflux occur in the last. The retrograde pumping region can also be seen in Figures 6.8, 6.10, 6.12 when $Q < 0$ and $\Delta p > 0$ and free pumping region can be seen when $Q = 0$ and $\Delta p = 0$. Moreover, augmented pumping region can also be seen in figures 6.8, 6.10, 6.12 when $Q > 0$ and $\Delta p < 0$.

Figures 6.9, 6.11, 6.13 show the frictional force for diverse values of $\alpha_1, \epsilon, \alpha_3$. Figures 6.14-6.16 describe the behaviour of pressure gradient for different values G_r, ϵ, N_b, N_t . Figure 6.14 describe that increasing value of ϵ the pressure gradient decreases in the region ($-1 \leq Z \leq 0.3$) and increases in the region ($0.2 \leq Z \leq 0.7$). Figures 6.15-6.16 it is depicted that with an increase in N_t, N_b, G_r pressure gradient decreases. Figures 6.17-6.19 illustrate the streamlines for different wave shapes. In these figures, it is depicted that by increasing value of α_1 , trapped bolus increases.

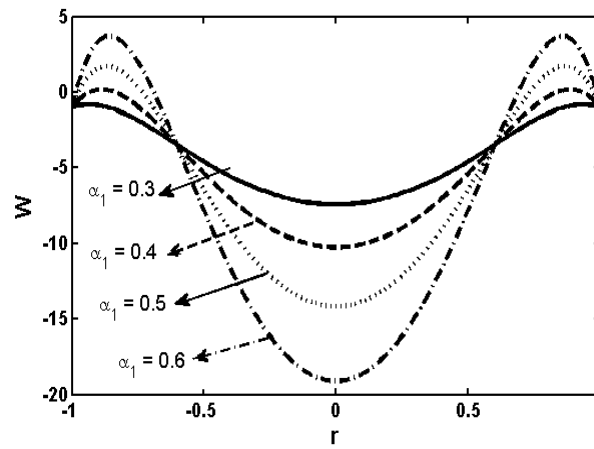


FIGURE 6.2: Velocity for different values of α_1 when $\alpha = 0.28$, $\delta = 0.43$, $B = 0.87$, $\epsilon = 0.12$, $N_t = 0.8$, $N_b = 0.7$, $G_r = 5.57$

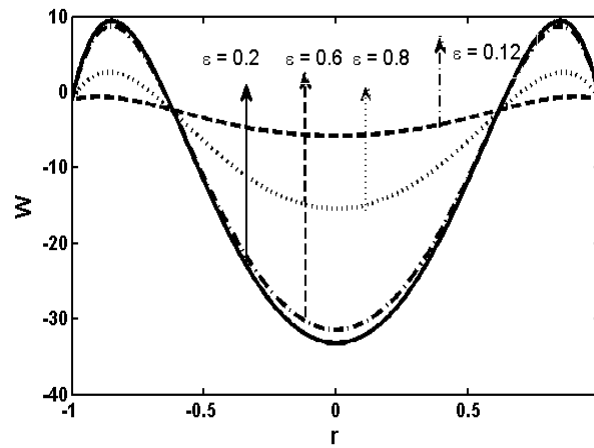


FIGURE 6.3: Velocity for different values of ϵ when $\alpha = 0.28$, $\delta = 0.43$, $B = 0.87$, $N_t = 0.8$, $N_b = 0.7$, $G_r = 5.57$

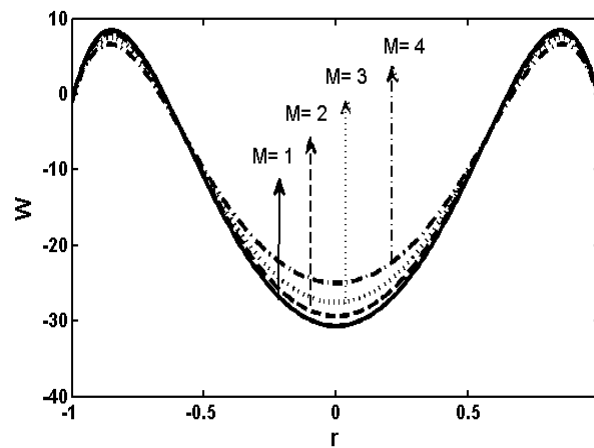


FIGURE 6.4: Velocity for different values of M when $\alpha = 0.28$, $\delta = 0.43$, $B = 0.87$, $\epsilon = 0.12$, $N_t = 0.8$, $N_b = 0.7$, $G_r = 5.57$

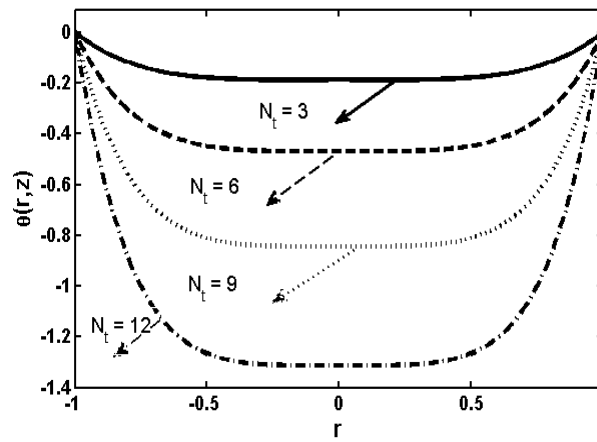


FIGURE 6.5: Temperature for different values of N_t when $\alpha = 0.28$, $\delta = 0.43$, $B = 0.87$, $\epsilon = 0.12$, $N_b = 0.7$, $G_r = 5.57$

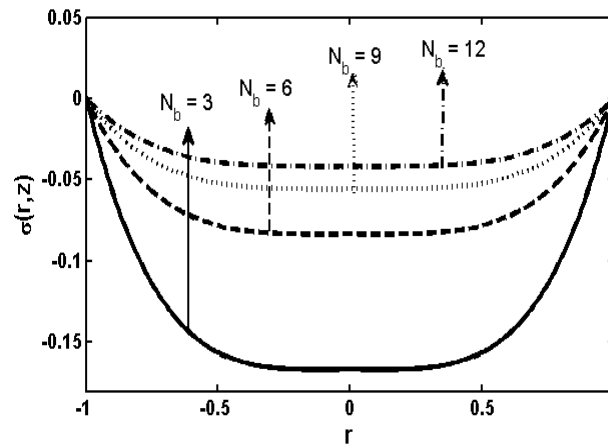


FIGURE 6.6: Concentration for different values of N_b when $\alpha = 0.28$, $\delta = 0.43$, $B = 0.87$, $\epsilon = 0.12$, $N_t = 0.8$, $G_r = 5.57$

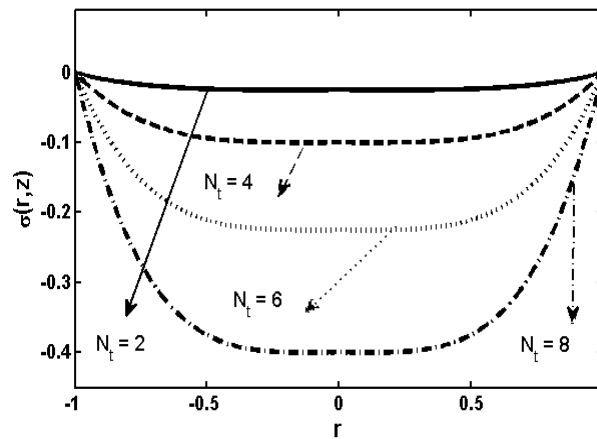


FIGURE 6.7: Concentration for different values of N_t when $\alpha = 0.28$, $\delta = 0.43$, $B = 0.87$, $\epsilon = 0.12$, $N_b = 0.7$, $G_r = 5.57$

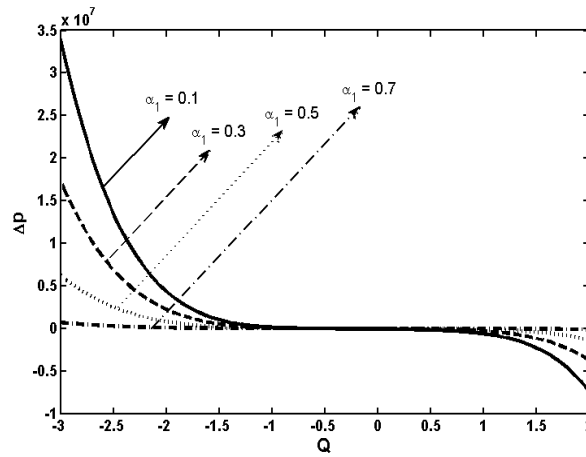


FIGURE 6.8: Pressure rise for different values of α_1 when $\alpha = 0.28$, $\delta = 0.43$, $B = 0.87$, $\epsilon = 0.12$, $N_t = 0.8$, $N_b = 0.7$, $G_r = 5.57$, $M = 0.9$

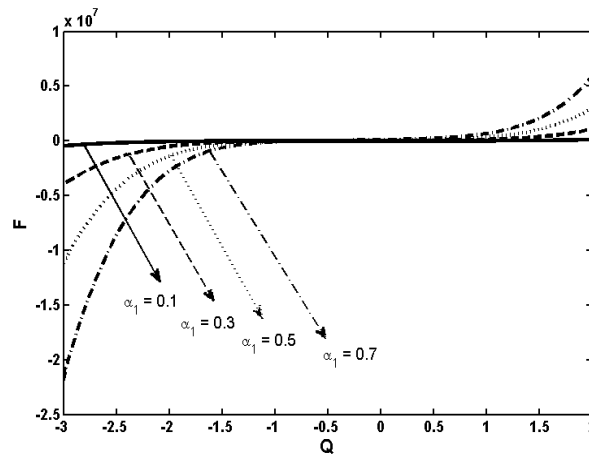


FIGURE 6.9: Frictional forces for different values of α_1 when $\alpha = 0.28$, $\delta = 0.43$, $B = 0.87$, $\epsilon = 0.12$, $N_t = 0.8$, $N_b = 0.7$, $G_r = 5.57$, $M = 0.9$

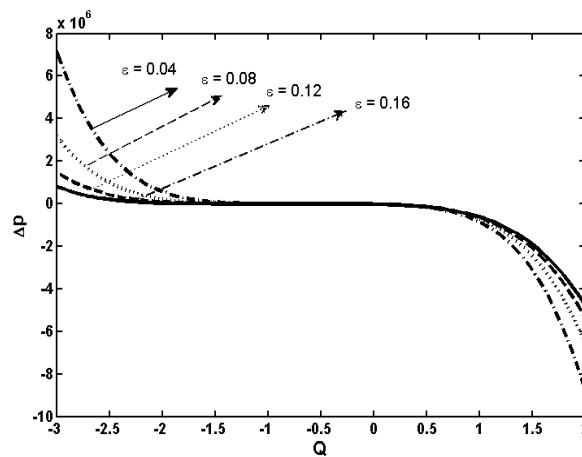


FIGURE 6.10: Pressure rise for different values of ϵ when $\alpha = 0.28$, $\delta = 0.43$, $B = 0.87$, $N_t = 0.8$, $N_b = 0.7$, $G_r = 5.57$, $M = 0.9$

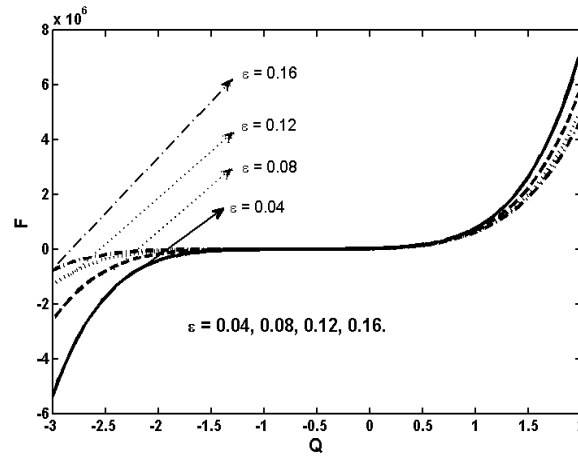


FIGURE 6.11: Frictional forces for different values of ϵ when $\alpha = 0.28$, $\delta = 0.43$, $B = 0.87$, $N_t = 0.8$, $N_b = 0.7$, $G_r = 5.57$, $M = 0.9$

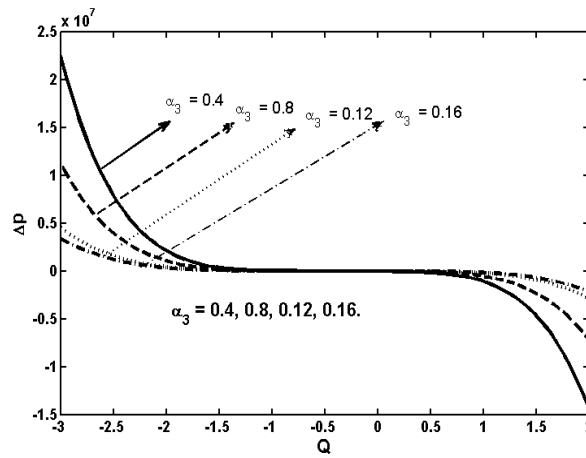


FIGURE 6.12: Pressure rise for different values of α_3 when $\alpha = 0.28$, $\delta = 0.43$, $B = 0.87$, $\epsilon = 0.12$, $N_t = 0.8$, $N_b = 0.7$, $G_r = 5.57$, $M = 0.9$

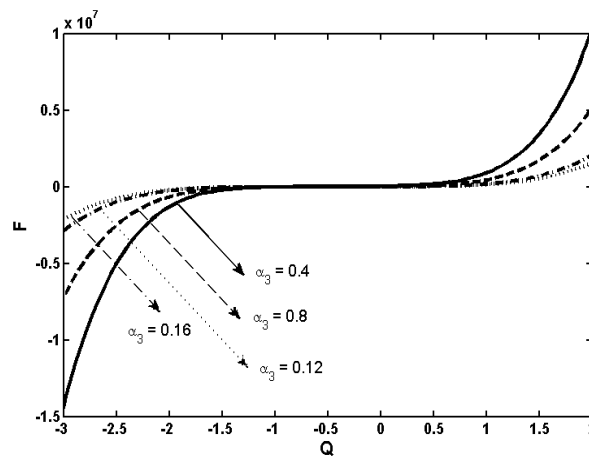


FIGURE 6.13: Frictional forces for different values of α_3 when $\alpha = 0.28$, $\delta = 0.43$, $B = 0.87$, $\epsilon = 0.12$, $N_t = 0.8$, $N_b = 0.7$, $G_r = 5.57$, $M = 0.9$

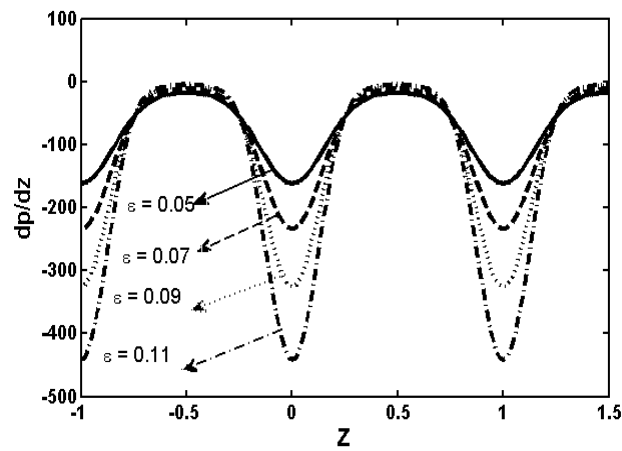


FIGURE 6.14: Pressure gradient for different values of ϵ when $\alpha = 0.28$, $\delta = 0.43$, $B = 0.87$, $\alpha_3 = 0.12$, $N_t = 0.8$, $N_b = 0.7$, $G_r = 5.57$, $M = 0.9$

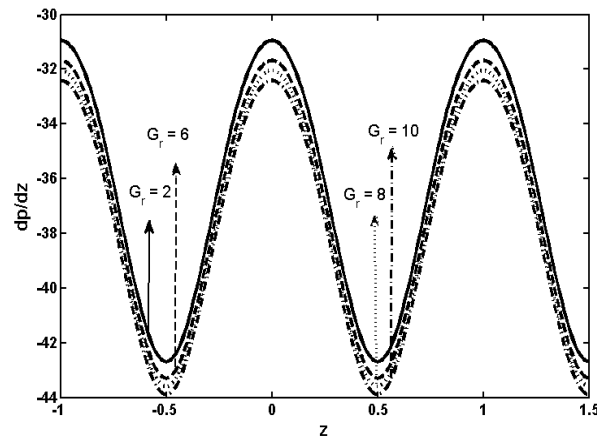


FIGURE 6.15: Pressure gradient for different values of G_r when $\alpha = 0.28$, $\delta = 0.43$, $B = 0.87$, $\epsilon = 0.12$, $N_t = 0.8$, $N_b = 0.7$, $\alpha_3 = 5.57$, $M = 0.9$

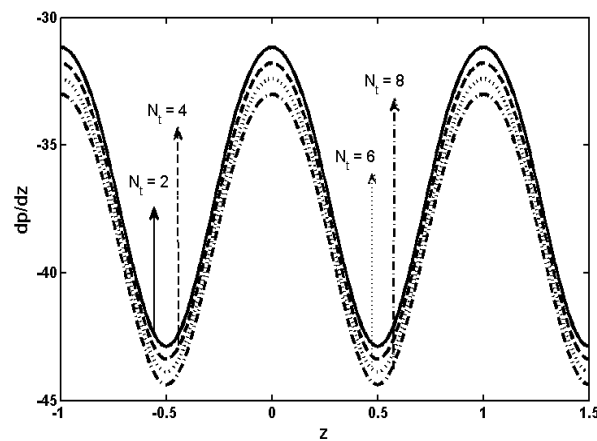


FIGURE 6.16: Pressure gradient for different values of N_t when $\alpha = 0.28$, $\delta = 0.43$, $B = 0.87$, $\epsilon = 0.12$, $\alpha_3 = 0.8$, $N_b = 0.7$, $G_r = 5.57$, $M = 0.9$

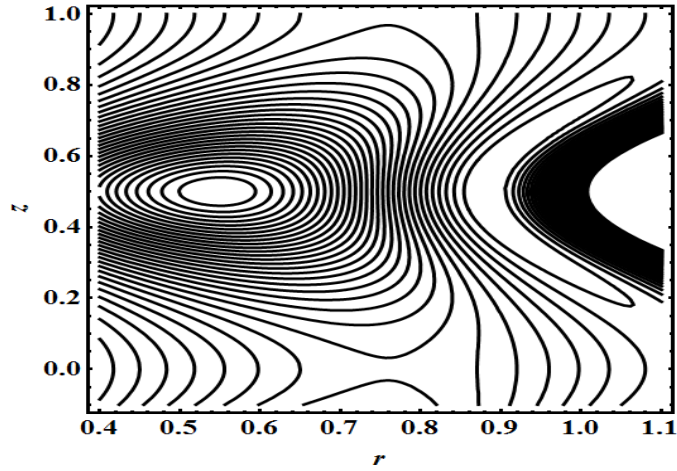


FIGURE 6.17: Streamlines for different values of $\alpha_1 = 0.1$ when $\alpha = 0.28$, $\delta = 0.43$, $B = 0.87$, $\epsilon = 0.12$, $N_t = 0.8$, $N_b = 0.7$, $G_r = 5.57$, $M = 0.9$

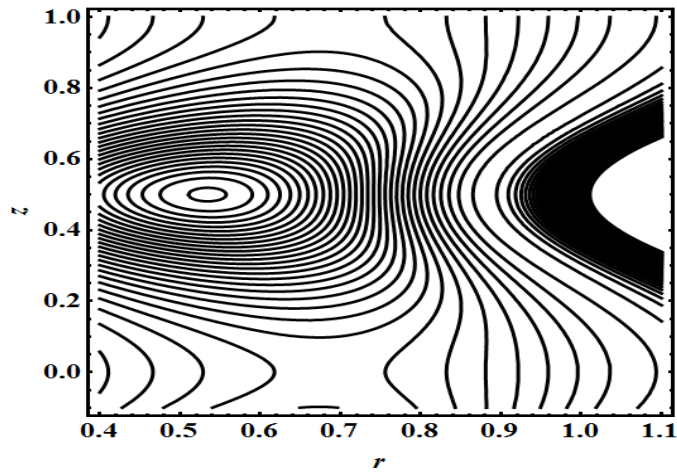


FIGURE 6.18: Streamlines for different values of $\alpha_1 = 0.3$ when $\alpha = 0.28$, $\delta = 0.43$, $B = 0.87$, $\epsilon = 0.12$, $N_t = 0.8$, $N_b = 0.7$, $G_r = 5.57$, $M = 0.9$

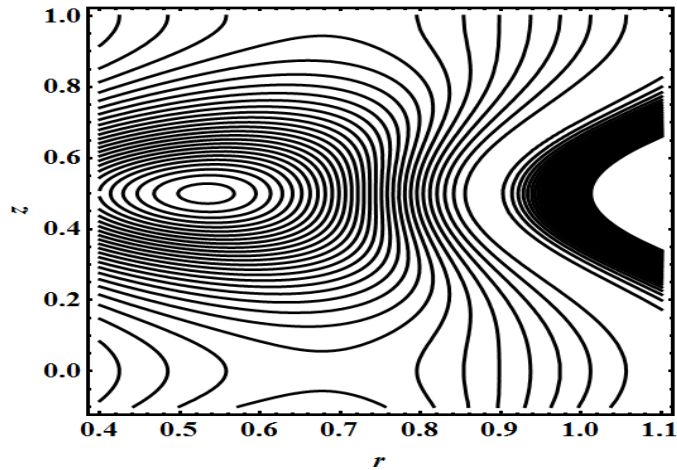


FIGURE 6.19: Streamlines for different values of $\alpha_1 = 0.5$ when $\alpha = 0.28$, $\delta = 0.43$, $B = 0.87$, $\epsilon = 0.12$, $N_t = 0.8$, $N_b = 0.7$, $G_r = 5.57$, $M = 0.9$

6.5 Conclusion

In this chapter, we have analysed the nanoparticle analysis for peristaltic flow of a non-Newtonian fluid due to ciliary motion. The main findings of the present study are as follow:

- The temperature profile is decreases for the increasing values of thermophersis parameters N_t .
- The nanoparticle concentration field is enhanced for the increasing values of Brownian motion N_b .
- It is clear that frictional forces and pressure rise have an opposite behaviour while compare to each other.
- The pressure gradient increases with the increasing value of ϵ .

Chapter 7

Physiological flow of Jeffrey six-constant fluid due to ciliary motion

This chapter deals with the physiological flow of Jeffrey six-constant fluid due to ciliary motion in an annulus. In this analysis, the peristaltic motion of non-Newtonian Jeffrey six-constant fluid is observed in an annulus with ciliated tips under the effect of heat and mass transfer. The effects of viscous dissipation are also taken into account. The governing equations of non-Newtonian fluid are modelled and simplified by using low Reynolds number and long wavelength assumptions. The velocity equation is solved by utilizing the regular perturbation technique in terms of a variant of small dimensionless parameter α . The obtained expressions for the velocity profiles are plotted and the impact of different physical parameters are investigated for different peristaltic waves.

7.1 Formulation of the Problem

The governing equations in the fixed frame for an incompressible fluid can be written as

$$\frac{\partial \bar{U}}{\partial \bar{R}} + \frac{\bar{U}}{\bar{R}} + \frac{\partial \bar{W}}{\partial \bar{Z}} = 0, \quad (7.1)$$

$$\rho \left(\frac{\partial}{\partial \bar{t}} + \bar{U} \frac{\partial}{\partial \bar{R}} + \bar{W} \frac{\partial}{\partial \bar{Z}} \right) \bar{U} = -\frac{\partial \bar{P}}{\partial \bar{R}} + \frac{1}{\bar{R}} \frac{\partial}{\partial \bar{R}} (\bar{R} \bar{\tau}_{\bar{R}\bar{R}}) + \frac{\partial}{\partial \bar{Z}} (\bar{\tau}_{\bar{R}\bar{Z}}) - \frac{\bar{\tau}_{\bar{\theta}\bar{\theta}}}{\bar{R}}, \quad (7.2)$$

$$\rho \left(\frac{\partial}{\partial \bar{t}} + \bar{U} \frac{\partial}{\partial \bar{R}} + \bar{W} \frac{\partial}{\partial \bar{Z}} \right) \bar{W} = -\frac{\partial \bar{P}}{\partial \bar{Z}} + \frac{1}{\bar{R}} \frac{\partial}{\partial \bar{R}} (\bar{R} \bar{\tau}_{\bar{R}\bar{Z}}) + \frac{\partial}{\partial \bar{Z}} (\bar{\tau}_{\bar{Z}\bar{Z}}), \quad (7.3)$$

$$\begin{aligned} \rho c_p \left(\frac{\partial}{\partial \bar{t}} + \bar{U} \frac{\partial}{\partial \bar{R}} + \bar{W} \frac{\partial}{\partial \bar{Z}} \right) \bar{T} &= \bar{\tau}_{\bar{R}\bar{R}} \frac{\partial \bar{U}}{\partial \bar{R}} + \bar{\tau}_{\bar{R}\bar{Z}} \frac{\partial \bar{W}}{\partial \bar{R}} + \bar{\tau}_{\bar{R}\bar{Z}} \frac{\partial \bar{U}}{\partial \bar{Z}} + \bar{\tau}_{\bar{Z}\bar{Z}} \frac{\partial \bar{U}}{\partial \bar{R}} + \bar{\tau}_{\bar{\theta}\bar{\theta}} \frac{\bar{U}}{\bar{R}} \\ &+ \bar{K} \left(\frac{\partial^2 \bar{T}}{\partial \bar{R}^2} + \frac{1}{\bar{R}} \frac{\partial \bar{T}}{\partial \bar{R}} + \frac{\partial^2 \bar{T}}{\partial \bar{Z}^2} \right), \end{aligned} \quad (7.4)$$

$$\begin{aligned} \left(\frac{\partial}{\partial \bar{t}} + \bar{U} \frac{\partial}{\partial \bar{R}} + \bar{W} \frac{\partial}{\partial \bar{Z}} \right) \bar{C} &= D \left(\frac{\partial^2 \bar{C}}{\partial \bar{R}^2} + \frac{1}{\bar{R}} \frac{\partial \bar{C}}{\partial \bar{R}} + \frac{\partial^2 \bar{C}}{\partial \bar{Z}^2} \right) \\ &+ \frac{D \bar{k}_T}{\bar{T}_0} \left(\frac{\partial^2 \bar{T}}{\partial \bar{R}^2} + \frac{1}{\bar{R}} \frac{\partial \bar{T}}{\partial \bar{R}} + \frac{\partial^2 \bar{T}}{\partial \bar{Z}^2} \right). \end{aligned} \quad (7.5)$$

The constitutional equation for a Jeffrey six-constant fluid model is defined as

$$\begin{aligned} \bar{\tau} + \epsilon_1 \left[\frac{d\bar{\tau}}{dt} - W \cdot \bar{\tau} + \bar{\tau} \cdot W + d(\bar{\tau} \cdot D + D \cdot \bar{\tau}) + b\bar{\tau} : DI + cDtr\bar{\tau} \right] \\ = 2\mu \left[D + \epsilon_2 \left(\frac{dD}{dt} - W \cdot D + D \cdot W + 2dD \cdot D + bD : DI \right) \right], \end{aligned} \quad (7.6)$$

in which

$$\begin{aligned} D(\text{symmetric measurement of velocity gradient}) &= \frac{\nabla \bar{V} + (\nabla \bar{V})^{t_1}}{2}, \\ W(\text{antisymmetric measurement of velocity gradient}) &= \frac{\nabla \bar{V} - (\nabla \bar{V})^{t_1}}{2}. \end{aligned}$$

Let us examine that the envelopes of the cilia tips can be denoted mathematically as

$$\bar{R} = \bar{h} = \bar{f}(\bar{Z}, \bar{t}) = \left[a + \epsilon a \cos \left(\frac{2\pi}{\lambda} \right) (\bar{Z} - c\bar{t}) \right], \quad (7.7)$$

$$\bar{Z} = \bar{g}(\bar{Z}, \bar{Z}_0, \bar{t}) = \bar{Z}_0 + \epsilon \beta a \sin \left(\frac{2\pi}{\lambda} \right) (\bar{Z} - c\bar{t}), \quad (7.8)$$

where a represents the radius of the ciliated tube, ϵ is the mean non-dimensional measure with respect to the cilia length, λ presented by wavelength and c denotes the wave speed. β is the measure of the eccentricity of the elliptical motion of the cilia tips. The velocities of the transporting fluid are just those caused by the cilia tips, which can be expressed as

$$\bar{W} = \frac{\partial \bar{Z}}{\partial \bar{t}} \Big|_{z_0} = \frac{\partial \bar{g}}{\partial \bar{t}} + \frac{\partial \bar{g}}{\partial \bar{Z}} \cdot \frac{\partial \bar{Z}}{\partial \bar{t}} = \frac{\partial \bar{g}}{\partial \bar{t}} + \frac{\partial \bar{g}}{\partial \bar{X}} \bar{W}, \quad (7.9)$$

$$\bar{U} = \frac{\partial \bar{R}}{\partial \bar{t}} \Big|_{z_0} = \frac{\partial \bar{f}}{\partial \bar{t}} + \frac{\partial \bar{f}}{\partial \bar{Z}} \cdot \frac{\partial \bar{Z}}{\partial \bar{t}} = \frac{\partial \bar{f}}{\partial \bar{t}} + \frac{\partial \bar{f}}{\partial \bar{X}} \bar{W}. \quad (7.10)$$

Using Eqs. (7.7) and (7.8) in Eqs. (7.9) and (7.10), we obtain

$$\bar{W} = -\frac{\left(\frac{2\pi}{\lambda}\right) (\epsilon \beta a c \cos\left(\frac{2\pi}{\lambda}\right) (\bar{Z} - c\bar{t}))}{1 - \left(\frac{2\pi}{\lambda}\right) (\epsilon \beta a \cos\left(\frac{2\pi}{\lambda}\right) (\bar{Z} - c\bar{t}))} = \bar{\chi}(\bar{Z}, \bar{t}),$$

$$\bar{U} = \frac{\left(\frac{2\pi}{\lambda}\right) (\epsilon \beta a c \sin\left(\frac{2\pi}{\lambda}\right) (\bar{Z} - c\bar{t}))}{1 - \left(\frac{2\pi}{\lambda}\right) (\epsilon \beta a \cos\left(\frac{2\pi}{\lambda}\right) (\bar{Z} - c\bar{t}))} \quad \text{at} \quad \bar{r} = \bar{h}.$$

The transformations between the two frames are

$$\bar{r} = \bar{R}, \quad \bar{z} = \bar{Z} - c\bar{t},$$

$$\bar{u} = \bar{U}, \quad \bar{w} = \bar{W} - c_1.$$

$$\frac{\partial \bar{W}}{\partial \bar{r}} = 0, \quad \frac{\partial \bar{T}}{\partial \bar{r}} = 0, \quad \frac{\partial \bar{C}}{\partial \bar{r}} = 0, \quad \text{at} \quad \bar{r} = 0, \quad (7.11)$$

$$\bar{W} = \bar{\chi}(\bar{Z}, \bar{t}), \quad \bar{T} = \bar{T}_0, \quad \bar{C} = \bar{C}_0, \quad \text{at} \quad \bar{r} = \bar{h} = a + a \cos\left[\frac{2\pi}{\lambda} (\bar{Z} - c\bar{t})\right]. \quad (7.12)$$

Introducing the following non-dimensional variables

$$\begin{aligned}
R &= \frac{\bar{R}}{a}, & r &= \frac{\bar{r}}{a}, & Z &= \frac{\bar{Z}}{\lambda}, & z &= \frac{\bar{z}}{\lambda}, & W &= \frac{\bar{W}}{c}, & w &= \frac{\bar{w}}{c}, & \tau &= \frac{a\bar{\tau}}{c\mu_0}, \\
U &= \frac{\lambda\bar{U}}{ac}, & u &= \frac{\lambda\bar{u}}{ac}, & t &= \frac{c_1\bar{t}}{\lambda}, & \lambda_1 &= \frac{\epsilon_1 c_1}{a}, & \lambda_2 &= \frac{\epsilon_2 c_1}{a}, \\
R_e &= \frac{ac_1\rho}{\mu_0}, & \delta &= \frac{a}{\lambda}, & h &= \frac{\bar{h}}{a} = 1 + \epsilon \cos(2\pi z), & P_r &= \frac{\mu_0 C_p}{k}, \\
E_c &= \frac{c^2}{C_p T_0}, & \theta &= \frac{\bar{T} - \bar{T}_0}{\bar{T}_0}, & \Pi &= \frac{a\bar{\Pi}}{c}, & \alpha &= \frac{k}{(\rho c)_f}, & p &= \frac{a^2 \bar{p}}{c_1 \lambda \mu_0}, \\
S_T &= \frac{\rho D k_T \bar{T}_0}{\mu T_0 \bar{C}_0}, & S_H &= \frac{\mu}{D\rho}, & \sigma &= \frac{\bar{C} - \bar{C}_o}{\bar{C}_o}.
\end{aligned}$$

Under the assumption of low Reynolds number and long wavelength $\delta \ll 1$ are estimated

$$0 = \frac{\partial u}{\partial r} + \frac{u}{r} + \frac{\partial w}{\partial z}, \quad (7.13)$$

$$0 = \frac{\partial p}{\partial r}, \quad (7.14)$$

$$0 = -\frac{\partial p}{\partial z} + \frac{1}{r} \frac{\partial}{\partial r} (r \tau_{rz}), \quad (7.15)$$

$$0 = \frac{1}{r} \frac{\partial}{\partial r} \left(r \frac{\partial \theta}{\partial r} \right) + B_k \frac{\partial w}{\partial r} (\tau_{rz}), \quad (7.16)$$

$$0 = \frac{1}{S_H} \frac{1}{r} \frac{\partial}{\partial r} \left(r \frac{\partial \sigma}{\partial r} \right) + S_T \frac{1}{r} \frac{\partial}{\partial r} \left(r \frac{\partial \theta}{\partial r} \right). \quad (7.17)$$

$$\frac{\partial w}{\partial r} = 0, \quad \frac{\partial \theta}{\partial r} = 0, \quad \frac{\partial \sigma}{\partial r} = 0, \quad \text{at } r = 0,$$

$$w = -1 - 2\pi\epsilon\delta\beta \cos(2\pi z), \quad \theta = 0, \quad \sigma = 0, \quad \text{at } r = h = 1 + \epsilon \cos(2\pi z).$$

Finally, in simplified form Eqs. (7.13)-(7.17) can be written as

$$\frac{\partial p}{\partial r} = 0, \quad (7.18)$$

$$\begin{aligned}
\frac{\partial p}{\partial z} &= \frac{1}{r} \frac{\partial}{\partial r} \left(r \frac{\partial w}{\partial r} \right) + \frac{1}{r} \frac{\partial}{\partial r} \left(\alpha \alpha_1 r \left(\frac{\partial w}{\partial r} \right)^3 \right) \\
&\quad + \frac{1}{r} \frac{\partial}{\partial r} \left(\alpha^2 \alpha_2 r \left(\frac{\partial w}{\partial r} \right)^5 \right), \quad (7.19)
\end{aligned}$$

$$\frac{1}{r} \frac{\partial}{\partial r} \left(r \frac{\partial \theta}{\partial r} \right) + B_k \frac{\partial w}{\partial r} (\tau_{rz}) = 0, \quad (7.20)$$

$$\frac{1}{S_H} \frac{1}{r} \frac{\partial}{\partial r} \left(r \frac{\partial \sigma}{\partial r} \right) + S_T \frac{1}{r} \frac{\partial}{\partial r} \left(r \frac{\partial \theta}{\partial r} \right) = 0. \quad (7.21)$$

The corresponding boundary conditions are defined as

$$\begin{aligned} \frac{\partial w}{\partial r} = 0, \quad \frac{\partial \theta}{\partial r} = 0, \quad \frac{\partial \sigma}{\partial r} = 0, & \quad \text{at } r = 0, \\ w = -1 - 2\pi\epsilon\delta\beta \cos(2\pi z), \quad \theta = 0, \quad \sigma = 0 & \quad \text{at } r = h = 1 + \epsilon \cos(2\pi z). \end{aligned}$$

7.2 Solution Methodology

7.2.1 Perturbation solution

We apply the regular perturbation method in terms of a variant of Jeffrey six-constant fluid parameter α . As perturbation technique, following expansion of w , θ , σ , and p in terms of small parameter α are used

$$\begin{aligned} w &= w_0 + \alpha w_1 + \alpha^2 w_2 + \mathcal{O}(\alpha^3), \\ \theta &= \theta_0 + \alpha \theta_1 + \alpha^2 \theta_2 + \mathcal{O}(\alpha^3), \\ \sigma &= \sigma_0 + \alpha \sigma_1 + \alpha^2 \sigma_2 + \mathcal{O}(\alpha^3), \\ p &= p_0 + \alpha p_1 + \alpha^2 p_2 + \mathcal{O}(\alpha^3). \end{aligned}$$

The perturbation solution for velocity, temperature and concentration profile is given in Eqs. (7.22)-(7.24)

$$\begin{aligned} W &= -1 - 2\pi\epsilon\delta\beta \cos(2\pi z) + \frac{r^4 - h^4}{4} \left(\frac{dp}{dz} \right) - \frac{1}{32} \alpha_2 \left(\frac{\partial p_0}{\partial z} \right)^3 (r^4 - h^4) \\ &\quad - \frac{3\alpha_1}{32} \left(\frac{\partial p_0}{\partial z} \right)^2 \left(\frac{\partial p_1}{\partial z} \right) (r^4 - h^4) + \frac{9\alpha_1^2}{576} (r^6 - h^6) \left(\frac{\partial p_0}{\partial z} \right)^3 - \frac{3\alpha_2}{576} (r^6 - h^6). \end{aligned} \quad (7.22)$$

$$\begin{aligned} \theta &= -\frac{1}{64} B_\kappa P_0^2 (r^4 - h^4) - \frac{1}{32} B_\kappa P_0 p_1 (r^4 - h^4) + \frac{1}{576} B_\kappa P_0^4 (r^4 - h^4) \alpha_1 \\ &\quad - \frac{1}{64} B_\kappa P_1^2 (r^4 - h^4) + \frac{1}{32} P_0 p_2 (r^4 - h^4) - \frac{1}{288} P_0^3 p_1 (r^6 - h^6) \alpha_1 \\ &\quad + \frac{1}{288} B_\kappa P_0^3 p_1 (r^6 - h^6) \alpha_1 + \frac{3}{2048} B_r P_0^4 p_1 (r^8 - h^8) \alpha_1^2 - \frac{1}{2048} P_0^6 (r^8 - h^8) \alpha_1^2 \\ &\quad - \frac{1}{4096} B_\kappa P_0^6 (r^8 - h^8) \alpha_1^2 - \frac{1}{4096} P_0^6 (r^8 - h^8) \alpha_2. \end{aligned} \quad (7.23)$$

$$\begin{aligned}
\sigma = & \frac{1}{64}B_\kappa S_T S_H P_0^2 (r^4 - h^4) + \frac{1}{32}B_\kappa S_T S_H P_0 p_1 (r^4 - h^4) - \frac{1}{576}B_\kappa P_0^4 (r^6 - h^6) \\
& + \frac{1}{64}B_\kappa S_T S_H P_1^2 (r^4 - h^4) - \frac{1}{32}S_T S_H P_0 p_2 (r^4 - h^4) + \frac{1}{288}P_0^3 (r^6 - h^6)\alpha_1 \\
& + \frac{1}{288}B_\kappa S_T S_H P_0^3 p_1 (r^6 - h^6)\alpha_1 - \frac{3}{2048}S_T S_H P_0^4 p_1 (r^8 - h^8)\alpha_1^2 + \frac{1}{1024}(r^8 - h^8) \\
& + \frac{1}{4096}B_\kappa S_T S_H P_0^6 p_1 (r^8 - h^8)\alpha_1^2 + \frac{1}{4096}S_T S_H P_0^6 p_1 (r^8 - h^8)\alpha_2, \tag{7.24}
\end{aligned}$$

$$\frac{dp}{dz} = \frac{16}{-h^4}[F + A1], \tag{7.25}$$

where

$$A1 = \frac{h^2}{2} + h^2 \pi \epsilon \delta \beta \cos(2\pi z) - \frac{1}{96}h^6 p_0^3 \alpha_1 - \frac{1}{32}h^6 p_0^2 p_1 \alpha_1 + \frac{3}{512}h^8 p_0^3 \alpha_1^2 - \frac{1}{512}h^8 p_0^5 \alpha_2. \tag{7.26}$$

Flow rate in the dimensionless form can be written as

$$F = Q - \frac{1}{2} \left(1 + \frac{\epsilon^2}{2} \right). \tag{7.27}$$

The pressure rise Δp can be written as

$$\Delta p = \int_0^1 \left(\frac{dp}{dz} \right) dz. \tag{7.28}$$

Velocities in terms of streamfunctions are defined as

$$u = -\frac{1}{r} \left(\frac{\partial \psi}{\partial z} \right), \quad w = \frac{1}{r} \left(\frac{\partial \psi}{\partial r} \right).$$

For the flow analysis, we have considered three waveforms sinusoidal wave, trapezoidal wave and multisinusoidal wave. The dimensionless equations can be written as

1. Sinusoidal wave

$$h(z) = 1 + \epsilon \cos(2\pi z)$$

2. Multisinusoidal wave

$$h(z) = 1 + \epsilon \cos(2m\pi z)$$

3. Trapezoidal wave

$$h(z) = 1 + \epsilon \left[\frac{32}{\pi^2} \frac{4}{\pi} \sum_{n=1}^{\infty} \frac{\sin \frac{\pi}{8}(2n-1)}{(2n-1)^2} \sin(2\pi(2n-1)z) \right]$$

7.3 Results and discussions

In this section, we have analyzed the solution for physiological flow of Jeffrey six-constant fluid due to ciliary motion through graphs. We have presented the solution attained by perturbation by framing velocity, pressure rise, pressure gradient, temperature, concentration and streamline graphs for diverse values of the parameters α , Q , ξ , δ and γ , S_T , S_H respectively. Figures 7.1-7.2 show that with the increase in α_1, α_2 temperature profile decreases. Figures 7.3-7.4 show that with the increase in B_r, ϵ temperature profile increases. Figures 7.5-7.8, it is depicted that with the increase in $\alpha_1, \alpha_2, S_T, S_H$ concentration profile increases. Figures 7.9 show that increases the value of α_2 while the velocity profile in the centre of the tube decreases whereas it gets opposite behaviour near the tube or near the peristaltic wave. Figures 7.10 it is depicted that, at the centre of the tube, the velocity profile is minimum whereas it gets opposite behaviour near the tube or near the peristaltic wave. Pressure rise and frictional forces for diverse values of $\alpha_1, \alpha_2, \beta$ and is plotted in Figures 7.11-7.16. In these figures, it is depicted that by increasing value of $\alpha_1, \alpha_2, \beta$ pressure rise increasing in the region ($Q \in [-2, -1]$) whereas reflux occur in the last. Three different regions can be recognized from these figures. The retrograde pumping region can also be seen in Figures 7.11, 7.13, 7.15 when $Q < 0$ and $\Delta p > 0$ and free pumping region can be seen when $Q = 0$ and $\Delta p = 0$. Moreover, augmented pumping region can also be seen in figures 7.11, 7.13, 7.15 when $Q > 0$ and $\Delta p < 0$. Figures 7.12, 7.14, 7.16 show the forces have an opposite behaviour as well as the pressure rise. Figures 7.17-7.18, it is depicted that by increasing value of α_1, α_2 pressure rise decreasing. Figures 7.19-7.21 illustrate the streamlines for different wave shapes.

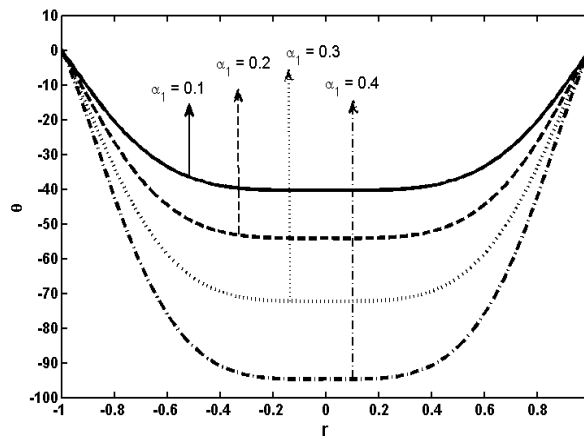


FIGURE 7.1: Variation of temperature graph for α_1 when $Z = 0.75$, $\epsilon = 0.22$, $M = 0.2$, $B_r = 0.22$, $\alpha = 0.22$, $\beta = 1.5$, $\alpha_2 = 0.6$.

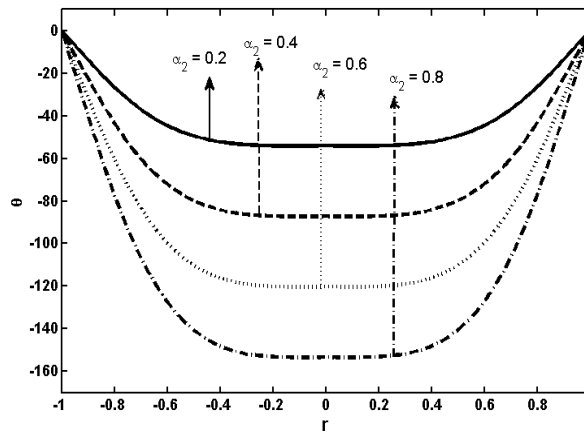


FIGURE 7.2: Variation of temperature for α_1 when $Z = 0.75$, $\epsilon = 0.22$, $M = 0.2$, $B_r = 0.22$, $\alpha = 0.22$, $\beta = 1.5$, $\alpha_1 = 0.6$.

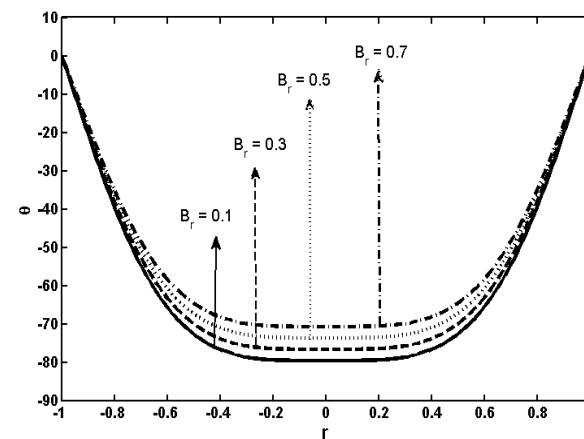


FIGURE 7.3: Variation of temperature for B_r when $Z = 0.75$, $\epsilon = 0.22$, $M = 0.2$, $\alpha_1 = 0.22$, $\alpha = 0.22$, $\beta = 1.5$, $\alpha_2 = 0.6$.

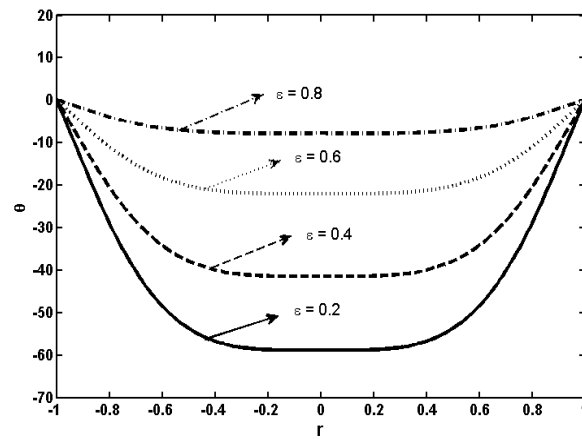


FIGURE 7.4: Variation of temperature for ϵ when $Z = 0.75$, $B_r = 0.22$, $M = 0.2$, $\alpha_1 = 0.22$, $\alpha = 0.25$, $\beta = 1.5$, $\alpha_2 = 0.6$.

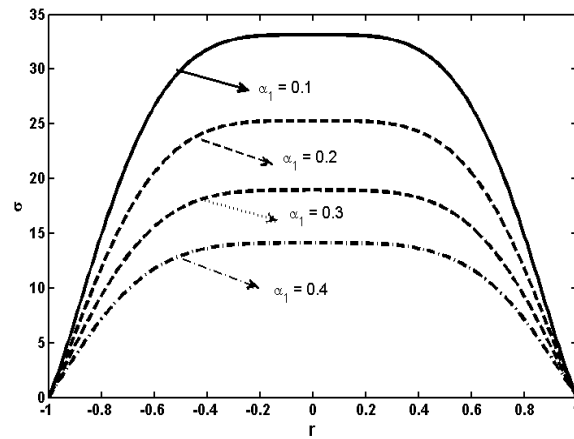


FIGURE 7.5: Variation of nanoparticle concentration for α_1 when $Z = 0.75$, $B_r = 0.22$, $M = 0.2$, $\epsilon = 0.22$, $\alpha = 0.25$, $\beta = 1.5$, $\alpha_2 = 0.6$, $S_T = 0.7$, $S_H = 0.5$.

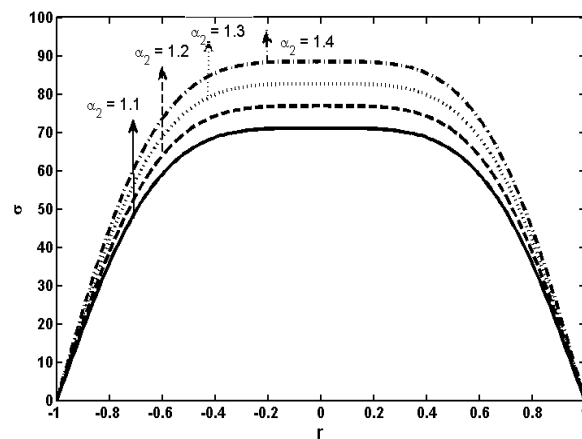


FIGURE 7.6: Variation of nanoparticle concentration for α_2 when $Z = 0.75$, $B_r = 0.22$, $M = 0.2$, $\epsilon = 0.22$, $\alpha = 0.25$, $\beta = 1.5$, $\alpha_1 = 0.6$, $S_T = 0.7$, $S_H = 0.5$.

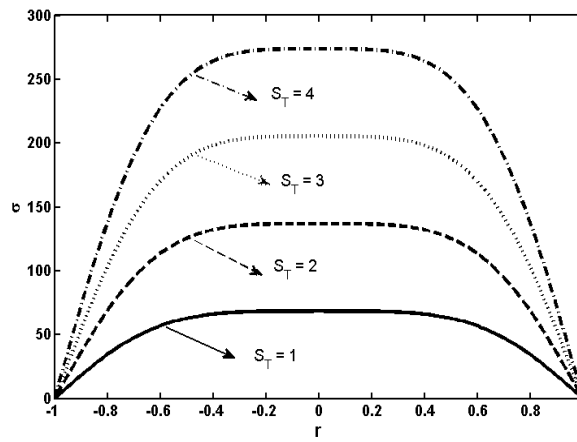


FIGURE 7.7: Variation of nanoparticle concentration for S_T when $Z = 0.75$, $B_r = 0.22$, $M = 0.2$, $\epsilon = 0.22$, $\alpha = 0.25$, $\beta = 1.5$, $\alpha_1 = 0.6$, $\alpha_2 = 0.7$, $S_H = 0.5$.

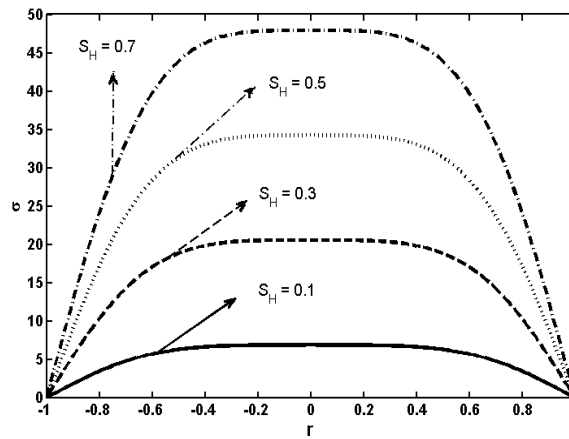


FIGURE 7.8: Variation of nanoparticle concentration for S_H when $Z = 0.75$, $B_r = 0.22$, $M = 0.2$, $\epsilon = 0.22$, $\alpha = 0.25$, $\beta = 1.5$, $\alpha_1 = 0.6$, $\alpha_2 = 0.7$, $S_T = 0.5$.

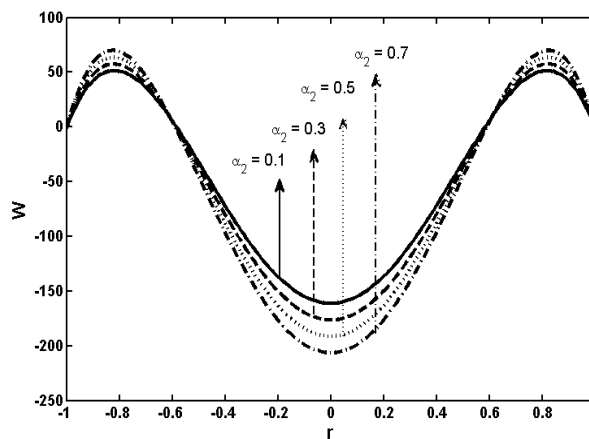


FIGURE 7.9: Variation of velocity for α_2 when $Z = 0.75$, $B_r = 0.22$, $M = 0.2$, $\epsilon = 0.22$, $\alpha = 0.25$, $\beta = 1.5$, $\alpha_1 = 0.7$

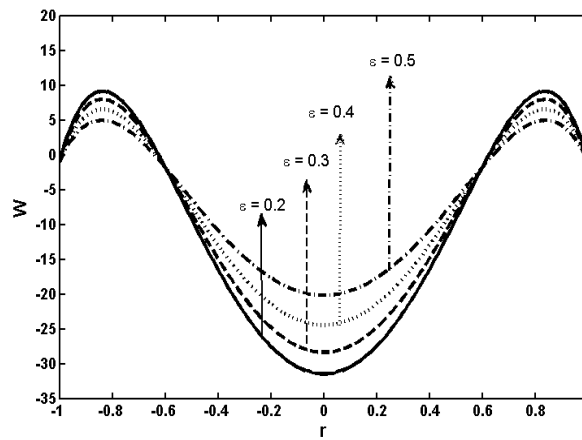


FIGURE 7.10: Variation of velocity for ϵ when $Z = 0.75$, $B_r = 0.22$, $M = 0.2$, $\alpha_1 = 0.22$, $\alpha = 0.25$, $\beta = 1.5$, $\alpha_2 = 0.27$

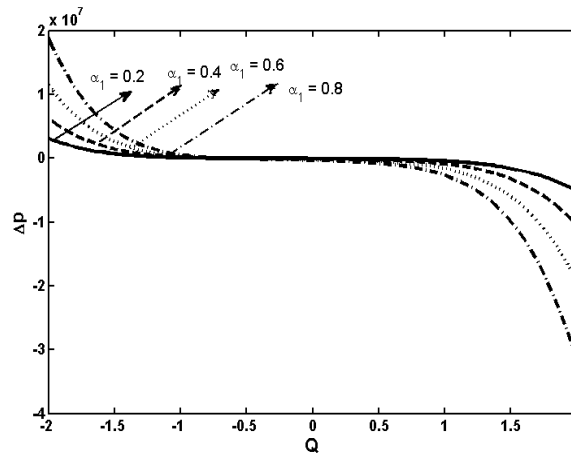


FIGURE 7.11: Variation of Pressure rise for α_1 when $Z = 0.23$, $\epsilon = 0.01$, $\alpha_1 = 0.22$, $\alpha_2 = 0.4$, $\beta = 1.5$, $B = 1.5$, $S_T = 0.7$, $S_H = 0.5$.

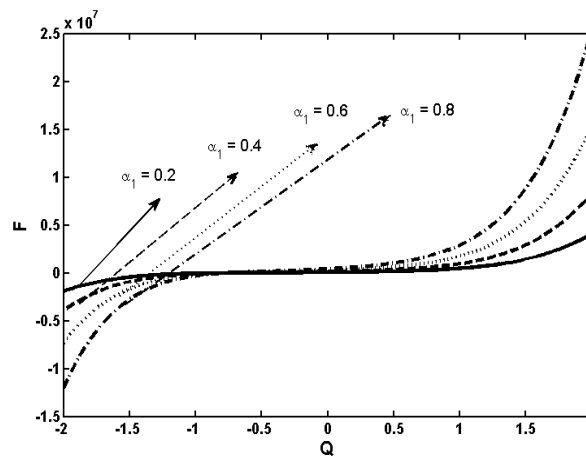


FIGURE 7.12: Variation of frictional force for α_1 when $Z = 0.23$, $\epsilon = 0.01$, $\alpha = 0.22$, $\alpha_2 = 0.4$, $\beta = 1.5$, $B_r = 1.5$, $S_T = 0.7$, $S_H = 0.5$.

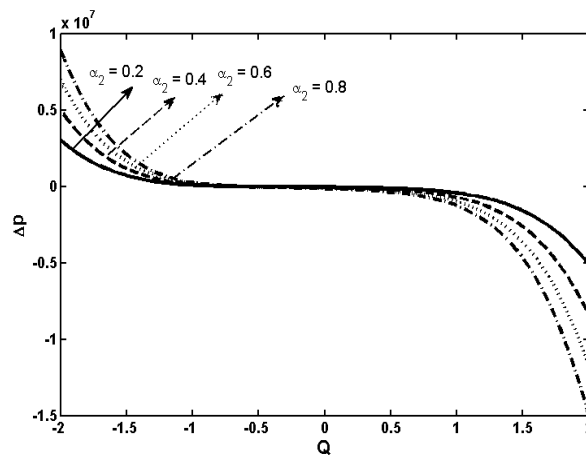


FIGURE 7.13: Variation of Pressure rise for α_2 when $Z = 0.23$, $\epsilon = 0.01$, $\alpha_1 = 0.22$, $\alpha = 0.4$, $\beta = 1.5$, $B_r = 1.5$, $S_T = 0.7$, $S_H = 0.5$.

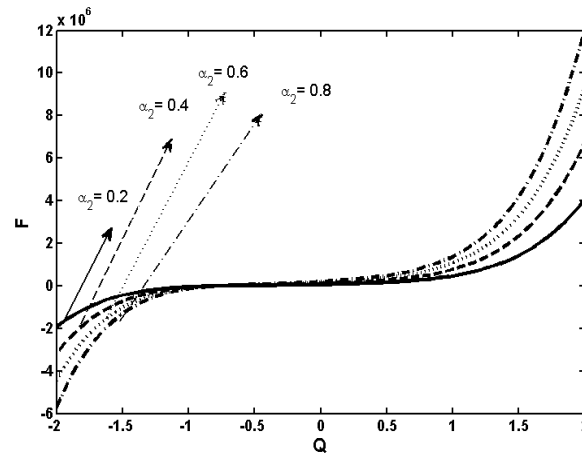


FIGURE 7.14: Variation of frictional force for α_2 when $Z = 0.23$, $\epsilon = 0.01$, $\alpha_1 = 0.22$, $\alpha = 0.4$, $\beta = 1.5$, $B_r = 1.5$, $S_T = 0.7$, $S_H = 0.5$.

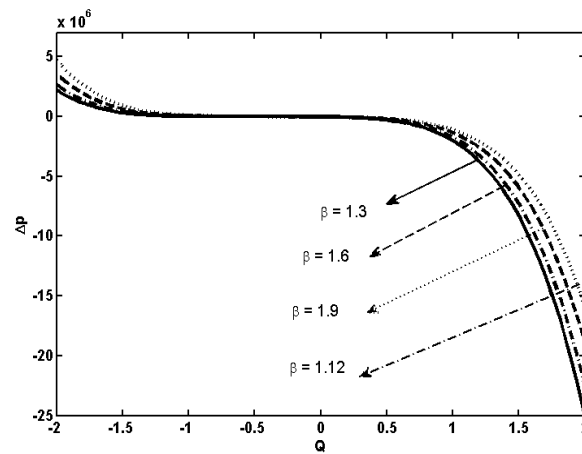


FIGURE 7.15: Variation of Pressure rise for β when $Z = 0.23$, $\epsilon = 0.01$, $\alpha_1 = 0.22$, $\alpha = 0.4$, $\alpha_2 = 0.5$, $B_r = 1.5$, $S_T = 0.7$, $S_H = 0.5$.

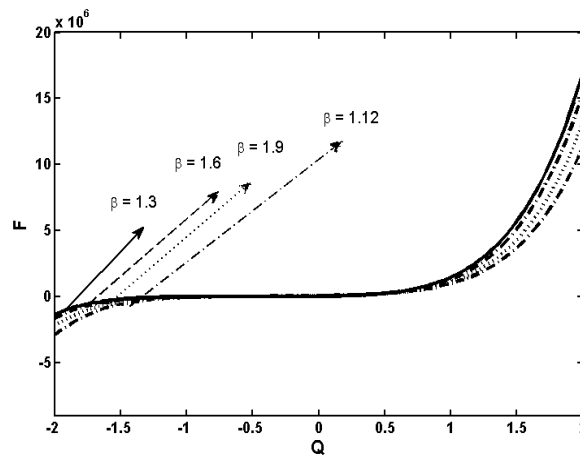


FIGURE 7.16: Variation of frictional force for β when $Z = 0.23$, $\epsilon = 0.01$, $\alpha_1 = 0.22$, $\alpha = 0.4$, $\alpha_2 = 0.5$, $B_r = 1.5$, $S_T = 0.7$, $S_H = 0.5$.

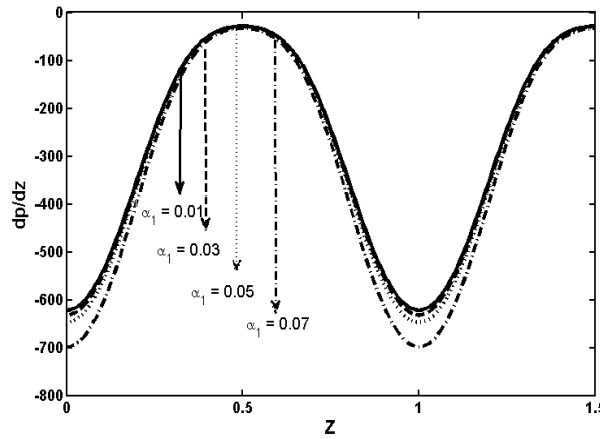


FIGURE 7.17: Pressure gradient $\frac{dp}{dz}$ for sinusoidal wave when $Z = 0.23$, $\epsilon = 0.01$, $\alpha = 0.4$, $\alpha_2 = 0.5$, $B_r = 1.5$, $S_T = 0.7$, $S_H = 0.5$.

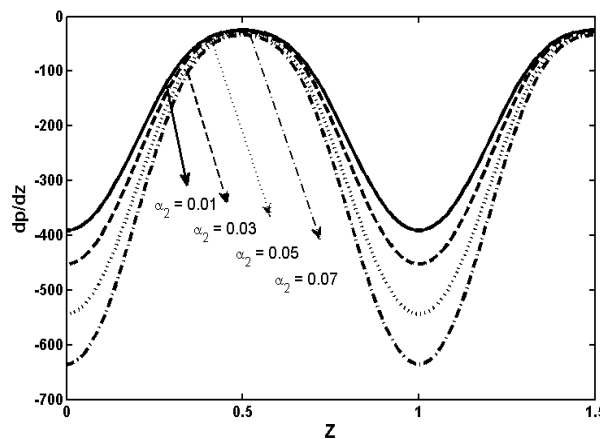


FIGURE 7.18: Pressure gradient $\frac{dp}{dz}$ for sinusoidal wave when $Z = 0.23$, $\epsilon = 0.01$, $\alpha_1 = 0.22$, $\alpha = 0.4$, $B_r = 1.5$, $S_T = 0.7$, $S_H = 0.5$.

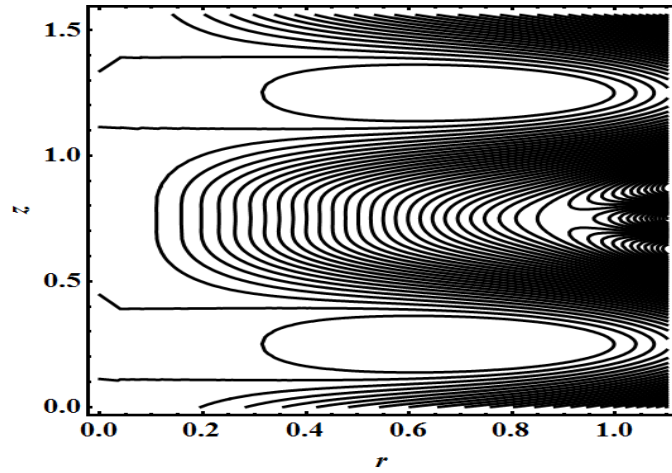


FIGURE 7.19: Streamlines pattern for sinusoidal wave $Z = 0.23$, $\epsilon = 0.01$, $\alpha_1 = 0.22$, $\alpha = 0.4$, $\alpha_2 = 0.5$, $B_r = 1.5$, $S_T = 0.7$, $S_H = 0.5$.

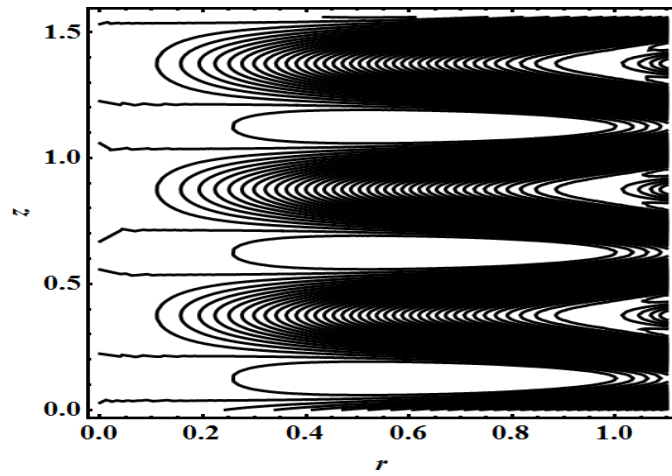


FIGURE 7.20: Streamlines pattern for multisinusoidal wave $Z = 0.23$, $\epsilon = 0.01$, $\alpha_1 = 0.22$, $\alpha = 0.4$, $\alpha_2 = 0.5$, $B_r = 1.5$, $S_T = 0.7$, $S_H = 0.5$.

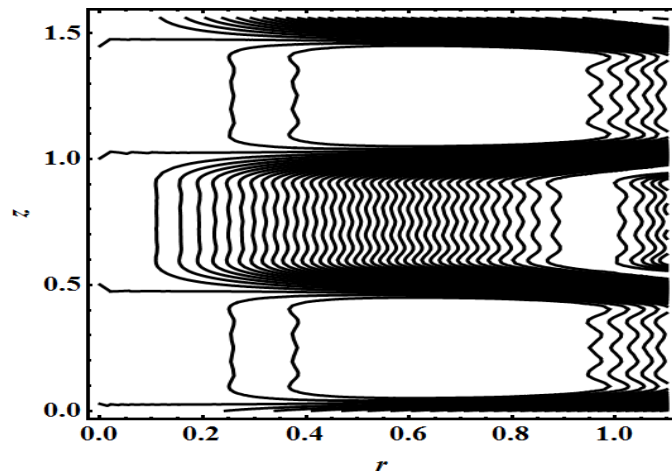


FIGURE 7.21: Streamlines pattern for Trapezoidal $Z = 0.23$, $\epsilon = 0.01$, $\alpha_1 = 0.22$, $\alpha = 0.4$, $\alpha_2 = 0.5$, $B_r = 1.5$, $S_T = 0.7$, $S_H = 0.5$.

7.4 Conclusion

In this chapter, we have analysed the physiological breakdown of Jeffrey six-constant flow due to ciliary motion. The main findings of the present study are as follows:

- The temperature profile is enhanced corresponding to increasing values of parameters B_r and parameter ϵ ,
- The nanoparticle concentration field is enhanced corresponding to increasing values of S_T and S_H ,
- It is clear that frictional forces and pressure rise have an opposite behaviour while compared to each other.
- The pressure gradient increases with the increasing value of ϕ .

Chapter 8

Conclusion

In this thesis, we have investigated the incompressible, laminar and two dimensional peristaltic flow of different non-Newtonian fluids for different flow geometries in the presence of heat transfer. The governing equations of non-Newtonian nanofluid along with heat and mass transfer are modelled and simplified by using low Reynolds number and long wavelength assumptions. The momentum equation is solved by utilizing the homotopy perturbation technique while the exact solutions are computed for temperature and concentration equations. The obtained expressions for the velocity, temperature and nanoparticles concentration are plotted and the impact of various physical parameters are investigated for different peristaltic waves. The main conclusion of this thesis is concluded in the coming paragraph.

In general, temperature profile increases by increasing Brownian motion parameter (N_b) due to increase in the collision between the particles which produces heat as a result temperature field increases. As particles can diffuse under the effects of temperature gradient so increase in thermophoresis parameter (N_t) results in the reduction of concentration field. Increasing the Brinkman number (B_κ) means greater viscous dissipation, thus by increasing Brinkman number, the collision in the flow causes an enhancement in the internal energy of the fluid, which is responsible for the resulting enhancement in the temperature field. By increasing the value of amplitude ratio (ϕ), the pressure gradient increases. Streamlines bolus takes the form of the shape of the geometry. The trapped bolus increases with the increasing value of ϕ . It is found that in the peristaltic flows of different non-Newtonian fluids that non-Newtonian parameters have strong effects

on the velocity profile, thus the theoretical study of non-Newtonian peristaltic flows for various flow geometries are very important for new physical models and their analytical computations. The main findings of the thesis are as follows:

- Velocity profile enhances near the endoscopic tube by increasing values of α because buoyancy forces play a dominant role near the endoscopic tube, also reflux case occurs near the peristaltic waves.
- The trapping bolus phenomenon shows that the bolus decreases with an increase in Jeffrey six-constant parameter α_1 .
- Temperature profile decreases for increasing values of the Biot number.
- Temperature of the fluid decreases with an increase in the nanoparticle volume fraction ϕ because high thermal conductivity plays an important role in dissipating heat.
- Pressure rise and frictional forces have an opposite behaviour as compared to each other.

8.1 Future work

The analysis performed in this thesis can be extend in many directions e.g., slip conditions, no-slip conditions, convective boundary conditions and temperature dependent viscosity. An interesting research of this field to analyze in future will be to study the effects of different nanoparticles, viscous dissipation and heat transfer of non-Newtonian fluids. Some of them are listed as follows.

- Peristaltic flow of a Maxwell nanofluid in an endoscope with non-Newtonian fluids.
- Physiological breakdown of a second grade nanofluid flow in an endoscope embedded in a porous medium.
- Peristaltic flow of a Williamson nanofluid in an endoscope with non uniform wall.
- Simulation of variable thermal conductivity in the flow of peristaltic flow of a non-Newtonian fluid model.

-
- Simulation of thermally stratified fluid in the flow of a peristaltic flow of a Newtonian and non-Newtonian fluids.
 - Simulation of viscous nanofluid in the flow of peristaltic flow of third grade fluid.
 - Physiological flow of Sisko fluid due to ciliary motion.
 - Peristaltic flow of a non-Newtonian fluids due to ciliary motion.
 - Physiological flow of Jeffrey fluid induced by ciliary motion.

Bibliography

- [1] C. Pozrikidis. A study of peristaltic flow. *Journal of Fluid Mechanics*, 180:515–527, 7 1987.
- [2] O. Eytan and E. David. Analysis of intra-uterine fluid motion induced by uterine contractions. *Bulletin of Mathematical Biology*, 61(2):221–238, 1999.
- [3] S. Nadeem and N. S. Akbar. Influence of heat transfer on peristaltic transport of a Johnson-Segalman fluid in an inclined asymmetric channel. *Communications in Nonlinear Science and Numerical Simulation*, 15(10):2860 – 2877, 2010.
- [4] M. Naseer, M. Y. Malik, S. Nadeem, and A. Rehman. The boundary layer flow of hyperbolic tangent fluid over a vertical exponentially stretching cylinder. *Alexandria Engineering Journal*, 53(3):747 – 750, 2014.
- [5] M. Y. Jaffrin and A. H. Shapiro. Peristaltic pumping. *Annual Review of Fluid Mechanics*, 3(1):13–37, 1971.
- [6] S. Srinivas, R. Gayathri, and M. Kothandapani. The influence of slip conditions wall properties and heat transfer on MHD peristaltic transport. *Computer Physics Communications*, 180(11):2115 – 2122, 2009.
- [7] B. B. Gupta and V. Seshadri. Peristaltic pumping in non-uniform tubes. *Journal of Biomechanics*, 9(2):105 – 109, 1976.
- [8] S. K. Guha, H. Kaur, and A. M. Ahmed. Mechanics of spermatic fluid transport in the vas deferens. *Medical and Biological Engineering*, 13(4):518–522, 1975.
- [9] S. K. Batra. Sperm transport through vas deferens: Review of hypotheses and suggestions for a quantitative model. *Fertility and Sterility*, 25(2):186–202, 1974.

-
- [10] T. Hayat and N. Ali. A mathematical description of peristaltic hydromagnetic flow in a tube. *Applied Mathematics and Computation*, 188(2):1491 – 1502, 2007.
- [11] A. E. Hakeem, A. E. Naby, A. E. M. Misiery, and I. I. E. Shamy. Hydromagnetic flow of fluid with variable viscosity in a uniform tube with peristalsis. *Journal of Physics A: Mathematical and General*, 36(31):8535, 2003.
- [12] S. Nadeem and N. S. Akbar. Influence of heat transfer on a peristaltic transport of Herschel-Bulkley fluid in a non-uniform inclined tube. *Communications in Nonlinear Science and Numerical Simulation*, 14(12):4100 – 4113, 2009.
- [13] K. Vajravelu, S. Sreenadh, and V. R. Babu. Peristaltic transport of a Herschel-Bulkley fluid in an inclined tube. *International Journal of non linear Mechanics*, 40(1):83 – 90, 2005.
- [14] A. M. Siddiqui, A. A. Farooq, and M. A. Rana. A mathematical model for the flow of a Casson fluid due to metachronal beating of cilia in a tube. *The Scientific World Journal*, 2015:13–37, 2015.
- [15] A. E. Hakeem, A. E. Naby, A. E. M. Misery, and I. I. E. Shamy. Effects of an endoscope and fluid with variable viscosity on peristaltic motion. *Applied Mathematics and Computation*, 158(2):497 – 511, 2004.
- [16] N. S. Akbar and Z. H. Khan. Metachronal beating of cilia under the influence of Casson fluid and magnetic field. *Journal of Magnetism and Magnetic Materials*, 378:320 – 326, 2015.
- [17] R. Ellahi, A. Riaz, S. Nadeem, and M. Ali. Peristaltic flow of Carreau fluid in a rectangular duct through a porous medium. *Mathematical Problems in Engineering*, 2012:320 – 326, 2012.
- [18] W. A. Khan and I. Pop. Boundary layer flow of a nanofluid past a stretching sheet. *International Journal of Heat and Mass Transfer*, 53(1112):2477 – 2483, 2010.
- [19] S. Nadeem, A. Shaheen, and S. Hussain. Physiological breakdown of Carreau fluid due to ciliary motion. *Journal of Applied Physics Letter*, 134:1 – 8, 2015.
- [20] N. S. Akbar, S. Nadeem, T. Hayat, and H. Awatif. Peristaltic flow of a nanofluid in a non-uniform tube. *Heat and Mass Transfer*, 48(2):425–425, 2012.

- [21] K. S. Das, N. Putra, and W. Roetzel. Pool boiling of nano fluids on horizontal narrow tubes. *International Journal of Multiphase Flow*, 29(8):1237 – 1247, 2003.
- [22] N. S. Akbar, S. Nadeem, and Z. H. Khan. Numerical simulation of peristaltic flow of a Carreau nanofluid in an asymmetric channel. *Alexandria Engineering Journal*, 53(1):191 – 197, 2014.
- [23] S. Nadeem, N. S. Akbar, and K. Vajravelu. Peristaltic flow of a Sisko fluid in an endoscope: Analytical and numerical solutions. *International journal of Computer Mathematics*, 88(5):1013–1023, 2011.
- [24] N. S. Akbar and S. Nadeem. Characteristics of heating scheme and mass transfer on the peristaltic flow for an Eyring-Powell fluid in an endoscope. *International Journal of Heat and Mass Transfer*, 55(13):375 – 383, 2012.
- [25] K. S. Mekheimer and Y. A. Elmaboud. The influence of heat transfer and magnetic field on peristaltic transport of a Newtonian fluid in a vertical annulus: Application of an endoscope. *Physics Letters A*, 372(10):1657 – 1665, 2008.
- [26] R. Ellahi, M. Raza, and K. Vafai. Series solutions of non-Newtonian nanofluids with Reynolds model and Vogels model by means of the homotopy analysis method. *Mathematical and Computer Modelling*, 55(78):1876 – 1891, 2012.
- [27] S. Nadeem, N. S. Akbar, and S. Ashiq. Numerical solutions of peristaltic flow of a Jeffrey six-constant fluid with variable MHD. *International Journal of Nonlinear Sciences and Numerical Simulation*, 11(10):873–885, 1993.
- [28] N. S. Akbar, M. Raza, and R. Ellahi. Endoscopic effects with entropy generation analysis in peristalsis for the thermal conductivity of $H_0 + Cu$ nanofluid. *Journal of Applied Fluid Mechanics*, 134:43 – 51, 2016.
- [29] A. E. Hakeem, A. E. Naby, and A. E. Misiery. Effects of an endoscope and generalized Newtonian fluid on peristaltic motion. *Applied Mathematics and Computation*, 128(1):19 – 35, 2002.
- [30] K. S. Mekheimer and A. elmaboud. Peristaltic transport of a particle fluid suspension through a uniform and non-uniform annulus. *Applied Bionics Biomechanics*, 5(2):47–57, 2008.

-
- [31] S. Nadeem, A. Shaheen, and S. Hussain. Physiological breakdown of Jeffrey six-constant nanofluid flow in an endoscope with non-uniform wall. *Journal of Applied Physics Letter*, 134:1 – 8, 2015.
- [32] S. Nadeem and N. S. Akbar. Effects of induced magnetic field on peristaltic flow of Johnson-Segalman fluid in a vertical symmetric channel. *Applied Mathematics and Mechanics*, 31(8):969–978, 2010.
- [33] M. Fadzilah, R. Nazar, M. Arifin, and I. Pop. Boundary layer flow and heat transfer over a stretching sheet with induced magnetic field. *Journal of Heat Mass Transfer*, 47:155–162, 2011.
- [34] A. Ishak, R. Naza, and I. Pop. Heat transfer over an unsteady stretching permeable surface with prescribed wall temperature. *Real World Application*, 10:2909–2913, 2009.
- [35] K. Vajravelu, G. Radhakrishnamacharya, and V. Radhakrishnamurty. Peristaltic flow and heat transfer in a vertical porous annulus with long wave approximation. *International Journal of non-Linear Mechanics*, 42(5):754 – 759, 2007.
- [36] M. Elbashbeshy and D. Aldawody. Heat transfer over an unsteady stretching surface with variable heat flux in the presence of a heat source or sink. *Computer and Mathematics with Application*, 60:2806–2812, 2010.
- [37] O. Manca, S. Nardini, and D. Ricci. A numerical study of nanofluid forced convection in ribbed channels. *Applied Thermal Engineering*, 37:280 – 292, 2012.
- [38] N. S. Akbar, D. Tripathi, N. Kazmi, and N. A. Mir. Study of heat transfer on physiological driven movement with CNT nanofluids and variable viscosity. *Computer Methods and Programs in Biomedicine*, 128:21–29, 2016.
- [39] J. Buongiorno. Convective transport in nanofluids. *Journal of Heat Transfer*, 128(3):240–250, 2005.
- [40] M. Abdou. Effect of radiation with temperature dependent viscosity and thermal conductivity on unsteady astretching sheet through porous media, nonlinear analysis. *Modeling and Control*, 15:257–270, 2010.
- [41] J. P. Meyer, T. J. Mckrell, and K. Grote. The influence of multi walled carbon nanotubes on single phase heat transfer and pressure drop characteristics in the

- transitional flow regime of smooth tubes. *International Journal of Heat and Mass Transfer*, 58(12):597 – 609, 2013.
- [42] M. A. Elsayed, T. G. Emam, and K. M. Abdelgaber. Effects of thermal radiation and magnetic field on unsteady mixed convection flow and heat transfer over an exponentially stretching surface with suction in the presence of internal heat generation/absorption. *Journal of the Egyptian Mathematical Society*, 20(3):215 – 222, 2012.
- [43] K. S. Mekheimer. Effect of the induced magnetic field on peristaltic flow of a couple stress fluid. *Physics Letters A*, 372(23):4271 – 4278, 2008.
- [44] Kh.S. Mekheimer. Peristaltic flow of blood under effect of a magnetic field in a non-uniform channels. *Applied Mathematics and Computation*, 153(3):763 – 777, 2004.
- [45] S. Ray and D. Chatterjee. MHD mixed convection in a lid driven cavity including heat conducting circular solid object and corner heaters with Joule heating. *International Communications in Heat and Mass Transfer*, 57:200 – 207, 2014.
- [46] N. Ali, T. Hayat, and S. Asghar. Peristaltic flow of a Maxwell fluid in a channel with compliant walls. *Chaos and Solitons Fractals*, 39(1):407 – 416, 2009.
- [47] B. Sreenivasulu and B. Srinivas. Mixed convection heat transfer from a spheroid to a Newtonian fluid. *International Journal of Thermal Sciences*, 87:1 – 18, 2015.
- [48] C. H. Chen. Magnetohydrodynamic mixed convection of a power law fluid past a stretching surface in the presence of thermal radiation and internal heat generation absorption. *International Journal of Non Linear Mechanics*, 44(6):596 – 603, 2009.
- [49] M. K. Choudhary, S. Chaudhary, and R. Sharma. Unsteady MHD flow and heat transfer over a stretching permeable surface with suction or injection. *Procedia Engineering*, 127:703 – 710, 2015.
- [50] R. Muthuraj and S. Srinivas. Mixed convective heat and mass transfer in a vertical channel with traveling thermal waves and porous medium. *Computers and Mathematics with Applications*, 59(11):3516 – 3528, 2010.
- [51] D. Pal and H. Mondal. Effects of temperature dependent viscosity and variable thermal conductivity on MHD non-Darcy mixed convective diffusion of species over

- a stretching sheet. *Journal of the Egyptian Mathematical Society*, 22(1):123 – 133, 2014.
- [52] S.U.S Choi. Enhancing thermal conductivity of fluids with nanoparticles developments and applications of non-Newtonian flows. *Argonne National Laboratory*, 66: 99–105, 1993.
- [53] N. S. Akbar and S. Nadeem. Endoscopic effects on peristaltic flow of a nanofluid. *Communications in Theoretical Physics*, 56(4):761, 2011.
- [54] N. S. Akbar and S. Nadeem. Thermal and velocity slip effects on the peristaltic flow of a six-constant Jeffrey fluid model. *International Journal of Heat and Mass Transfer*, 55(1516):3964 – 3970, 2012.
- [55] M. A. Elsayed, Elbashbeshy, and A. D. Aldawody. Heat transfer over an unsteady stretching surface with variable heat flux in the presence of a heat source or sink. *Computers and Mathematics with Applications*, 60(10):2806 – 2811, 2010.
- [56] N. S. Akbar and A. W. Butt. Bio mathematical venture for the metallic nanoparticles due to ciliary motion. *Computer Methods and Programs in Biomedicine*, 134: 43 – 51, 2016.
- [57] N. S. Akbar, M. Raza, and R. Ellahi. Copper oxide nanoparticles analysis with water as base fluid for peristaltic flow in permeable tube with heat transfer. *Computer Methods and Programs in Biomedicine*, 130:22 – 30, 2016.
- [58] N. S. Akbar, D. Tripathi, O. Anwar, and Z.H. Khan. MHD dissipative flow and heat transfer of Casson fluids due to metachronal wave propulsion of beating cilia with thermal and velocity slip effects under an oblique magnetic field. *Acta Astronautica*, 128:1 – 12, 2016.

Appendix A

In this appendix, we present the constants appearing in homotopy perturbation solution for velocity in Equation (2.35).

$$\begin{aligned}
A_1 &= \frac{1}{\kappa} \left(\frac{Bh}{2} + \frac{B\kappa h}{2} \right), \quad A_2 = \sin[\eta], \quad A_3 = BG_r A_2, \quad A_4 = -G_r A_1 A_2, \\
A_5 &= -\frac{p_0}{4}, \quad A_6 = \frac{1}{32} \alpha_1 p_0^3 \alpha - \frac{1}{32} \alpha_1 p_1^3 \alpha + \frac{A_3}{64} + \frac{A_4}{4}, \quad A_7 = \frac{1}{64} \alpha_1 p_0^3 p_1^2 \alpha, \\
A_8 &= -\frac{3\alpha_1 p_0^6 p_1 \alpha}{1024} + \frac{3\alpha_1 p_0^5 p_1^2 \alpha}{1024} + \frac{5\alpha_2 p_0^3 p_1^4 \alpha^2}{1024} + \frac{3\alpha_1 p_0^3 p_1 \alpha A_3}{1024} - \frac{5\alpha_2 p_1^4 \alpha^2 A_3}{2048} \\
&\quad - \frac{3\alpha_1 p_1 \alpha A_3^2}{4096} + \frac{3\alpha_1 p_0^3 p_1 \alpha A_4}{64} - \frac{3\alpha_2 p_1^4 \alpha^2 A_4}{128} - \frac{3\alpha_1 p_1 \alpha A_3 A_4}{128} - \frac{3\alpha_1 p_1 \alpha A_4^2}{16}, \\
A_9 &= \frac{\alpha_1 p_0^4 \alpha}{5120} - \frac{3\alpha_1 p_0^8 p_1 \alpha}{2560} - \frac{\alpha_2 p_0^6 p_1^3 \alpha^2}{512} + \frac{\alpha_2 p_0^5 p_1^4 \alpha^2}{1024} - \frac{3\alpha_1 p_0^6 \alpha A_3}{10240} + \frac{3\alpha_1 p_0^5 p_1 \alpha m_3}{5120} \\
&\quad + \frac{\alpha_2 p_0^3 p_1^3 \alpha^2 A_3}{512} + \frac{3\alpha_1 p_0^3 \alpha A_3^2}{20480} - \frac{\alpha_2 p_1^3 \alpha^2 A_3^2}{2048} - \frac{\alpha_1 \alpha A_3^3}{40960} - \frac{3\alpha_1 p_0^6 \alpha A_4}{640} + \frac{3\alpha_1 p_0^5 p_1 \alpha A_4}{320} \\
&\quad + \frac{\alpha_2 p_0^3 p_1^3 \alpha^2 A_4}{32} + \frac{3\alpha_1 p_0^3 \alpha A_3 A_4}{640} - \frac{\alpha_2 p_1^3 \alpha^2 A_3 A_4}{64} - \frac{3\alpha_1 \alpha m_3^2 m_4}{2560} + \frac{3\alpha_1 p_0^3 \alpha m_4^2}{80} \\
&\quad - \frac{\alpha_2 p_1^3 \alpha^2 m_4^2}{8} - \frac{3\alpha_1 \alpha A_3 A_4^2}{160} - \frac{\alpha_1 \alpha m_4^3}{16}, \\
A_{10} &= \frac{\alpha_1 p_0^{11}}{8192} - \frac{\alpha_1 p_0^{10} p_1 \alpha}{8192} + \frac{5\alpha_2 p_0^4 p_1^2 \alpha^2}{12288} - \frac{5\alpha_2 p_0^8 p_1^3 \alpha^2}{6144} - \frac{\alpha_1 p_0^8 \alpha m_3}{8192} - \frac{5\alpha_2 p_0^6 p_1^2 \alpha^2 m_3}{8192} \\
&\quad + \frac{5\alpha_2 p_0^5 p_1^3 \alpha^2 m_3}{12288} + \frac{\alpha_1 p_0^5 \alpha A_3^2}{32768} + \frac{5\alpha_2 p_0^3 p_1^2 \alpha^2 m_3^2}{16384} - \frac{5\alpha_2 p_1^2 \alpha^2 m_3^3}{98304} - \frac{\alpha_1 p_0^8 \alpha m_4}{512} \\
&\quad - \frac{5\alpha_2 p_0^6 p_1^2 \alpha^2 m_4}{512} + \frac{5\alpha_2 p_0^5 p_1^3 \alpha^2 m_4}{768} + \frac{\alpha_1 p_0^5 \alpha m_3 m_4}{1024}, \\
A_{11} &= \frac{3\alpha_1 p_0^{13} \alpha}{114688}, \quad A_{12} = \frac{5\alpha_2 p_0^{12} p_1 \alpha^2}{114688} + \frac{15\alpha_2 p_0^{11} p_1^2 \alpha^2}{57344}, \quad A_{13} = \frac{5\alpha_2 p_0^{10} p_1^3 \alpha^2}{57344} \\
A_{14} &= \frac{15\alpha_2 p_0^5 p_1^2 \alpha^2 m_3^2}{229376} + \frac{15\alpha_2 p_0^3 p_1 \alpha^2 m_3^2 m_4^2}{896} - \frac{15\alpha_2 p_1 \alpha^2 m_3^2 m_4^2}{3584} + \frac{5\alpha_2 p_0^3 p_1 \alpha^2 m_4^3}{56}.
\end{aligned}$$

Appendix B

In this appendix, we present the constants appearing in homotopy perturbation solution for velocity in Equation (3.25).

$$\begin{aligned}
m_5 &= \frac{1}{32}\alpha_1 p_0^3 \alpha - \frac{1}{32}\alpha_1 p_1^3 \alpha + \frac{m_3}{64} + \frac{m_4}{4}, \quad m_6 = \frac{dp_0}{dz}, \quad m_7 = \frac{dp_1}{dz}, \\
m_8 &= \frac{1}{64}\alpha_1 p_0^3 p_1^2 \alpha + \frac{1}{192}\alpha_2 p_0^5 \alpha^2 - \frac{1}{192}\alpha_2 p_1^5 \alpha^2 - \frac{1}{128}\alpha_1 p_1^2 \alpha m_3 - \frac{1}{8}\alpha_1 p_1^2 \alpha m_4, \\
m_9 &= -\frac{3\alpha_1 p_0^6 p_1 \alpha}{1024}, \quad m_{10} = \frac{3\alpha_1 p_0^5 p_1^2 \alpha}{1024} + \frac{5\alpha_2 p_0^3 p_1^4 \alpha^2}{1024}, \quad m_{11} = \frac{3\alpha_1 p_0^3 p_1 \alpha m_3}{1024} \\
&\quad - \frac{3\alpha_1 p_1 \alpha m_3^2}{4096} + \frac{3\alpha_1 p_0^3 p_1 \alpha m_4}{64} - \frac{3\alpha_2 p_1^4 \alpha^2 m_4}{128}, \quad m_{12} = \frac{3\alpha_1 p_1 \alpha m_3 m_4}{128}, \\
m_{13} &= \frac{\alpha_1 p_0^4 \alpha}{5120} - \frac{3\alpha_1 p_0^8 p_1 \alpha}{2560} - \frac{\alpha_2 p_0^6 p_1^3 \alpha^2}{512}, \quad m_{14} = \frac{\alpha_2 p_0^5 p_1^4 \alpha^2}{1024} - \frac{3\alpha_1 p_0^6 \alpha m_3}{10240} \\
&\quad + \frac{\alpha_2 p_0^3 p_1^3 \alpha^2 m_3}{512} + \frac{3\alpha_1 p_0^3 \alpha m_3^2}{20480} - \frac{\alpha_2 p_1^3 \alpha^2 m_3^2}{2048} - \frac{\alpha_1 \alpha m_3^3}{40960} - \frac{3\alpha_1 p_0^6 \alpha m_4}{640} \\
&\quad + \frac{\alpha_2 p_0^3 p_1^3 \alpha^2 m_4}{32} + \frac{3\alpha_1 p_0^3 \alpha m_3 m_4}{640} - \frac{\alpha_2 p_1^3 \alpha^2 m_3 m_4}{64} - \frac{3\alpha_1 \alpha m_3^2 m_4}{2560} \\
&\quad - \frac{\alpha_2 p_1^3 \alpha^2 m_4^2}{8} - \frac{3\alpha_1 \alpha m_3 m_4^2}{160} - \frac{\alpha_1 \alpha m_4^3}{16}, \\
m_{15} &= \frac{\alpha_1 p_0^{11}}{8192}, \quad m_{16} = \frac{\alpha_1 p_0^{10} p_1 \alpha}{8192} + \frac{5\alpha_2 p_0^4 p_1^2 \alpha^2}{12288} + \frac{5\alpha_2 p_0^8 p_1^3 \alpha^2}{6144} - \frac{\alpha_1 p_0^8 \alpha m_3}{8192} \\
&\quad + \frac{5\alpha_2 p_0^5 p_1^3 \alpha^2 m_3}{12288} + \frac{\alpha_1 p_0^5 \alpha m_3^2}{32768} + \frac{5\alpha_2 p_0^3 p_1^2 \alpha^2 m_3^2}{16384} - \frac{5\alpha_2 p_1^2 \alpha^2 m_3^3}{98304} - \frac{\alpha_1 p_0^8 \alpha m_4}{512} \\
&\quad - \frac{5\alpha_2 p_0^6 p_1^2 \alpha^2 m_4}{512} + \frac{5\alpha_2 p_0^5 p_1^3 \alpha^2 m_4}{768} + \frac{\alpha_1 p_0^5 \alpha m_3 m_4}{1024}, \\
m_{17} &= \frac{3\alpha_1 p_0^{13} \alpha}{114688} - \frac{5\alpha_2 p_0^{12} p_1 \alpha^2}{114688} + \frac{15\alpha_2 p_0^{11} p_1^2 \alpha^2}{57344} - \frac{5\alpha_2 p_0^{10} p_1^3 \alpha^2}{57344} - \frac{3\alpha_1 p_0^{10} \alpha^2 m_3}{229376} \\
&\quad + \frac{15\alpha_2 p_0^5 p_1^2 \alpha^2 m_3^2}{229376} + \frac{15\alpha_2 p_0^3 p_1 \alpha^2 m_3^2 m_4}{896} - \frac{15\alpha_2 p_1 \alpha^2 m_3^2 m_4}{3584} + \frac{5\alpha_2 p_0^3 p_1 \alpha^2 m_4^3}{56} \\
&\quad - \frac{5\alpha_2 p_1 \alpha^2 m_3 m_4^3}{112} - \frac{5\alpha_2 p_1 \alpha^2 m_4^4}{28}.
\end{aligned}$$

Appendix C

In this appendix, we present the constants appearing in homotopy perturbation solution for velocity in Equation (4.21).

$$\begin{aligned}
 A_1 &= \frac{\alpha_1 p_0^{15} \alpha}{524288}, \quad A_2 = \frac{\alpha_2 p_0^{15} \alpha^2}{524288} - \frac{5\alpha_2 p_0^{14} p_1 \alpha^2}{131072}, \quad A_3 = \frac{15\alpha_2 p_0^{13} p_1^2 \alpha^2}{262144} - \frac{5\alpha_2 p_0^{12} \alpha^2 A_3}{1048576} \\
 &\quad + \frac{15\alpha_2 p_0^{11} p_1 \alpha^2 m_3}{262144}, \quad A_4 = \frac{15\alpha_2 p_0^{10} p_1^2 \alpha^2 m_3}{524288}, \quad A_5 = \frac{5\alpha_2 p_0^9 p_1 \alpha^2 m_3^2}{1048576}, \\
 A_6 &= \frac{1}{64} \alpha_1 p_0^3 p_1^2 \alpha + \frac{1}{192} \alpha_2 p_0^5 \alpha^2 - \frac{1}{192} \alpha_2 p_1^5 \alpha^2 - \frac{1}{128} \alpha_1 p_1^2 \alpha A_3 - \frac{1}{8} \alpha_1 p_1^2 \alpha A_4 \\
 &\quad - \frac{5\alpha_2 p_0^6 \alpha^2 m_3^2}{2097152} + \frac{5\alpha_2 p_0^5 p_1 \alpha^2 m_3^3}{1048576}, \quad A_7 = \frac{\alpha_2 \alpha^2 m_3^5}{16777216} - \frac{5\alpha_2 p_0^{12} \alpha^2 m_4}{131072} + \frac{15\alpha_2 p_0^5 \alpha}{65536} \\
 A_7 &= \frac{5\alpha_2 p_0^{17} \alpha^2}{2359296}, \quad A_8 = \frac{5\alpha_2 p_0^{16} p_1 \alpha^2}{393216} + \frac{5\alpha_2 p_0^{15} \alpha^2}{1179648} - \frac{5\alpha_2 p_0^{14} \alpha^2 m_3}{1179648} - \frac{5\alpha_2 p_0^{13} p_1 \alpha^2 m_3}{393216}.
 \end{aligned}$$